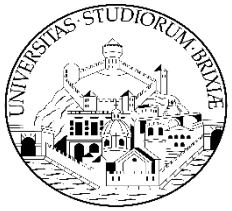


UNIVERSITÀ
DEGLI STUDI
DI BRESCIA

**PhD Course in**

**Precision Medicine**

**Settore scientifico-disciplinare BIO/10**

**XXXVI Cycle**

# Ferroptosis and Iron Metabolism in Cancer Growth

**PhD Student:**

**Luca Cantamessa**

**Supervisor:** **Prof. Maura Poli**

**Co-supervisor:** **Michela Asperti, PhD**

**Magdalena Edyta Gryzik, PhD**

# Index

# Abstract

Iron is an essential micronutrient for most living organisms, and it is also required to sustain the accelerated metabolism of cancer cells. On the other hand, increased amount of iron causes cellular oxidative stress, promoting the peroxidation of phospholipid-bound polyunsaturated fatty acids (PL-PUFAs) and causing ferroptotic cell death. Thus, the double-edged sword of essentiality and toxicity of iron makes it a promising target to counteract tumor growth.

In light of this lines of evidence, this PhD thesis investigated the effects of ferroptosis inducers and iron modulation in two different tumor types, glioblastoma and rhabdomyosarcoma which are poorly characterized regarding iron metabolism and ferroptosis mechanism.

Glioblastoma (GBM) is the most common tumor of the central nervous system in adults, and it is characterized by extreme aggressiveness and elevated risk of tumor recurrence, resulting in poor patient prognosis. Recently, stem-like GBM cells, named glioblastoma cancer stem cells (GBM-CSCs), have been identified as being responsible for the resistance to current therapies and tumor relapse, therefore, new therapeutic approaches are required. In this context, the study investigated whether ferroptosis-inducing agents could affect the viability of GBM-CSCs.

It was demonstrated that ferroptosis inducers can potently inhibit the growth of GBM-CSC lines. Moreover, ferroptosis inducers were found to increase the efficacy of temozolomide, encouraging further studies for unravelling the mechanism of ferroptosis in GBM-CSCs.

The other type of tumor studied in the present PhD thesis is rhabdomyosarcoma (RMS), an aggressive and metastatic pediatric cancer that develops from undifferentiated myocytes. Current therapies for RMS include surgical resection followed, when required, by different strategies of aggressive chemotherapy and radiotherapy. These treatments, however, are often not curative thus requiring new therapeutic tools. Recently, since it was reported that iron chelators can efficiently impair RMS tumor growth, the current study investigated the effects on RMS cells of didox, a synthetic inhibitor of the regulatory subunit of ribonucleotide reductase RRM2 with iron-chelating properties. It was found that didox can effectively inhibit the *in vitro* growth of RMS cell lines representative of the most frequent

subtypes, embryonal (ERMS) and alveolar (ARMS), also altering their motility, their clonogenic capability, and their iron status. Moreover, the findings demonstrated that didox was able to impair the *in vivo* growth of ARMS cells, suggesting that the use of this inhibitor could be effective in the treatment of RMS.

Additionally, among the many molecular alterations identified in RMS, the overexpression of caveolin-1 (Cav-1) has been demonstrated to correlate with an increased sensitivity of RMS cells to ferroptosis inducers. Therefore, the mechanism of ferroptosis in Cav-1-overexpressing ERMS cells, with a particular focus on the alterations on lipid metabolism in these cells were investigated. The data demonstrated that RMS cells that overexpressed Cav-1 are characterized by an altered expression of various lipid metabolism-related genes and proteins. Interestingly, Cav-1-overexpressing cells showed increased expression of both mRNA and protein level of long-chain-fatty-acid-CoA ligase 4 (ACSL4), the enzyme responsible for the insertion of polyunsaturated fatty acids (PUFAs) in cell membrane. Thus, further studies investigated the role of ACSL4 in the ferroptosis sensitivity of these cells. By inhibiting both its activity and its expression, it was found that ACSL4 seems not directly involved in the increased susceptibility to ferroptosis of these cells. Moreover, it was found that the modulation of lipid content of Cav-1-overexpressing cells can alter their sensitivity to ferroptosis inducer RSL3. Cells pre-treated with PUFAs showed increased sensitivity to the cytotoxic effect of RSL3, whereas the pre-treatment with MUFAs protected cells towards RSL3-induced ferroptosis.

In conclusion, the data from the current study showed that both iron modulation and ferroptosis induction could be promising alternative therapeutic tools to counteract the growth of tumor that showed resistance to the current therapies, such as glioblastoma and rhabdomyosarcoma.

# Riassunto

Il ferro è un micronutriente essenziale per la vita, ma è anche necessario per sostenere il metabolismo accelerato delle cellule tumorali. Inoltre, l'aumento dei livelli di questo metallo causa stress ossidativo nelle cellule, promuovendo la perossidazione degli acidi grassi polinsaturi legati ai fosfolipidi di membrana e causando morte cellulare per ferroptosi. Perciò, la doppia natura del ferro (essenziale e tossico allo stesso tempo) lo rende un promettente target terapeutico nella lotta al cancro.

Considerato ciò, in questa tesi di dottorato abbiamo indagato gli effetti degli induttori di ferroptosi e della chelazione del ferro in due diversi tipi di tumore, entrambi poco caratterizzati per il loro metabolismo del ferro e per il meccanismo di ferroptosi: il glioblastoma e il rabdomiosarcoma.

Il glioblastoma (GBM) è in tumore del sistema nervoso centrale più frequente negli adulti, ed è caratterizzato da un'estrema aggressività e da un elevato rischio di recidive, risultanti in una scarsa prognosi dei pazienti. Recentemente, cellule staminali di glioblastoma, note come glioblastoma cancer stem cells (GBM-CSCs), sono state identificate come responsabili della ricaduta della malattia, rendendo necessario lo sviluppo di nuove strategie antitumorali. Perciò, abbiamo investigato sull'efficacia degli induttori di ferroptosi nel ridurre la vitalità cellulare delle GBM-CSCs.

Abbiamo dimostrato che gli induttori di ferroptosi inibiscono potentemente la crescita di linee di GBM-CSCs *in vitro*. Inoltre, abbiamo osservato che gli induttori di ferroptosi aumentano l'efficacia della temozolomide, incoraggiando ulteriori analisi sul meccanismo della ferroptosi nelle GBM-CSCs.

L'altra tipologia di tumore studiata nel presente lavoro di tesi, in collaborazione con il gruppo di ricerca del Prof. Fanzani (all'Università di Brescia) è il rabdomiosarcoma, un tumore dell'età pediatrica aggressivo e metastatico che si sviluppa da miociti non differenziati. Le terapie attuali contro il RMS includono l'asportazione chirurgica, seguita, dove necessario, da diverse strategie combinate di chemio- e radioterapia; ciononostante, questi trattamenti risultano spesso non curativi, richiedendo lo sviluppo di strategie alternative. Recentemente, abbiamo dimostrato che i chelanti del ferro possono impedire efficacemente la crescita del RMS, perciò abbiamo investigato gli effetti su linee cellulari di

RMS del didox, un inibitore sintetico della subunità regolatrice della ribonucleotide reduttasi RRM2, caratterizzato anche da proprietà di chelante del ferro. Abbiamo scoperto che il didox inibisce significativamente la crescita *in vitro* di linee cellulari di RMS rappresentative dei due sottotipi più frequenti, embrionale e alveolare, riducendo inoltre la loro motilità, la loro clonogenicità e alterando il loro metabolismo del ferro. Inoltre, abbiamo dimostrato che il didox contrasta la crescita *in vivo* di linee cellulari di RMS alveolare, suggerendo che l'uso di questo inibitore potrebbe essere efficace nel trattamento dei rabdomiosarcomi.

Inoltre, tra le varie alterazioni molecolari identificate nei RMS, l'overespressione di caveolina-1 (Cav-1) è stata correlata con un aumento della sensibilità di linee cellulari di RMS agli induttori di ferroptosi. Perciò, abbiamo investigato sul meccanismo della ferroptosi in linee cellulari di RMS embrionale overesprimenti Cav-1. Abbiamo dimostrato che queste cellule esprimono livelli alterati di geni e proteine correlati al metabolismo lipidico. Inoltre, abbiamo rilevato, nelle cellule overesprimenti Cav-1, un aumento dei livelli di espressione, sia genica sia proteica, della long-chain-fatty-acid-CoA ligase 4 (ACSL4), l'enzima responsabile dell'inserzione nelle membrane cellulari degli acidi grassi polinsaturi. Di conseguenza, abbiamo investigato sul ruolo di ACSL4 nella sensibilità alla ferroptosi di queste cellule. Inibendo sia la sua attività sia la sua espressione, abbiamo scoperto che ACSL4 non sembra direttamente coinvolto nell'aumentata sensibilità alla ferroptosi di queste cellule. In aggiunta, abbiamo dimostrato che la modulazione del contenuto lipidico delle cellule overesprimenti Cav-1 può alterare la loro sensibilità all'induttore di ferroptosi RSL3: il trattamento in combinazione con acidi grassi polinsaturi ne riduce ulteriormente la vitalità, mentre la combinazione con acidi grassi monoinsaturi protegge queste cellule dall'azione citotossica di RSL3.

In conclusione, i nostri dati dimostrano che la modulazione del metabolismo del ferro e l'induzione della ferroptosi sono entrambe due promettenti strategie nel contrastare la crescita di tumori resistenti agli attuali trattamenti antitumorali, come il glioblastoma e il rabdomiosarcoma.

# 1- Introduction

# Iron metabolism

## *Systemic and cellular iron metabolism*

Iron is an essential micronutrient for virtually all life forms, being involved in many fundamental biological processes such as DNA synthesis and repair, energy production in mitochondria and the component of heme groups in numerous enzymes Fe-S clusters and other proteins (Papanikolaou and Pantopoulos, 2005). In the extracellular environment, iron can be found in its $Fe^{3+}$ form bound to transferrin, which, binding two ferric iron atoms per molecule (Holo-Tf), is mainly recognized by transferrin receptor 1 (TfR1) on the cell membrane. Then, the complex (Holo-Tf/TfR1) is internalized via clathrin-mediated endocytosis (Hentze, Muckenthaler and Andrews, 2004), and, after the acidification of the endosome, iron atoms are dissociated, while transferrin and TfR1 are recycled. Iron can be reduced to its ferrous ($Fe^{2+}$) form by the metalloreductase six-transmembrane epithelial antigen of prostate 3 (STEAP3), and transported to the cytoplasm by divalent metal transporter 1 (DMT1) (Brown *et al.*, 2020). The cytosolic free ferrous ions constitute the labile iron pool (LIP), the source of iron available for the incorporation into iron-dependent enzymes, for the synthesis of Fe-S clusters and heme, and for the regulation of gene expression (Lane *et al.*, 2015). When in the cytoplasm, free $Fe^{2+}$ can interact with hydrogen peroxide leading to the production of free radicals through the Fenton reaction, thus increasing oxidative stress. To avoid this, cells store excess iron in ferritin (Ft), a 24-polymeric protein composed by a light (FtL) and a heavy (FtH) chains, which are expressed differentially in a tissue-depending manner (Bystrom and Rivella, 2015). With FtL performing a structural function, FtH exerts ferroxidase action, allowing the oxidation of iron to its $Fe^{3+}$ form, which can be safely stored in ferritin (Arosio, Elia and Poli, 2017). Alternatively, iron is exported through the transmembrane channel ferroportin (FPN, also known as SLC40A1), the only known iron exporter (Torti and Torti, 2020), negatively regulated by the peptide hormone hepcidin, which induces FPN ubiquitination and proteasomal degradation (Nemeth and Ganz, 2021). In Figure 1.1 are schematized the main proteins involved in cellular iron metabolism.

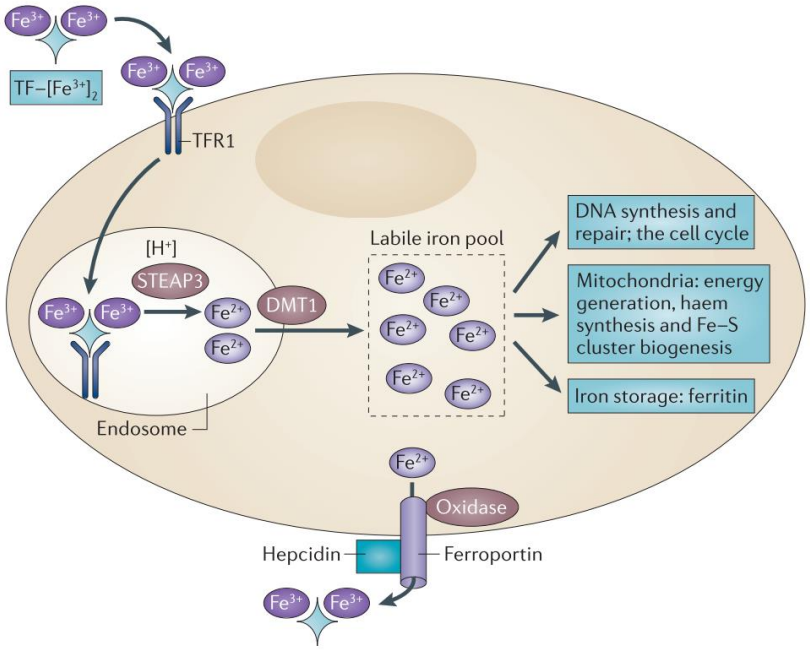


**Figure 1.1 – The key players in cellular iron metabolism.** Transferrin (Tf)-bound $Fe^{3+}$ iron is recognized by Transferrin receptor 1 (TfR1) and internalized by clathrin-dependent endocytosis. In the endosome, the acidic environment causes ferric iron to dissociate from transferrin; then, $Fe^{3+}$ is reduced to ferrous $Fe^{2+}$ by the metalloreductase six transmembrane epithelial antigen of prostate 3 (STEAP3) and is transported to the cytoplasm by divalent metal transporter 1 (DMT1), forming the so-called Labile Iron Pool (LIP). Free cytoplasmic iron can finally be incorporated in iron-dependent enzymes, used for the synthesis of heme and Fe-S clusters, or be safely stocked in the iron storage protein ferritin. Excessive iron is then exported by the transmembrane channel ferroportin, whose activity is inhibited by the systemic hormone hepcidin, which also causes its internalization and degradation (from Torti and Torti, 2013).

## *Iron metabolism in cancer*

In the context of iron metabolism, it is known that cancer cells are characterized by the so-called "iron addiction" (Figure 1.2), hallmarked by the alteration of iron-related proteins to guarantee an increase of intracellular iron availability to sustain their accelerated metabolism. It means that cancer cells generally show an increased iron uptake due to upregulation of TfR1, decreased iron efflux with downregulation of FPN and decreased iron storage with downregulation of ferritin (Torti *et al.*, 2018), increasing the amount of free $Fe^{2+}$ iron in the cytoplasm.

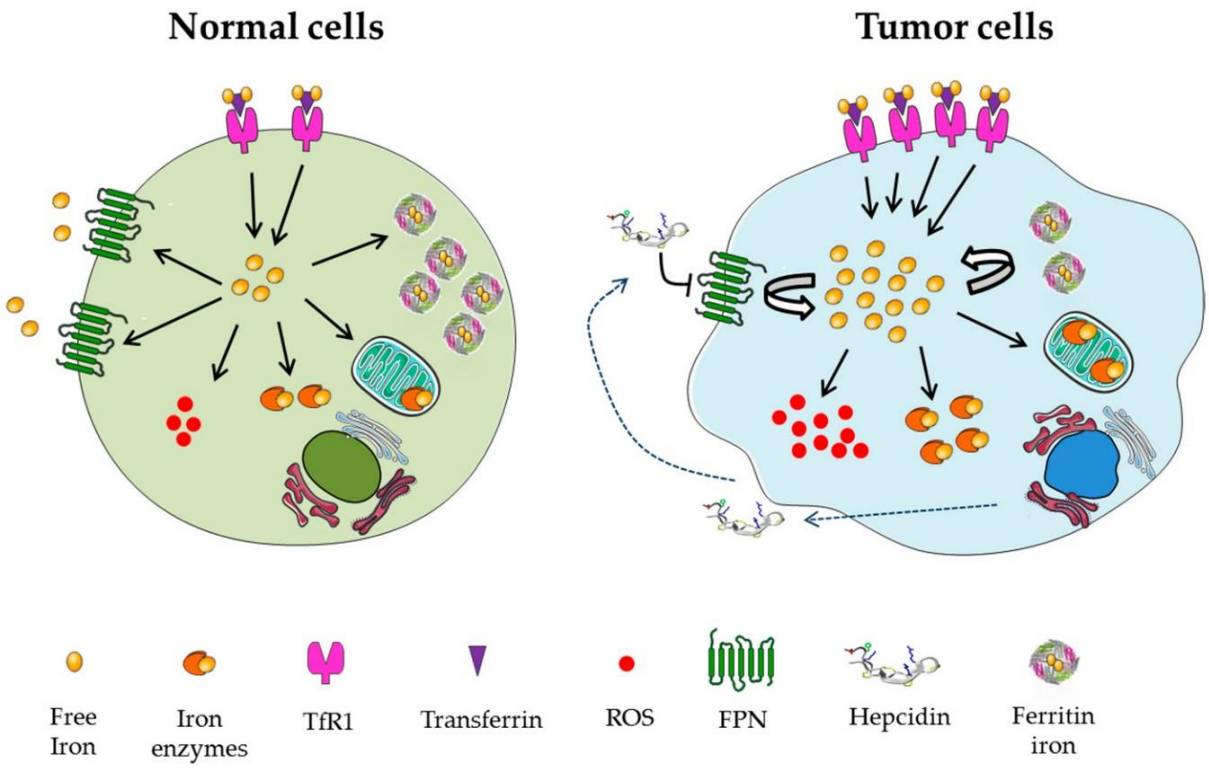


**Figure 1.2 – The "iron addiction" of cancer cells.** In normal cells, adequate levels of transferrin receptor 1 (TfR1) supply the cell with enough iron, which is incorporated in iron enzymes to sustain DNA synthesis and repair, energy production in mitochondria and generation of heme groups and Fe-S clusters, while the excess amount of iron is safely stored in ferritin polymers. Cancer cells, having increased metabolic demands, resolve their higher need of iron with the upregulation of TfR1 and the degradation of ferritin, increasing the labile iron pool and, in turn, its incorporation in iron enzymes but, on the other hand, this iron increase leads to the production of free radicals through the Fenton reaction. Also, tumor cells are able to produce and secrete hepcidin, the main systemic iron-regulating hormone, which binds ferroportin-1 (FPN, the only known cellular iron exporter) and mediates its internalization and degradation that further increases intracellular iron (Fanzani and Poli, 2017).

From a therapeutic point of view, there are two alternative modalities to take advantage of iron dysregulation in cancer. The first one is the use of iron chelating agents to decrease the amount of bioavailable iron, which in turn attenuates tumor proliferation and metastatic potential by inducing cell cycle arrest and apoptotic death (Abdelaal and Veuger, 2021). The most used chelating compounds are deferiprone (DFP), deferoxamine (DFO) and deferasirox (DFX) (Ibrahim and O'Sullivan, 2020). These compounds have also been tested in preclinical studies in pancreatic, breast, liver, gastric, hepatic and esophageal cancers, showing promising results (Brown et al., 2020).

The second strategy, named "iron overload" induction, takes into consideration the toxic effect of iron excess, whereby treatment with iron would further increase its already critical levels in cancer cells, promoting the Fenton reaction and the production of reactive oxygen species (ROS) (Torti and Torti, 2013). Despite its proved efficacy in *in vitro* cell lines, the application of this strategy in cancer patients is controversial, since the presence of iron

promotes tumor proliferation and resistance to therapies (Brown et al., 2020). However, some works showed that the use of iron oxide nanoparticles is effective against mammary tumor (Zanganeh et al., 2016), and that the combination of iron and some chemotherapeutic agents is effective in potentiating the anti-tumor effect in prostatic cancer (Bordini et al., 2020) and multiple myeloma (Campanella et al., 2013; Bordini et al., 2017).

# Fatty acid metabolism

## *Cellular fatty acid metabolism*

Fatty acids are important structural components of the cell membrane and they are involved in the regulation of intracellular mechanisms, in the storage and production of energy (de Carvalho and Caramujo, 2018). Biochemically classified as carboxylic acids, the fatty acids that are used in cells can be classified based on their length and by the number and location of double bonds between the carbon atoms that compose the aliphatic chain. Typically, the fatty acids that can be found in the cell membrane contain from 16 to 20 carbon atoms, and are divided in three main categories, that are saturated (SFAs), monounsaturated (MUFAs) and polyunsaturated fatty acids (PUFAs), depending on the presence of, respectively, no double bonds, a single double bond, or multiple double bonds between the carbon atoms of the chain (White, 2009).

The regulation of cellular lipid metabolism relies on the transcription factors Sterol Regulatory Element Binding Proteins (SREBP1 and 2). These proteins are present in the cell in their inactive form, which localizes on the membrane of the endoplasmic reticulum (Nohturfft and Shao, 2009). In case of low sterols concentrations, these precursors are transported to the Golgi apparatus, where they are proteolytically cleaved (Brown and Goldstein, 1997). This modification enables the translocation of mature SREBPs to the nucleus, where they can bind to sterol regulatory elements on the DNA, thus promoting gene transcription. More precisely, SREBP1 is involved in the regulation of genes for fatty acids and triacylglycerols synthesis, while SREBP2 regulates the transcription of genes involved in cholesterol synthesis (Santos and Schulze, 2012).

The synthesis of fatty acids starts from the production of acetyl-CoA, from citrate deriving from the Krebs cycle through the action of ATP-citrate lyase (ACLY) (Wei *et al.*, 2020). Then, acetyl-CoA is converted to malonyl-CoA by the enzyme acetyl-CoA carboxylase (ACC), the second building block in fatty acid synthesis (Wang *et al.*, 2022). Then, several malonyl-CoA molecules, together with a priming acetyl-CoA molecule, are condensed by the enzyme fatty acid synthase (FASN), which, in repeated steps, leads to the production of palmitic acid, a 16-carbon saturated fatty acid.

After this, the chain can be elongated by fatty acid elongase (ELOVL) and further desaturated by fatty acid desaturases. Among these, δ-5 desaturase (D5D, or FADS2) and δ-6 desaturase (D6D, or FADS1) are responsible for the production of PUFAs (Tosi *et al.*, 2014), whereas stearoyl-CoA desaturase 1 (SCD1) catalyzes the conversion of palmitoyl- and stearoyl-CoA (which are saturated fatty acids) into, respectively, palmitoleyl- and oleoyl-CoA (which are monounsaturated fatty acids), that is the first step for the synthesis of MUFAs (Ntambi and Miyazaki, 2004). Alternatively, the import of essential PUFAs (which cannot be synthetized by the cell) is mediated by fatty acid transport proteins (FATPs) and fatty acid translocase (FAT, or CD36), thus playing an essential role in lipid metabolism (Koundouros and Poulogiannis, 2020).

Then, fatty acids can be either inserted in the cell membrane or redirected to mitochondria for energy production via the β-oxidation, while excess fatty acids are stored in lipid droplets. These cytosolic structures are formed in the cytoplasmic reticulum and are composed of a neutral lipid core (where triacylglycerols and sterol esters are located) covered by a single monolayer of phospholipids and endowed with various regulatory proteins. Due to their dynamic nature, lipid droplets are continuously degraded and reformed based on the needs of the cell (Olzmann and Carvalho, 2019). Figure 1.3 summarizes the main proteins involved in fatty acids synthesis.

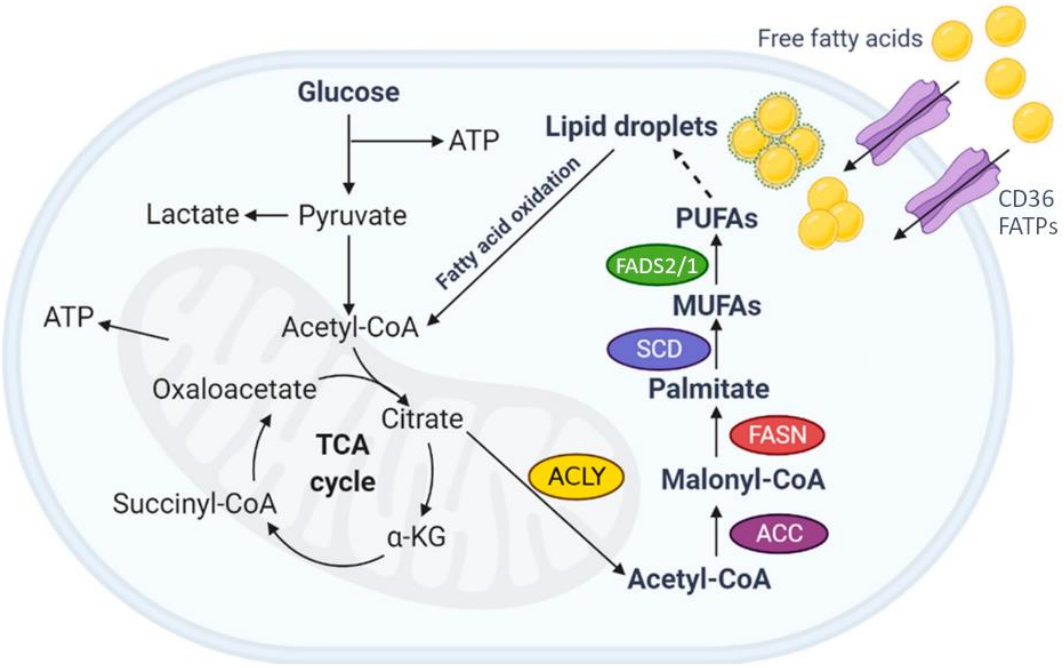


**Figure 1.3 – The key players in cellular fatty acids biosynthesis.** ATP-citrate lyase (ACLY) mediates the production of acetyl-CoA from citrate derived from the TCA cycle. Then, acetyl-CoA carboxylase (ACC) mediates the production of malonyl-CoA, of which, together with a priming acetyl-CoA molecule, multiple units are sequentially condensed by fatty acid synthase (FASN) to form palmitate, a saturated fatty acid. Then, stearoyl-CoA desaturase mediates the first step in monounsaturated fatty acids (MUFAs) synthesis, and fatty acid desaturase 2 and 1 (FADS2/1) mediate the further production of polyunsaturated fatty acids (PUFAs), which will be either inserted in the cell membrane or stored in lipid droplets. Moreover, the import of fatty acids, both essentials and non-essentials, from the extracellular space is mediated by fatty acid translocase (FAT, or CD36) and by fatty acid transport proteins (FATPs) (modified from Yoon and Lee, 2022).

## *Lipid metabolism and cancer*

Due to their accelerated metabolism and growth rate, tumor cells are characterized by increased need of fatty acids, which results in the alteration of the expression of fatty acids metabolism mediators (Currie *et al.*, 2013).

Firstly, the expression of SREBPs is altered in cancer, promoting tumor growth and metastasis, and their expression is also associated with poor prognosis (Röhrig and Schulze, 2016). These alterations in SREBPs levels also modify the expression of downstream proteins. It has been demonstrated that downregulation of ACLY, both by chemical inhibition or by silencing RNA, can impair the growth of tumors, both *in vitro* and *in vivo* (Hatzivassiliou *et al.*, 2005; Migita *et al.*, 2008). Also, the knockdown of ACC has been revealed to cause cell death in both prostate (Brusselmans *et al.*, 2005) and breast cancer (Chajès *et al.*, 2006). Moreover, the expression of FASN is extremely increased in various cancer types and has been correlated to poorer prognosis of patients (Menendez and Lupu,

2007), while its inhibition causes cell death by apoptosis, probably induced by excessively high concentrations of malonyl-CoA (Pizer *et al.*, 2000).

Also, SCD1, which mediates MUFAs synthesis, has been found overexpressed in tumors compared to normal cells (Li *et al.*, 1994), and it has been proven to promote oncogenic transformation of human lung fibroblasts (Scaglia, Matías Caviglia and Ariel Igal, 2005). Moreover, its pharmacological inhibition causes cell cycle arrest between the $G_1$ and S phase, thereby inducing cells to apoptosis (Hess, Chisholm and Igal, 2010). Contrarily, FADS2 and FADS1, responsible for PUFAs synthesis, are reported to promote *in vivo* tumor growth of various tumor types, and their inhibition has been observed to reduce tumor proliferation (Hansen-Petrik *et al.*, 2002; He *et al.*, 2012; R. Zhao *et al.*, 2020).

Since tumor cells are characterized by elevated oxidative stress, fatty acids and in particular PUFAs are subjected to peroxidation, leading to the formation of lipid peroxides that are detrimental and could cause a regulated form of cell death named ferroptosis.

# Ferroptosis

An important consequence of intracellular iron increase is the onset of a form of cell death associated with excessive iron-dependent membrane lipid peroxidation, named "ferroptosis", a name coined in 2012 by the laboratory of Dr. Brent R. Stockwell (Dixon *et al.*, 2012).

Ferroptosis was originally discovered by a high-throughput screening of potential lethal molecules to RAS-mutated tumor cells, with the identification of two compounds called erastin (in 2003) and RSL3 (in 2008) that did not trigger markers of any already known type of regulated cell death, such as caspase activation, cleavage of poly [ADP-ribose] polymerase (PARP) and DNA fragmentation. Moreover, neither the treatment with chemical inhibitors of apoptosis or necroptosis nor knockout of apoptotic related-genes can rescue the viability of the cells exposed to ferroptosis inducers (also called "FINs") (Yang and Stockwell, 2016). Indeed, ferroptotic cell death can be mitigated by antioxidants, ROS and lipid ROS scavengers, and iron chelators, and these are referred to as "ferroptosis inhibitors" (Dixon and Stockwell, 2019).

During the early stages of ferroptosis, increase of cell membrane permeability is observed, progressively leading to membrane rupture at the end of the process. Also, the structure of the endoplasmic reticulum is altered, and this organelle plays a pivotal role in lipid peroxides initiation and propagation (von Krusenstiern *et al.*, 2023). Moreover, while the nucleus appears of normal dimensions without any sign of chromatin condensation, some other organelles contribute to drive ferroptosis. For example, the release of iron from lysosomes can propagate non-enzymatic lipid peroxides formation, as explained later, and peroxisomal $H_2O_2$ can also damage membrane-bound lipids. Finally, mitochondrial membrane rupture can be observed, suggesting that the leakage of electrons from the mitochondrial electron transport chain could contribute to superoxide formation and, ultimately, lipid membrane damage (Stockwell, 2022).

From a biochemical point of view, ferroptosis is characterized by increased iron concentration, which accumulates both in the cytoplasm (LIP) and in mitochondria, and by the concomitant decrease of three main cellular antioxidant machineries, namely, the glutathione/glutathione peroxidase 4 (GPX4) axis, the NADPH/Ferroptosis Suppressor 1 (FSP1)/Coenzyme $Q_{10}$ ($CoQ_{10}$) axis, and the GTP cyclohydrolase-1

(GCH1)/Tetrahydrobiopterin ($BH_4$) axis. All these features favor the harmful peroxidation of phospholipid-bound polyunsaturated fatty acids (PL-PUFAs) chains, leading to cell death (Zheng and Conrad, 2020).

In addition, ferroptotic cells are characterized by the release of arachidonic acid (AA)-derived mediators and damage-associated molecular patterns (DAMPs), therefore making ferroptosis a pro-immunogenic form of cell death (Friedmann Angeli *et al.*, 2014; Xie *et al.*, 2016; Lv *et al.*, 2022).

## *Lipid peroxidation*

As mentioned before, ferroptosis is mainly caused by excessive lipid peroxidation of PUFA-containing phospholipids, hence this process cannot occur on MUFA chains.

The aberrant production of phosphatidylethanolamine (PE)-bound lipid peroxides is a self-propagating process (Ursini and Maiorino, 2020). Normally, the cells produce lipid peroxides by two modalities (the non-enzymatic and enzymatic processes), and their toxicity is prevented by antioxidants such as vitamin E or the tripeptide glutathione (GSH) (Cao and Dixon, 2016).

In the final steps of both the non-enzymatic and enzymatic peroxidation, the methylene carbon atom bridging two double bonds is deprived of a hydrogen atom by the interaction with a free radical, making it a radical specie. The new radical lipid compound is thermodynamically unstable, delocalizing a free electron between the $\pi$-orbitals to form a resonance hybrid. This leads to the conversion of the molecule to a more stable isomer with two adjacent double bonds and a free electron on the carbon near them. Then, the stabilized radical reacts with the molecular oxygen which, extracts a hydrogen atom to turn it into a lipid hydroperoxide, as schematized in Figure 1.4 (Gaschler and Stockwell, 2017).

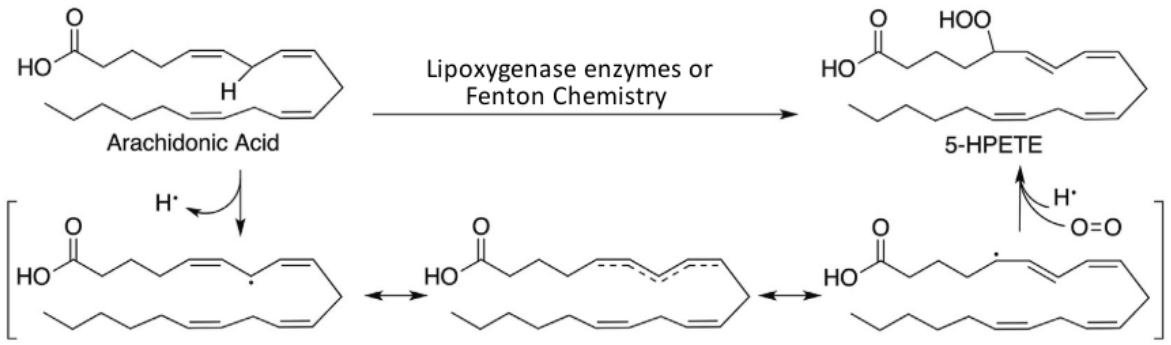


**Figure 1.4 – The general process of lipid peroxides formation.** Arachidonic acid, the most representative polyunsaturated fatty acid (PUFA) involved in ferroptotic lipid peroxidation, is taken as example. The reaction begins with the removal of a hydrogen atom on the methylene carbon, generating a free radical. Due to the formation of a resonance hybrid, the molecule is converted into its more stable isomer, which has the radical carbon near only one double bond. Then, the interaction with molecular oxygen leads to the generation of the final lipid hydroperoxide (Gaschler and Stockwell, 2017).

## *Synthesis of lipid peroxides by Fenton chemistry*

The formation of lipid hydroperoxides can be initiated by the so-called "Fenton chemistry", a non-enzymatic process, or by the activity of lipoxygenases, an enzymatic process. The "Fenton chemistry" process develops through three stages, initiation, propagation and termination, and involves the ferrous ion (or, less frequently, a $Cu^{2+}$ ion) derived from LIP, which is available to participate in redox processes (Torti and Torti, 2013).

In the initiation phase, the generation of the lipid radical is driven by the interaction between the labile $Fe^{2+}$ pool and hydrogen peroxide ($H_2O_2$), which causes the release of a ferric ($Fe^{3+}$) ion, a hydroxide anion ($OH^-$), and the highly reactive hydroxyl radical species (HO•). If another equivalent of $H_2O_2$ is available, $Fe^{3+}$ can be reduced back to $Fe^{2+}$ producing a peroxyl radical (ROO•). In the following propagation step, both the hydroxyl and peroxyl radical can remove a hydrogen from a PUFA, generating a carbon-centered radical able to react with molecular oxygen and form a lipid-peroxyl radical (LOO•) (Gaschler and Stockwell, 2017).

At this point, the lipid-peroxyl radical can repeat the process with another membrane PUFA, generating a lipid peroxide and a lipid radical that can interact with molecular oxygen, thus propagating the generation of lipid peroxides. Two of these lipid radicals can interact and generate a stable non-radical molecule, forming a bond between them and terminating the propagation reaction. Alternatively, if available, a lipophilic antioxidant like vitamin E can take part in the reaction and donate an electron to the radical, stabilizing it, as illustrated in Figure 1.5 (Gaschler and Stockwell, 2017). Contrarily, if their concentration is too high and

antioxidants are not available, lipid radicals continue to propagate the cascade, leading to the damage of macromolecules and to the cell death.

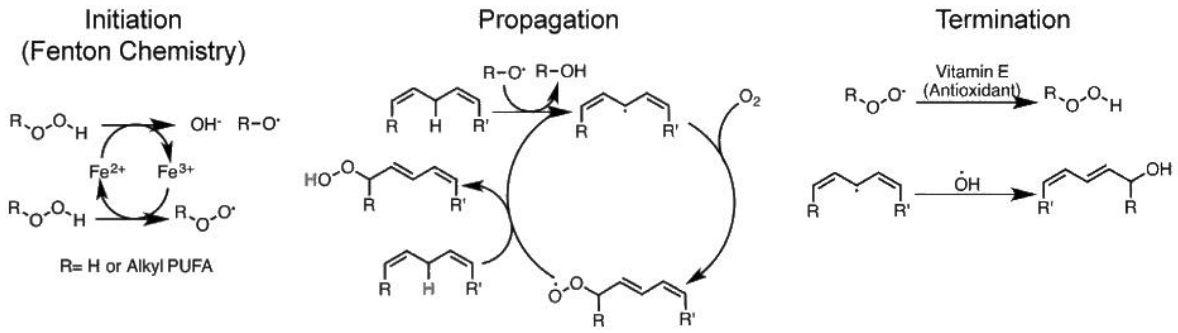


**Figure 1.5 – The three phases of non-enzymatic production of lipid peroxides.** First, the interaction of iron with hydrogen peroxide ($H_2O_2$) produces a reactive hydroxyl radical, which catalyzes the production of a lipid radical. Then, this organic radical can interact with molecular oxygen, producing a lipid-peroxyl radical that can further interact with another lipid molecule, producing a lipid radical while transforming itself in its corresponding lipid alcohol. This chain process can be terminated with the acquisition of an electron derived from another reactive radical or an antioxidant, typically vitamin E or other synthetic equivalents (Gaschler and Stockwell, 2017).

## *Synthesis of lipid peroxides by enzymatic catalysis*

The oxidized lipid can be also generated in a regulated manner with the involvement of enzymes which are part of three different families: cyclooxygenases (COXs), cytochrome P450s (CYPs) and lipoxygenases (LOXs). While the first two are involved in the production of biologically active signaling mediators (respectively, lipid endoperoxides and epoxyeicosatrienoic acids), lipoxygenases represent the major producers of lipid hydroperoxides, which are involved in ferroptotic cell death (Laneuville *et al.*, 1995; Gaschler and Stockwell, 2017). Using a nonheme ferrous ion in their catalytic center, LOXs are able to catalyze the conversion of PUFAs like arachidonic (AA) or linoleic acid (LA) into conjugated hydroperoxides (Latunde-Dada, 2017; Shintoku *et al.*, 2017).

Six different LOXs have been identified in the human body: 5-LOX, 12-LOX-1, 12-LOX-2, 15-LOX-1, 15-LOX-2, and the epithelial 3-LOX, and their names derive from the number of the carbon atom of the fatty chain on which the peroxidation occurs. While 3-LOX is essentially an isomerase designated to the interconversion of the various lipid peroxides, the most significant ones for ferroptosis-inducing lipid peroxides synthesis are 5-LOX, 12-LOX and 15-LOX. (Kagan *et al.*, 2017).

5-LOX mediates the production of free 5-hydroperoxyeicosatetraenoic acid (5-HPETE) which can be further converted in leukotriene $A_4$ ($LTA_4$) and various leukotrienes. When not active, it is localized in the nuclear matrix, but, upon the interaction with two $Ca^{2+}$ ions, it

translocates to the perinuclear zone, where it forms a complex with the cytosolic phospholipase $A_2$ ($cPLA_2$, responsible for the cleavage of AA from cell membranes) and with 5-lipoxygenase activating protein (FLAP, which facilitates the delivery of AA to 5-LOX). The complex then migrates on the cell membrane and catalyzes the peroxidation of arachidonic acid at carbon 5 (Chen and Funk, 2001; Kulkarni *et al.*, 2002; Gaschler and Stockwell, 2017).

12-LOX synthetizes 12-HPETE from AA and 9-hydroperoxyoctadecadienoic acid (9-HPODE) from LA. Unlike the 5-LOX complex, this protein can produce lipid peroxides directly from fatty acid chains that are still bound to membrane phospholipids and without requiring any activating protein (Shintoku *et al.*, 2017).

15-LOX is responsible of the production of 15-hydroxyeicosatetraenoic acid (15-HETE) from free AA and 13-hydroxyoctadecadienoic acid (13-HODE) from free LA (Wenzel *et al.*, 2017; Ye and Stockwell, 2017). Since this peroxide is the most produced in cells treated with ferroptosis inducers, 15-LOX is the most important lipoxygenases involved in ferroptosis. Moreover, 15-LOX overexpression accelerated the cell death rate caused by ferroptosis inducers, and both its chemical inhibition and siRNA-mediated knockdown reduced the cell death, more efficiently than 5-LOX or 12-LOX downregulation.

### *Fatty acid metabolism and ferroptosis*

As described in the previous paragraph, the main event in ferroptosis is the peroxidation of PUFAs contained in membrane phospholipids. Therefore, the amount of PUFAs inserted in cell membranes determines the sensitivity to ferroptosis, and so, the enzymes that catalyze the insertion of fatty acids in membrane phospholipids play a key role in this process. These enzymes are known as long-chain-fatty-acid-CoA ligases (ACSLs), and they catalyze the conjugation of fatty acids chains to coenzyme-A, which activates the fatty acids for their insertion in the cell membrane. In humans, five isoforms (ACSL1, ACSL3, ACSL4, ACSL5 and ACSL6) are present (Quan, Bode and Luo, 2021), and, among these, ACSL4 and ACSL3 have been strictly correlated to ferroptosis.

It has been reported that ACSL4 has a high specificity for the conversion of the polyunsaturated fatty acids arachidonic (AA) and adrenic acid (AdA) (Doll *et al.*, 2017). Coherently, ACSL4 knockdown caused the reduction of ferroptotic PE precursors (Kagan *et al.*, 2017), while its overexpression led to the induction of ferroptosis with the increase of 5-HETE production and of malonaldehyde (MDA) levels, the principal marker of lipid

peroxides production (Yuan *et al.*, 2016). Therefore, ACSL4 results to be a positive regulator of ferroptosis as well as a marker for ferroptosis sensitivity.

An opposite role has been postulated for ACSL3, which preferentially activates MUFAs for the insertion in the cell membrane. In turn, this incorporation essentially reduces the amount of PUFAs esterified in phospholipids, ultimately lowering the formation of the lipid peroxides. It has been reported that cells exposed to monounsaturated fatty acids (MUFAs) become resistant to ferroptosis inducers and that the absence of ACSL3 eliminated the ferroptosis-protecting effect of MUFAs (Magtanong *et al.*, 2019).

Recently, it has been described that the overexpression of SCD1, which catalyzes the first step in MUFAs synthesis, negatively regulates ferroptosis and protects from this type of cell death in ovarian (Tesfay *et al.*, 2019) and gastric cancer cells (Wang *et al.*, 2020); also, its expression in different tumor types has been associated with poorer prognosis, indicating SCD1 as a potential predictive marker (Sen, Coleman and Sen, 2023). Also, the chemical inhibition of FADS2 and FADS1 (involved in the production of arachidonic acid), has been observed to protect from RSL3-induced cell death and lipid peroxides accumulation in gastric cancer cells (Lee *et al.*, 2020).

## *The antioxidant mechanisms for ferroptosis suppression*

It is known that, in order to neutralize the reactive oxygen species and lipid peroxides produced by cellular stress conditions, cells developed some efficient antioxidant systems. Among them, the most important lipid peroxide protective enzyme is Glutathione Peroxidase 4 (GPX4), which depends on glutathione (GSH) as reducing agent. Of course, the amount of GSH is connected to the availability of glutamate, cysteine and glycine, the amino acids involved in its biosynthesis. Of these, cystine is transported into cytosol by system $X_c^-$, an antiporter channel that uses the intracellular gradient of glutamate to mediate the uptake of cystine, the thiol-condensed dimeric form of cysteine (Yang and Stockwell, 2016).

### *The system $X_c^-$*

Specifically, the system $X_c^-$ is a $Na^+$-independent amino acid transport complex localized in the cell membrane, and is composed of two subunits, SLC7A11 and SLC3A2, forming a disulfide-linked heterodimer. SLC7A11, also known as xCT, is a 55 kDa protein composed

of 501 residues, with 12 transmembrane domains that mediate the amino acid selectivity of the pore. SLC3A2, known also as 4F2hc, is a 68 kDa single-pass transmembrane regulatory protein composed of 630 residues and it can also interact with other SLC7A subunits, like SLC7A5, SLC7A6, SLCA7A7, SLC7A8, SLC7A10 for the transport of other amino acids (Mastroberardino *et al.*, 1998; Torrents *et al.*, 1998; Pineda *et al.*, 1999; Rossier *et al.*, 1999; Bröer *et al.*, 2001; Yanagida *et al.*, 2001; Yan *et al.*, 2019).

The main biological function of the system $X_c^-$ antiporter is to guarantee cellular cysteine supply, which is essential for the protein translation for glutathione synthesis, as represented in Figure 1.6 (Conrad and Sato, 2012).

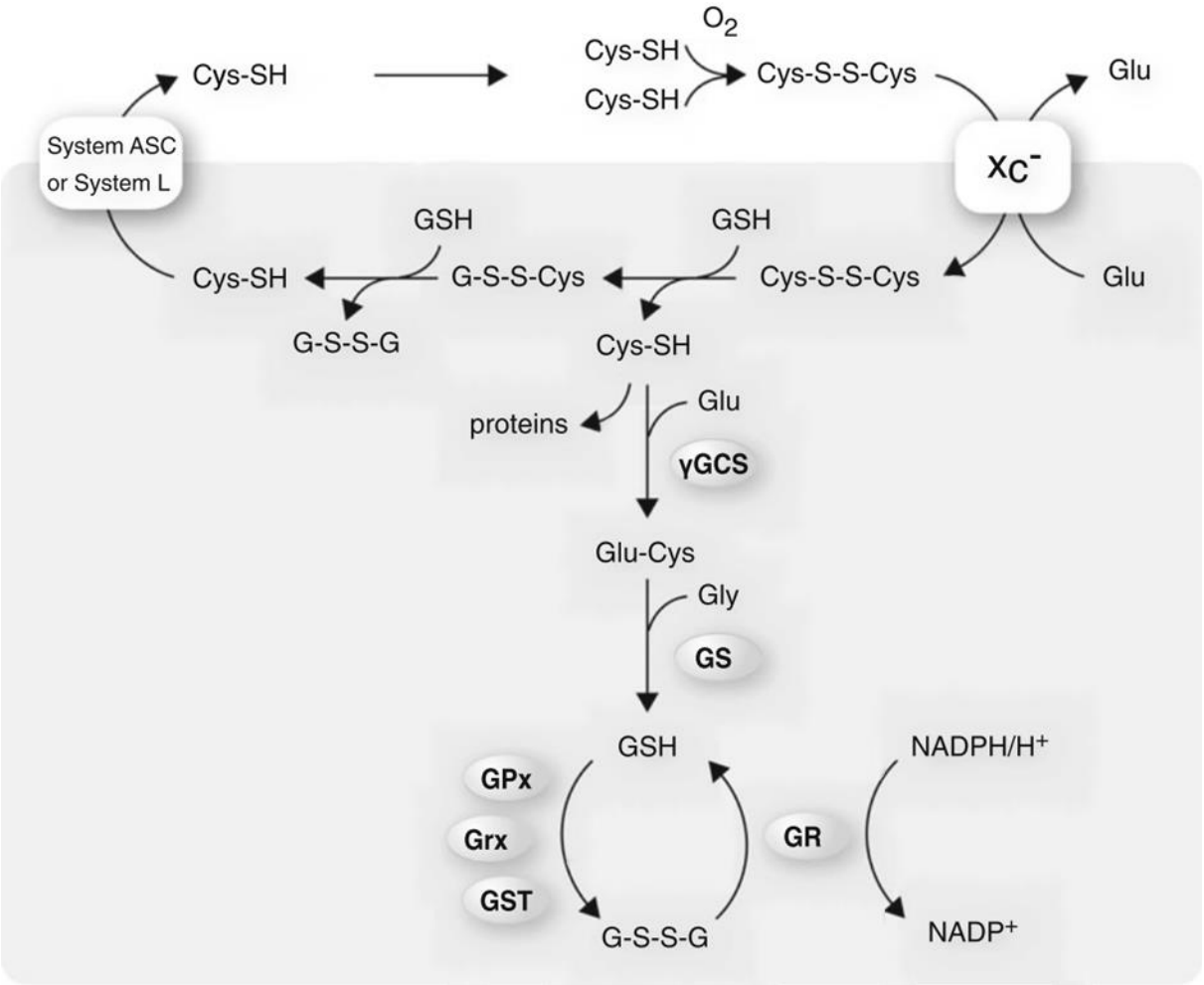


**Figure 1.6 – The cystine/cysteine cycle.** Cystine (Cys-S-S-Cys), internalized by the system $X_c^-$ with the extrusion of a glutamate (Glu) molecule, is made biologically available with the consecutive oxidation of two glutathione (GSH) molecule, liberating two free cysteine (Cys-SH) molecules. Cysteine can then be used for protein translation, glutathione synthesis or exported in the extracellular space, where, in oxidizing conditions, is converted to cystine or other cysteine-thiol conjugates. Then, cystine can be imported again in the cell, repeating the cycle (Conrad and Sato, 2012).

On the other hand, in case of system $X_c^-$ inhibition, the cells can ensure the proper levels of cysteine using the transsulfuration pathway (Figure 1.7). The transsulfuration pathway

mediates intracellular cysteine production with the conversion of methionine to homocysteine (through the loss of a methyl group). The sulfur atom is then passed to a molecule of serine by its condensation with homocysteine, and, finally, cysteine is produced by the enzyme cystathionine γ-lyase. The activation of this pathway has been observed to induce ferroptosis resistance in cells, conferring a protection towards various system $X_c^-$ inhibitors but not to GSH-depleting agents (Hayano *et al.*, 2016).

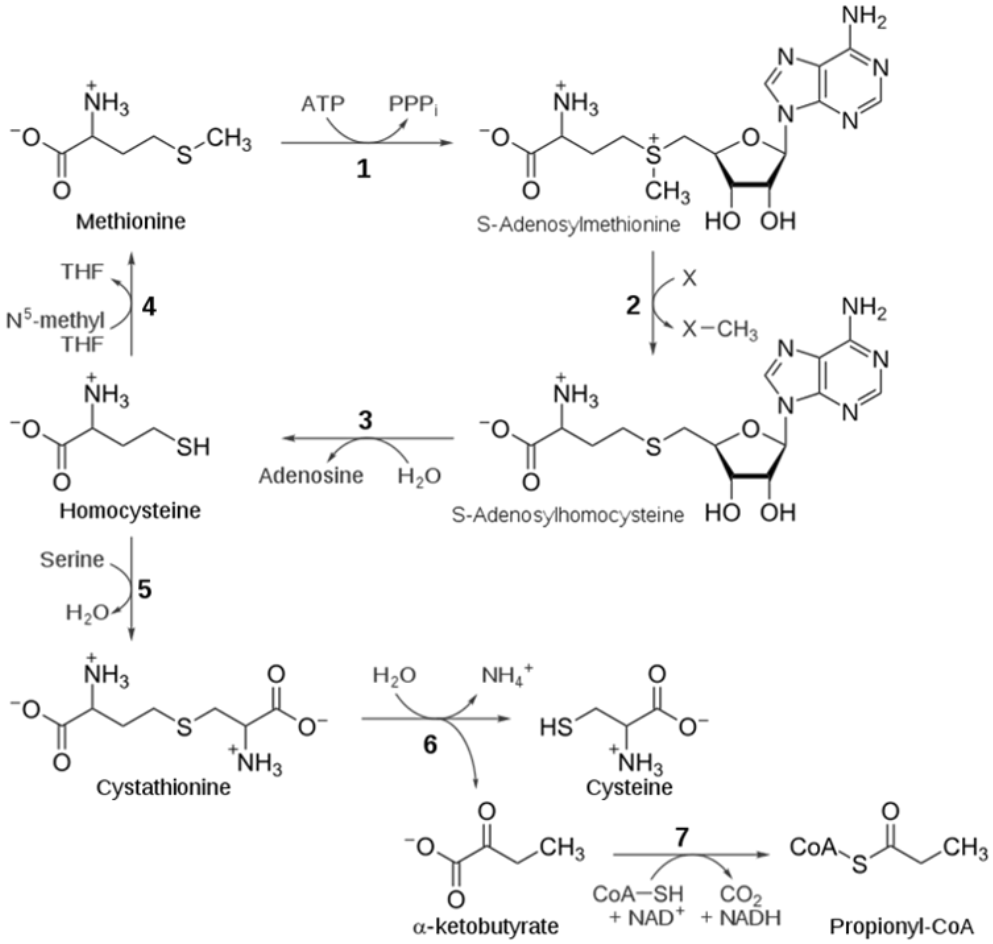


**Figure 1.7 – The transsulfuration pathway.** A molecule of methionine is ligated to adenosine, producing S-adenosylmethionine, which losses a methylene group to form S-adenosylhomocysteine. Adenosine is then removed leaving a homocysteine molecule, which is condensed with serine, producing cystathionine, which is further split into α-ketobutyrate and cysteine, thus providing an alternative pathway for cysteine supply in case of system $X_c^-$ inhibition. The activation of the transsulfuration pathway has been reported to induce ferroptosis resistance in cells (Hayano *et al.*, 2016).

## *Glutathione synthesis*

Glutathione is the most abundant antioxidant peptide among all lifeforms. Composed of the amino acids glutamate, cysteine and glycine and its synthesis occurs in sequential stages that require the hydrolysis of ATPs. First, the enzyme glutamate-cysteine ligase (GCL, also known as γ-glutamylcysteine synthetase, GCS) catalyzes the interaction of the γ-carboxyl group of glutamate with the amino group of cysteine, forming γ-glutamylcysteine, which is

then immediately added the amino acid glycine by glutathione synthetase (GS) with a classical peptide bond (Lu, 2013). This unusual **γ**-bond in glutathione protects it from intracellular peptidases, ensuring its bioavailability. Once oxidized, it forms a dimer with another oxidized glutathione molecule forming GSSG, in which the two glutathione monomers are covalently tied together with a thiol bond between the two sulfur atoms. GSSG is then reduced back to monomeric GSH by the NADPH-dependent glutathione reductase. Glutathione is produced in any cell type of the organism, while liver has been observed to act as an exporter of GSH for systemic oxidative stress reduction (Wu *et al.*, 2004).

Due to its small size, the GSH tripeptide can act as a cofactor for the regeneration of exhausted enzymes such as ribonucleotide reductase, function as a direct antioxidant molecule such as vitamin E, or as a cofactor for redox enzymes like glutathione peroxidase 4 (GPX4).

### *Glutathione peroxidase 4 (GPX4)*

Glutathione Peroxidase 4 (GPX4) is a 20-22 kDa monomeric protein and belongs to the glutathione peroxidase family. There are two GPX4 isoforms: the 23 kDa-mitochondrial isoform (which contains a leader sequence in the N-terminus that permits the translocation to mitochondria) and the 20 kDa-cytosolic isoform which can be localized in the endoplasmic reticulum, in the cytoplasm and in the nucleus (Arai *et al.*, 1999; Imai and Nakagawa, 2003).

GPX4 is the only enzyme that can reduce lipid hydroperoxides to their corresponding alcohols using a selenocysteine in its catalytic site (Brigelius-Flohé and Maiorino, 2013). Selenocysteine is structurally analogous to cysteine but with a selenium atom substituting the canonical sulfur one, which gives the residue a high polarizability that results in a highly increased redox potential compared to cysteine (Mousa, Notis Dardashti and Metanis, 2017). Thus, the interaction of GPX4 with lipid hydroperoxides produces the corresponding lipid alcohol, causing the selenium atom to be oxidized by binding a OH group, making the enzyme exhausted. The interaction with glutathione leads then to the loss of the hydroxyl group by the selenium atom, the production of a GSSG dimer and the release of a water molecule (Green, 2018).

The unique function of GPX4 cannot be replaced by other enzymes, and this is demonstrated by the fact that total GPX4$^{-/-}$ phenotype in mice is embryonically lethal due

to the lack of the protective system against lipid peroxidation (Yant *et al.*, 2003). Thus, GPX4 depletion leads to the increase of lipid peroxidation with the accumulation of oxidized PUFAs, causing cell death by ferroptosis (Friedmann Angeli *et al.*, 2014).

### *The $CoQ_{10}$/FSP1 axis*

Recently, it has been reported that ubiquinol (the reduced form of $CoQ_{10}$) protects cells from lipid peroxidation and inhibits ferroptotic cell death independently from the well-known glutathione/GPX4 axis (Stockwell, Jiang and Gu, 2020).

In particular, Ferroptosis Suppressor Protein 1 (FSP1, previously named AIFM2) has the capacity to block lipid peroxidation by regenerating $CoQ_{10}$ from ubiquinol, suppressing ferroptosis without the requirement of GSH or GPX4. Indeed, $CoQ_{10}$ has been postulated to act as a natural antioxidant in lipid membranes, thus scavenging eventual reactive molecules such as lipid peroxides, analogously to vitamin E (Bersuker *et al.*, 2019; Doll *et al.*, 2019). Also, due to similar structural properties, vitamin K has been recently found to inhibit the ferroptotic peroxidation of cell membranes acting as a radical trapping agent, with the regeneration of its reduced form being mediated by FSP1 (Mishima *et al.*, 2022).

Moreover, GTP cyclohydrolase-1 (GCH1) is the enzyme involved in the synthesis of tetrahydrobiopterin ($BH_4$), a metabolite that can both act as a radical trapping agent itself and contribute to the formation of the reduced $CoQ_{10}$, finally arresting lipid peroxidation. Indeed, the expression of this gene has been seen to protect from ferroptosis both in *in vitro* established tumor models and in patient-derived cell lines (Kraft *et al.*, 2020; Zheng and Conrad, 2020).

Figure 1.8 shows the interactions between the three antioxidant pathways for the suppression of ferroptosis.

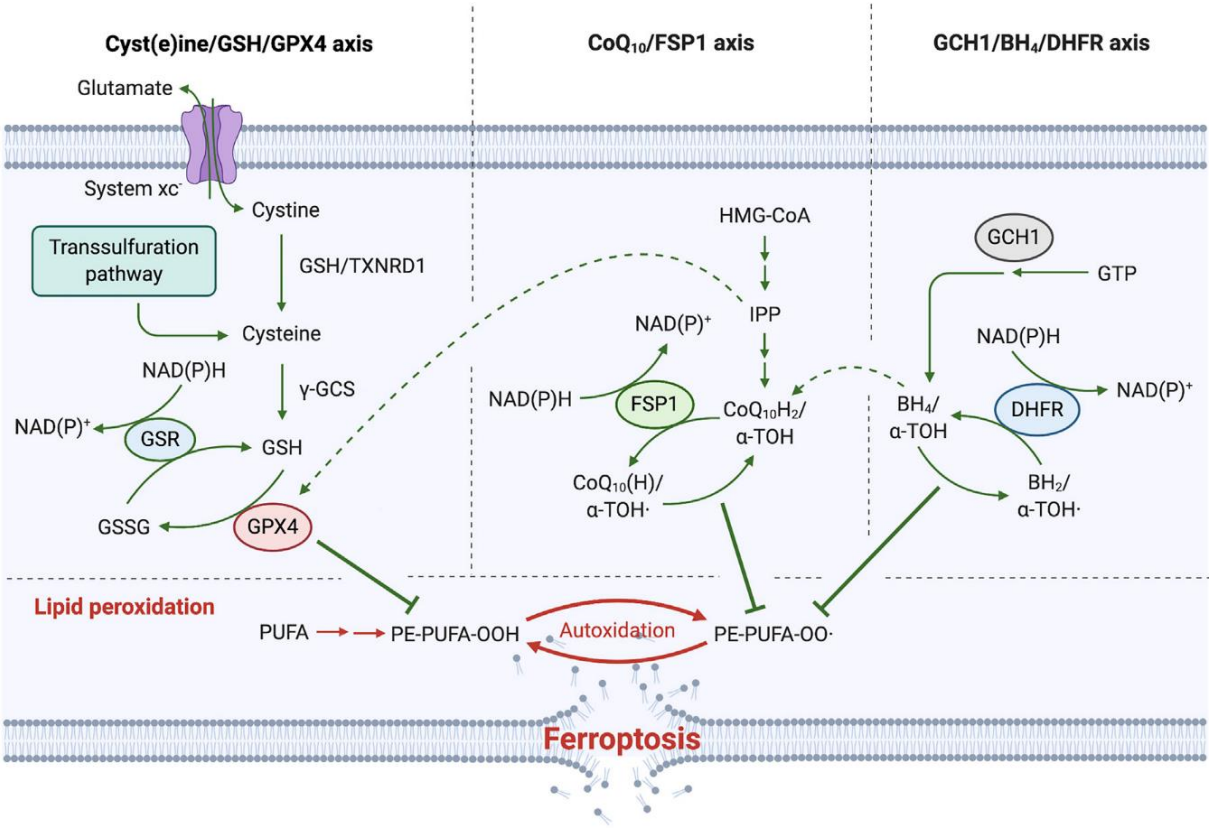


**Figure 1.8 – The antioxidant machineries involved in ferroptosis suppression.** The enzymatic neutralization of membrane lipid peroxides to their non-toxic lipid alcohol form is mediated by the enzyme Glutathione Peroxidase 4 (GPX4), which uses the antioxidant peptide glutathione (GSH) as a cofactor. GSH synthesis requires the amino acid cysteine, which is either imported in the cell by the antiporter System $X_c^-$ or derived from the transsulfuration pathway. Alternatively, the antioxidant molecules Coenzyme $Q_{10}$ ($CoQ_{10}$) and tetrahydrobiopterin ($BH_4$) can act as radical-trapping agents by non-enzymatically neutralizing lipid peroxides. Notably, interconnections exists between these three pathways because isopentenyl pyrophosphate (IPP) is involved in the production of the selenoenzyme GPX4, and $BH_4$ can contribute to the synthesis of $CoQ_{10}$ (modified from Zheng and Conrad, 2020).

## *Inducers and inhibitors of ferroptosis*

Since it is difficult to technically define its specific nature, ferroptosis has been mainly studied using chemical agents that could induce this type of cell death, known as ferroptosis inducers (or FINs), or by molecules that can prevent/inhibit it, known as ferroptosis inhibitors.

### *Ferroptosis inducers*

Based on the mechanism of action, ferroptosis-inducing molecules can be divided into three main categories, namely, system $X_c^-$ inhibitors, also known as class I FINs (which indirectly inactivate GPX4 by inducing GSH depletion), GPX4 inhibitors, also named class II and III FINs (which selectively inhibit GPX4) and class IV FINs (which induce non-canonical ferroptosis by increasing the LIP) (Hassannia, Vandenabeele and Vanden Berghe, 2019;

Stockwell and Jiang, 2020). Moreover, other pharmacological agents such as cisplatin and paracetamol have been linked to ferroptosis promotion, since their mechanism of action seems to be correlated to the increase of oxidative stress (Guo *et al.*, 2018; Gai *et al.*, 2020).

### System $X_c^-$ inhibitors (Class I FINs)

Class I FINs primarily interfere with the system $X_c^-$ antiporter, which is the main cellular mechanism of cysteine supply, essential for GSH synthesis. These molecules lead to GSH depletion with the indirect inactivation of GPX4 and the accumulation of the lethal lipid peroxides (Sato *et al.*, 2005; Su *et al.*, 2020). The most relevant class I FINs are erastin, piperazine erastin, imidazole ketone erastin (IKE), sorafenib, sulfasalazine (SAS), buthionine sulfoximine (BSO), and glutamate.

Erastin was discovered in 2003 during a high throughput screening of molecules which could induce selective death in cells harboring mutations in the RAS family (KRAS, HRAS, BRAF, NRAS). The first ultrastructural analyses on erastin-treated cells revealed mitochondrial shrinkage and vanishing of the cristae, which led to the discovery that this novel molecule targets two of the three mitochondrial voltage-dependent anionic channels, VDAC2 and VDAC3 (Yagoda *et al.*, 2007). Further studies revealed that the two channels are only secondary targets, and that the principal one is the system $X_c^-$, (Dixon *et al.*, 2012; Y. Zhao *et al.*, 2020).

To improve the *in vivo* bioavailability of erastin and to increase its metabolic stability, piperazine erastin and imidazole ketone erastin have been developed, resulting in, respectively, higher water solubility and stronger efficacy (Yang *et al.*, 2014; Zhang *et al.*, 2019).

Sorafenib is a multikinase inhibitor targeting receptor tyrosine kinases involved in growth signaling and angiogenesis such as VEGFRs and PDGFR and serine/threonine kinases involved in the MAPK cascade. Currently, it is the only FDA- and EMA-approved drug for the treatment of unresectable hepatocellular carcinoma (HCC), and is also used for advanced renal cell carcinoma (RCC) and recurrent thyroid carcinoma refractory to radioactive iodine treatment (Bronte *et al.*, 2017; Keating, 2017). In addition, recently it has been found that it also inhibits system $X_c^-$, with a mechanism of action that seems related to that of erastin, even though it is not completely clarified (Lachaier *et al.*, 2014).

Sulfasalazine (SAS) is an FDA- and EMA-approved anti-inflammatory drug used in the treatment of rheumatic polyarthritis and chronic ulcerative colitis. More recently, beyond the ROS scavenging ability and the apoptotic effect on inflammatory cells, sulfasalazine has been demonstrated to interfere with SLC7A11 (Sehm, Fan, *et al.*, 2016).

Buthionine sulfoximine (BSO) is a potent and specific inhibitor of the enzyme γ-glutamylcysteine synthase (GCL), which, preventing the production of γ-glutamylcysteine, causes glutathione depletion (Griffith, 1982; Yang *et al.*, 2014). BSO is less effective than erastin, showing 60% cell death with 10 μM erastin, and only 20% with BSO 1 mM in a human retinal pigment epithelial cell line (Sun *et al.*, 2018). Therefore, even though BSO reached phase I clinical trials with a good tolerability in patients, to date the addition of BSO to standard chemotherapy routines lacks of a strong clinical rationale (Dixon and Stockwell, 2019).

Glutamate can be considered as a class I FIN since, when present in high concentrations in the extracellular space, it can inhibit its export by system $X_c^-$, indirectly impairing cystine import and the redox cycle, lowering cysteine levels. However, this strategy is not applicable clinically because glutamate is the main excitatory neurotransmitter of the central nervous system, where high glutamate concentrations in the extracellular space induce continuous activation of glutamatergic receptors, causing neuronal cell death by excitotoxicity (Bridges, Natale and Patel, 2012).

### GPX4 inhibitors (class II and class III FINs)

These two classes of ferroptosis inducers can be discussed together because their final target is the inhibition of GPX4 activity, causing, respectively, its inactivation or its depletion.

Among the class II FINs, there are RSL3 (the chemical compound mainly used to study ferroptosis) and other molecules such as ML210, DPI compounds, altretamine, JKE-1674, NSC144988 and withaferin A.

RSL3 (which stands for "RAS-selective lethal 3"), similarly as erastin, was discovered during a screening of RAS-targeting molecules (Yang and Stockwell, 2008). Further studies elucidated that it causes lipid peroxide production without alterations of intracellular GSH pool. The explanation relies in the chloroacetamide moiety of this molecule, which can irreversibly bind to the selenocysteine in the active site of GPX4, which first interacts with the reduced form of the adaptor protein 14-3-3ε, inhibiting its activity and rapidly inducing

the accumulation of lipid peroxides and cell death (Yang *et al.*, 2014). Different published papers showed that *in vitro* treatment with RSL3 reduced GPX4 activity in different cancer cells and, interestingly, increased the levels of free cytoplasmic iron (Sui *et al.*, 2018); therefore, the increase of intracellular iron seems to be correlated with ferroptosis induction. Like erastin, RSL3 is characterized by poor solubility and biodistribution *in vivo*, which limits its use mainly in cellular models. However, some experiments in animal models have been conducted, revealing that RSL3 can either significantly inhibit the growth of tumors derived from HT-1080 cells and reduce a pre-existing cancerous mass (Yang *et al.*, 2014). Also, the combination of RSL3 and iron dextran were efficient in reducing the *in vivo* growth of HepG2 cells, suggesting a new promising antitumor strategy (Asperti et al., 2021).

Finally, FIN56 is a class III ferroptosis inducer. Although its mechanism of action has not been completely elucidated, it has been observed to induce GPX4 degradation via the autophagic machinery (Sun et al., 2021). Moreover, FIN56 could bind and activate squalene synthase (SQS, which is involved in cholesterol synthesis), thereby causing the depletion of some metabolites such as coenzyme $Q_{10}$, leading to oxidative stress and favoring the production of lipid peroxides (Shimada et al., 2016).

### Class IV FINs

Iron has a fundamental role in ferroptotic cell death since LIP (in the form of $Fe^{2+}$) is involved in the Fenton reaction and can sustain and propagate lipid peroxidation. Non-canonical ferroptosis is the phenomenon initiated by the increase of free intracellular iron levels that does not involve the GSH/GPX4 system. Indeed, even if the mechanism of action is still not properly defined, it has been demonstrated that loading cells with different sources of iron (such as iron chloride, hemoglobin, hemin, ferrous ammonium sulfate or ferric ammonium citrate) induces ferroptotic cell death (Li *et al.*, 2017; Fang *et al.*, 2018; Hassannia *et al.*, 2018; Imoto *et al.*, 2018). These different iron-containing molecules, causing iron overload, are therefore classified as class IV FINs (Hassannia, Vandenabeele and Vanden Berghe, 2019).

Also, salinomycin, an inhibitor of both the Wnt pathway and autophagy, has recently been demonstrated to induce ferroptosis. Directly interacting with iron in the lysosomes, salinomycin has been observed to prevent the release of iron into the cytosol. This causes further degradation of ferritin as a compensatory mechanism, resulting in iron release and

in the consequent increase of lipid peroxidation, and finally leading to ferroptotic cell death (Mai *et al.*, 2017).

To date, no specific marker for the assessment of ferroptotic cell death has been identified yet. Thus, the mostly used strategy to confirm that a specific molecule causes ferroptosis is the use of specific ferroptosis inhibitors, which are compounds that can counteract the progressive accumulation of membrane-bound lipid peroxides.

### *Ferroptosis inhibitors*

The two categories of molecules with the property to inhibit ferroptosis are radical trapping agents (RTAs) and iron chelators. Among RTAs, that act by blocking the lipid peroxidation process, are ferrostatins (the most potent, classified as first, second and third generation, with increasing efficacy), followed by, liproxstatin-1, phenoxazine and the less potent BHT and α-tocopherol (Dixon *et al.*, 2012; Friedmann Angeli *et al.*, 2014; Shah, Margison and Pratt, 2017). Iron chelators such as deferoxamine and deferiprone have also been reported to inhibit or mitigate ferroptosis by sequestering excess free reactive iron in the cytoplasm, thus blocking the non-enzymatic production of lipid peroxides (Yang and Stockwell, 2008; Bystrom and Rivella, 2015).

Figure 1.9 summarizes the main mechanisms of ferroptosis and its chemical modulation by inhibitors and inducers.

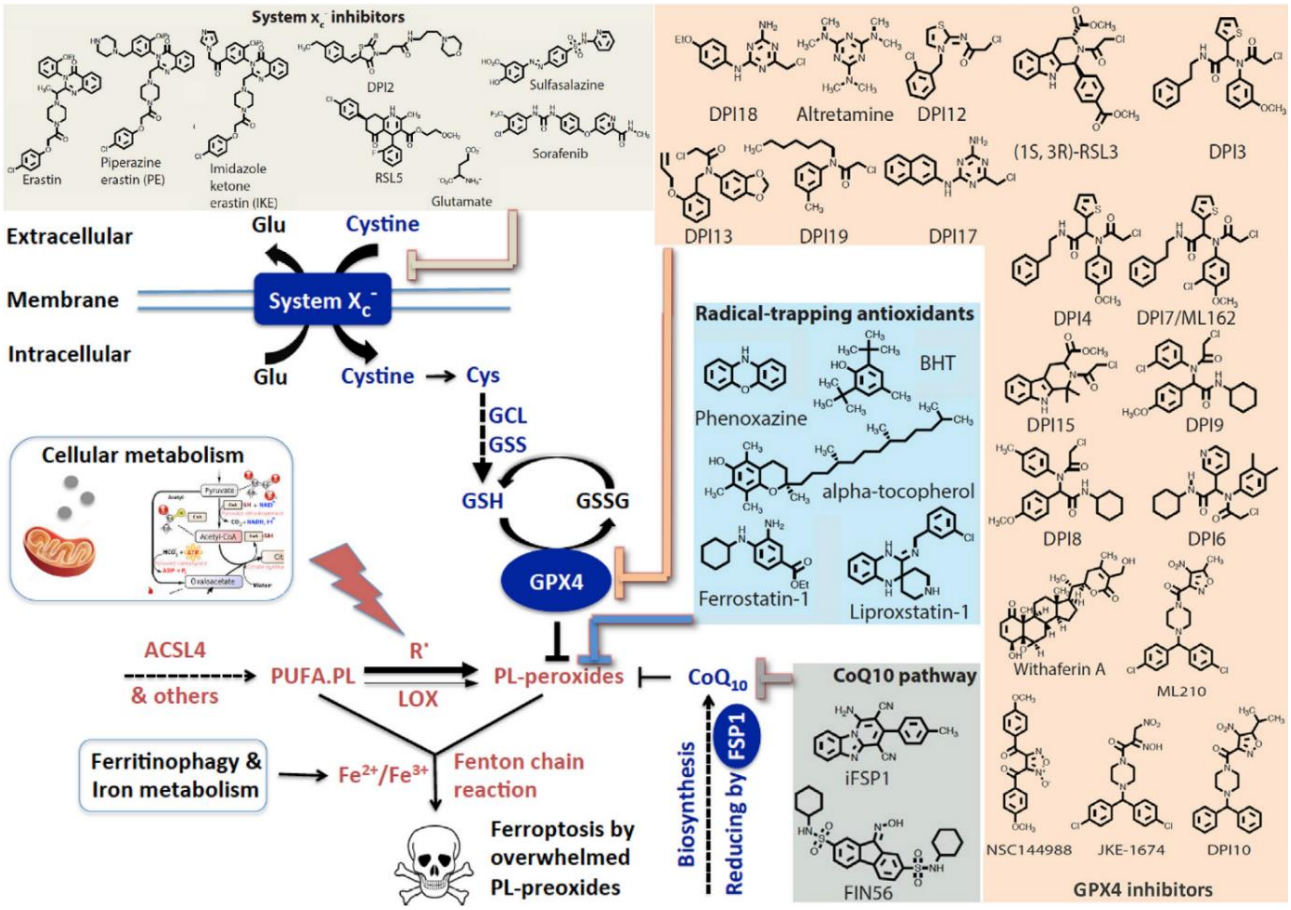


**Figure 1.9 – Schematic representation of ferroptosis pathway with its chemical inducers and inhibitors.** Ferroptosis inducers (FINs) can be divided into three categories. First, there are system Xc- inhibitors (also known as class I FINs), represented by erastin (and its derivatives, piperazine erastin and imidazole ketone erastin), sorafenib, sulfasalazine and RSL5, capable of reducing cystine and cysteine intracellular levels. Inhibitors of GPX4 (catalogued as class II and class III FINs, respectively direct and indirect inhibitors of GPX4) comprise RSL3, FIN56, ML210, DPI compounds, altretamine, JKE-1674, NSC144988 and withaferin A, causing the failure of the antioxidant system even in presence of GSH. Class IV FINs (such as ferric ammonium citrate, ferrous ammonium sulfate, hemoglobin, hemin, or iron chloride) can increase cellular iron levels, promoting lipid peroxidation and ferroptosis. Ferroptosis inhibitors, instead, can be divided into radical-trapping antioxidants (like ferrostatin-1, liproxstatin-1, phenoxazine, BHT and α-tocopherol), which scavenge reactive molecules such as ROS and lipid peroxides, and iron chelators (such as deferoxamine and deferiprone), which reduce the labile iron pool, thus preventing non-enzymatic lipid peroxidation. (Stockwell and Jiang, 2020).

## *Ferroptosis in cancer*

As mentioned in the previous paragraphs, ferroptosis is driven by iron accumulation, lipid peroxidation of cell membranes and the failure of the various antioxidant systems essential to neutralize lipid peroxides. Thus, cells with a basal high oxidative stress and high iron levels could be more sensitive to ferroptosis. In this context, these conditions can be frequently observed in tumor cells, where unbalanced redox status renders cancer cells highly susceptible to oxidative damage, iron toxicity and lipid peroxidation, conditions that can be exploited to pharmacologically induce ferroptosis. Moreover, since cancer cells frequently

develop resistance to therapies, the induction of ferroptosis could be a valid tool for the treatment of tumors.

A frequent feature of many cancer cells is the overexpression of xCT, suggesting a higher dependence on the system $X_c^-$ for cysteine supply and glutathione synthesis, essential for GPX4 activity. Thus, system $X_c^-$ inhibitors could represent a targeted cancer therapy. On the other hand, it is important to mention that many cancer cells rely on an alternative mechanism, the transsulfuration pathway, to synthesize cysteine from methionine when system $X_c^-$ is inhibited. This should be taken into account, since these cancer cells could be resistant to class I FINs but could still undergo ferroptosis using other inducers (Hirschhorn and Stockwell, 2019).

Tumors also have an increased activity of the enzymes involved in the synthesis, storage, and utilization of PUFAs, essential to synthetize membranes during cell proliferation. Since PUFAs are the main targets for lipid peroxidation, tumor cells have a high need of functional GPX4 for their survival to ensure protection against the accumulation of detrimental lipid peroxides (Xu *et al*., 2019). Thus, the inhibition of GPX4 could be a golden target to induce ferroptosis in these cancer cells.

Finally, tumor cells are characterized by high iron demand, to support their growth and metabolic functions, thus the increased amount of free cytoplasmic iron promotes lipid peroxides formation through Fenton chemistry, rendering tumor cells more sensitive to ferroptosis.

All these observations likely support the use of ferroptosis inducers in the treatment of aggressive cancers. Several compounds targeting ferroptosis have been widely tested *in vitro*, acting with three principal strategies: to target system $X_c^-$ (i.e., erastin, piperazine erastin or imidazole ketone erastin), to inhibit GPX4 activity (e.g., RSL3), and by the inhibition of GCL, with consequent lack of GSH (i.e., BSO).

Surprisingly, after a drug screening of various compounds already used clinically as anti-tumor agents, and thus FDA-approved, some of them were found able to promote ferroptotic cell death.

For example, sorafenib, a multikinase inhibitor used in the treatment of hepatocellular carcinoma and advanced renal cellular carcinoma, has been observed to increase the

amount of lipid peroxides in human HCC cell lines, inducing a caspase-independent type of cell death that could be reverted by the use of both the iron chelator DFX and of ferrostatin-1 (Louandre *et al.*, 2013). Also, likewise erastin, sorafenib has been demonstrated to reduce the release of glutamate of the human fibrosarcoma cell line HT1080, causing cytotoxic effects that can be prevented by antioxidant molecules. Besides, being a multikinase inhibitor, sorafenib has been hypothesized to cause, among the others types of cell death, ferroptosis by the inhibition of a still unknown kinase that is necessary for system $X_c^-$ activity (Dixon *et al.*, 2014).

Sulfasalazine, used as therapeutic agent against rheumatoid arthritis and inflammatory bowel diseases, was found to reduce the release of glutamate from both the fibrosarcoma cell line HT1080 and the prostate cancer cell line DU-145 (Dixon *et al.*, 2014); moreover, endoplasmic reticulum stress was observed after SAS exposure in the glioma cell line U251, causing a reduction of cell viability that could be rescued by the iron chelator DFO and by ferrostatin-1 (Sehm, Fan, *et al.*, 2016).

Recently, altretamine, an antineoplastic compound used to treat ovarian cancer and whose target has for long remained unknown, has been linked to ferroptosis, as whole lysates of altretamine-treated human B cell lymphoma lines were found to contain a significant amount of lipid peroxides. Since GPX4 is the only lipid peroxide-neutralizing enzyme, altretamine has been rediscovered as a "novel" GPX4 inhibitor (Woo *et al.*, 2015).

Another example of ferroptosis induction is the treatment with cisplatin, which lowers both glutathione and glutathione reductase levels while increasing both glutathione peroxidase and malondialdehyde levels in hepatic homogenates of Wistar rats (Pratibha *et al.*, 2006). Confirming these results, it has been observed that, in A549 and HCT116 cells, cisplatin-induced cytotoxicity could be partially reverted by the combined use of deferoxamine, ferrostatin-1 and the apoptosis inhibitor Z-VAD-FMK, indicating that, in addition to apoptosis, ferroptosis also contributes to the cytotoxic effect of cisplatin (Guo *et al.*, 2018).

# 2- Aims of the work

Cancer cells are often characterized by an increase of intracellular labile iron pool due to the upregulation of TfR1 (increasing iron uptake) and the downregulation of both FPN and ferritin (decreasing iron efflux and iron storage, respectively) (Torti *et al.*, 2018).

This mechanism is essential to sustain the accelerated metabolism of cancer cells. however, due to the double nature of iron, essential and toxic at the same time, targeting its homeostasis is a promising approach to prevent or slow down tumor growth (Torti and Torti, 2020).

The aim of this PhD work was to study, in glioblastoma and rhabdomyosarcoma tumors, the effect of iron alteration, taking into consideration both its toxicity, whereby iron excess likely promotes ferroptosis, and its requirement for tumor growth, whereby iron chelation could interfere with tumor cell survival.

Ferroptosis is a new type of cell death triggered by the increase of intracellular iron levels and by the failure of the cellular lipid peroxide-neutralizing systems. These two alterations ultimately cause the harmful peroxidation of membrane-bound polyunsaturated fatty acids, leading to membrane permeabilization, damage of macromolecules and cell death (Stockwell, 2022). Considering their high intracellular iron and their high oxidative stress, tumor cells seem to be more sensitive toward this type of cell death, compared to the normal ones. This means that exploiting the ferroptosis process, using ferroptosis inducers, could be a promising antitumor strategy (Z. Ye *et al.*, 2020). In fact, many papers have been published in these years, focusing on the study of ferroptosis induction in different tumors with varying results due to both the peculiarities of each tumor. The reasons for this are not yet exhaustive, hence knowledge and research of this tumor-specific features and metabolism are vital and desired.

On the other hand, depleting iron in tumor cells deprives them of an essential metal for the many iron-dependent enzymes involved in DNA replication, electron transport chain, etc., impacting on tumor metabolism (Ibrahim and O'Sullivan, 2020). In this context, the antitumor effects of iron chelators (such as deferoxamine and deferiprone) have been profoundly investigated in different cancer types, where they efficiently blocked tumor growth in both *in vitro* and *in vivo* experiments, giving promising results also in clinical trials

(Brown *et al.*, 2020; Abdelaal and Veuger, 2021). Therefore, taking advantage of the dysregulation of iron metabolism in cancer, both by promoting iron-dependent lipid peroxidation or by depriving tumor cells of this essential micronutrient has been demonstrated as a valid strategy for overcoming tumor growth.

The research studies focused, in two parts, on two different types of tumors, glioblastoma and rhabdomyosarcoma, which are not well studied regarding iron metabolism and for their susceptibility to iron excess or deprivation.

**Glioblastoma** (GBM) is the most frequent tumor of the central nervous system, and, nowadays, despite various antitumor strategies have been exploited, none of these can be considered curative, only increasing the survival of patients by few months (Khasraw *et al.*, 2022; Ostrom *et al.*, 2022). This is caused by a very frequent tumor recurrence, which relies on the persistence of a treatment-resistant staminal component of the tumor, also called glioblastoma cancer stem cells (GBM-CSCs) (Xie *et al.*, 2022). Thus, new therapeutic approaches are needed to improve the currently used strategies, and one of them could be ferroptosis induction.

Therefore, the aims of this part of the project were to characterize iron metabolism in GBM-CSC lines, which has been not investigated yet, and, mainly, to study the effects of ferroptosis-inducing agents in these tumor cell lines. In detail, the purposes were:

- To characterize the primary GBM-CSC lines used in this study for the expression of ferroptosis- and iron metabolism-related genes.
- To verify if the ferroptosis inducers erastin (which blocks the import of cystine, thereby impairing the production of the antioxidant peptide glutathione), RSL3 and ML162 (both inhibitors of the lipid peroxide-neutralizing enzyme GPX4) could reduce the viability of GBM-CSC lines.
- To confirm whether FINs could effectively induce ferroptosis in GBM-CSC lines, by co-treating cells with both ferroptosis inducers and ferroptosis inhibitors and successively assessing both cell viability and lipid ROS accumulation.
- To test if a treatment with ferroptosis inducers could sensitize GBM-CSC lines to the effects of temozolomide, the chemotherapeutic agent currently approved for GBM treatment, and to which GBM-CSCs have been reported to have reduced sensitivity.

**Rhabdomyosarcoma** (RMS) is the most frequent soft tissue sarcoma in children, developed from undifferentiated myocytes (Skapek *et al.*, 2019). It is a rare disease, and, despite the multimodal treatment schedule involves both surgery, chemo- and radiotherapy, tumor recurrence frequently develops in patients, along with therapy resistance and metastatic dissemination (Miwa *et al.*, 2020).

Our previous study demonstrated that rhabdomyosarcoma cells are sensitive to the deprivation of iron, making iron chelators interesting compounds to counteract RMS growth (Asperti *et al.*, 2023). Didox (3,4-dihydroxybenzohydroxamic acid) seems to be a very interesting compound and the reason is not only for its property to chelate iron (Fritzer-Szekeres *et al.*, 1997; Asperti *et al.*, 2019), but also for its great inhibitory activity on RRM2 function (Elford, Wampler and Riet, 1979).

RRM2 is one of the regulatory subunits of ribonucleotide reductase, and is responsible for the rapid *de novo* synthesis of deoxyribonucleotides and it is involved, consequently, in the duplication of the genome during cell division (Chabes and Thelander, 2000). Interestingly RRM2 is one of the 50 most overexpressed proteins in cancer, promoting tumor proliferation and invasiveness and concomitantly reducing patient prognosis (Hsu et al., 2011; Wang et al., 2021; Das, Jain and Mallick, 2022; Li et al., 2022). Since iron is an essential cofactor for RRM2 activity, didox, as both an iron chelator and an inhibitor of RRM2 activity, could be a promising approach for the treatment and management of rhabdomyosarcoma, a cancer type that shows high sensitivity to iron chelation and a high proliferative rate.

Therefore, the second part of this PhD project aimed to study the effects of didox on two RMS cell lines, RD and RH30, representative of the embryonal and alveolar subtype respectively, analyzing cell viability and aggressiveness markers such as motility and clonogenicity, as well as the expression of the main iron-related proteins, both *in vitro* and *in vivo*.

Also, working with rhabdomyosarcoma cell lines in collaboration with Prof. Alessandro Fanzani's group at the University of Brescia, we observed sensitivity to ferroptosis inducers in RD cells, and, in particular, in caveolin-1-overexpressing RD cells.

Caveolin-1 (Cav-1) is one of the proteins often overexpress in RMS. It is involved in the formation of caveolae in the membrane and has also been demonstrated to regulate several signaling pathways in RMS cell lines (Rossi, Poliani, Cominelli, *et al.*, 2011; Ketteler and Klein,

2018). Interestingly, its overexpression in RMS has been linked to increased tumor aggressiveness, metastatic behavior, and, as mentioned before, to high susceptibility to ferroptosis (Codenotti *et al.*, 2018, 2019).

Given the promising link between high expression of Cav-1 in RMS and high sensitivity toward ferroptosis, the study sought to analyze the expression of ferroptosis-related proteins in Cav-1-overexpressing cells. In addition, ACSL4 activity has been observed to increase the sensitivity to ferroptosis inducers in different *in vitro* models (Doll *et al.*, 2017; Magtanong *et al.*, 2022). This ligase is responsible for the activation of polyunsaturated fatty acids (PUFAs), supporting their insertion in cell membranes (Soupene and Kuypers, 2008; Quan, Bode and Luo, 2021). Thus, starting from these interesting connections, this study aimed to assess if increased expression of ACSL4 in Cav-1-overexpressing cells was involved in their higher sensitivity to ferroptosis inducers studying a possible link between Cav-1 and ACSL4.

Specifically, the aims of the second part of this PhD project were:

- To characterize the Cav-1-overexpressing RD cells versus RD cells in terms of expression of genes and proteins related to lipid metabolism and antioxidant enzymes that are directly associated with ferroptosis.
- To investigate if ACSL4 inhibition could reduce the sensitivity to ferroptosis inducers in Cav-1-overexpressing RD cells by inhibiting ACSL4-mediated PUFA activation with pan-ACSL inhibitor triacsin C and the ACSL4 specific RNA silencing.
- To investigate if a pre-treatment with monounsaturated or polyunsaturated fatty acids could modulate the sensitivity of Cav-1-overexpressing RD cells to the ferroptosis inducer RSL3.

# 3- Glioblastoma and ferroptosis

# Introduction

## *Clinical features*

Glioblastoma (GBM) represents the most common malignant tumor of the central nervous system (CNS) that accounts for the 14.2% of all CNS tumors and 50.1% of all CNS malignant tumors diagnosed in the United States. Glioblastoma more frequently occurs in adults than in children, with a global incidence of 3.26 cases per 100,000 population (Ostrom *et al.*, 2022).

GBMs are extremely aggressive and infiltrative, invasive with elevated risk of tumor recurrence in the CNS. This causes the prognosis of glioblastoma patients to be very poor with median survival of newly diagnosed patients of 12-15 months and with only 6.9% of the patients surviving 5 years after diagnosis (Khasraw *et al.*, 2022; Ostrom *et al.*, 2022; Thakur *et al.*, 2022).

## *Classification and molecular alterations*

According to the fifth edition of the World Health Organization classification of CNS tumors, glioblastomas belong to the group of "adult-type diffuse gliomas", and are referred to as "glioblastoma, IDH-wildtype". The mutational status of either the *IDH1* or *IDH2* genes, which encode the isoform 1 and 2 of the enzyme isocitrate dehydrogenase, respectively discriminate between GBM, which are wildtype, and "astrocytoma, *IDH*-mutant" or "oligodendroglioma, *IDH*-mutant and 1p/19q-codeleted", the latter harboring a deletion of both chromosomal arms 1p and 19q (Louis *et al.*, 2021).

The mutation status of the *IDH1* and *IDH2* genes has also a prognostic value in which multiple studies indicate that *IDH*-mutant gliomas have significantly better prognosis than *IDH*-wildtype ones (Ichimura *et al.*, 2009; SongTao *et al.*, 2012; Sun *et al.*, 2013; Yang *et al.*, 2015).

The second genetic alteration used in the diagnostic is the loss of both chromosomal arms 1p and 19q, specific of oligodendrogliomas, which represent the less aggressive type of this class of tumors. Indeed, various studies confirmed that gliomas harboring 1p/19q codeletion are characterized by reduced aggressiveness and increased responsiveness to therapies (Cairncross *et al.*, 2014; Cancer Genome Atlas Research Network *et al.*, 2015; Eckel-Passow *et al.*, 2015).

| WHO Classification of Tumors of the Central Nervous System, 5th ed. |
|---|
| Gliomas, glioneural tumors, and neuronal tumors |
| Adult-type diffuse gliomas |
| Astrocytoma, IDH-mutant |
| Oligodendroglioma, IDH-mutant, and 1p/19q-codeleted |
| **Glioblastoma, IDH-wildtype** |
| Pediatric-type diffuse low-grade gliomas |
| Pediatric-type diffuse high-grade gliomas |
| Circumscribed astrocytic gliomas |
| Glioneural and neuronal tumors |
| Ependymal tumors |

Table 3.1 – Graphical scheme of the subtypes comprised in "adult-type diffuse gliomas" (modified from Louis *et al.*, 2021). Adult-type diffuse gliomas can be further subclassified in astrocytoma, IDH-wildtype, oligodendroglioma, IDH-wildtype (whose characteristic alteration, other than IDH1/2 genes mutations, is the codeletion of chromosome 1p and 19q), and glioblastoma, IDH-wildtype (which represents the most aggressive subtype of adult-type diffuse gliomas).

### *Glioblastomas, IDH-wildtype*

The mutational landscape of "glioblastomas, IDH-wildtype" is very wide. However, three specific molecular features have been identified as distinctive of this tumor type: the amplification of the *EGFR* gene, the mutation of the *TERT* gene promoter and the combined gain/loss of, respectively, the whole chromosome 7 and the whole chromosome 10 (also referred to as "+7/-10"). The presence in an IDH-wildtype glioma of at least one of these alterations is considered sufficient to identify the tumor as "glioblastoma, IDH-wildtype", thus improving and simplifying the diagnostic process (Louis *et al.*, 2021; Śledzińska *et al.*, 2021).

The most amplified gene in glioblastomas is *EGFR* (encoding for the epidermal growth factor receptor, EGFR), which occurs in about 50% of the cases. In half of these, it is associated with the deletion of exons from 2 to 7, leading to the expression of the EGFR

variant III (EGFRvIII) (Wong *et al.*, 1987; Frederick *et al.*, 2000), a receptor lacking the extracellular portion for ligand binding, and whose intracellular part constitutively binds its non-mutated counterpart (Fan *et al.*, 2013; Gan, Cvrljevic and Johns, 2013). This results in the hyperactivation of the downstream pathways, such as the MAPK and the PI3K/Akt ones, increasing tumor aggressiveness (Hegi, Rajakannu and Weller, 2012). Moreover, *EGFR* amplification strongly correlates with aggressive behavior of gliomas, and has been detected in about 36% of GBM, IDH-wildtype, showing low sensitivity but high specificity (100%) for this entity (Brat *et al.*, 2018; Stichel *et al.*, 2018).

Secondly, two well-established mutations can occur on the promoter sequence that regulates the *TERT* gene, leading to its overexpression. The encoded protein, the catalytic reverse transcriptase subunit of telomerase, which is normally absent in somatic cells, is therefore re-expressed, permitting cells to avoid telomere shortening and to escape cellular senescence (Gomez *et al.*, 2012). Coherently, the presence of mutations in the *TERT* promoter has been reported to negatively affect the survival of GBM patients (Killela *et al.*, 2013; Labussière *et al.*, 2014; Eckel-Passow *et al.*, 2015).

The presence of +7/-10 karyotypic alteration in glial tumors has been reported to correlate with poor survival of patients and high aggressiveness of the disease, both in glioblastomas, IDH-wildtype and in glial tumors that did not fulfill the morphological criteria for their classification as glioblastoma, IDH-wildtype (Reuss *et al.*, 2015; Wijnenga *et al.*, 2017; Hasselblatt *et al.*, 2018; Tesileanu *et al.*, 2020). Therefore, this molecular signature has been identified as typical of glioblastoma, IDH-wildtype in the latest classification guidelines (Stichel *et al.*, 2018).

Finally, It has been found that, in about 40% of glioblastoma, IDH-wildtype cases, methylation of CpG islands on the *MGMT* promoter occurs, causing the silencing of this gene (Molinaro *et al.*, 2019) encoding the enzyme methylated-DNA-protein-cysteine methyltransferase (MGMT, also known as 6-O-methylguanine-DNA methyltransferase). This leads to increased sensitivity to both chemo- and radiotherapy, making the methylation status of the *MGMT* gene the most predictive marker for therapy effectiveness and prognosis evaluation (Hegi *et al.*, 2005; Stupp *et al.*, 2009).

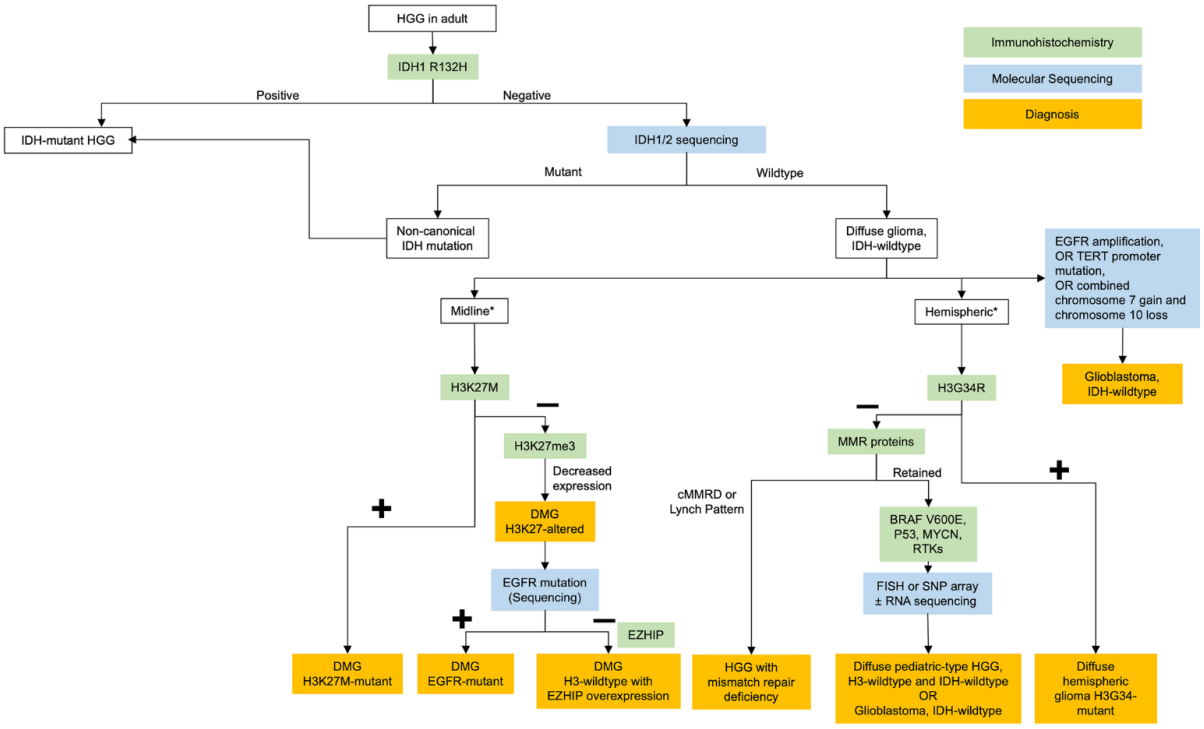


**Figure 3.1 – The diagnostic algorithm used in clinical practice for the diagnosis of gliomas (from Melhem *et al.*, 2022).**

## *Molecular subtypes of GBM*

In 2010, a work from the Cancer Genome Atlas Network highlighted molecular differences between GBM samples, leading to the identification of three different subtypes, namely proneural, classical and mesenchymal (Verhaak *et al.*, 2010).

The proneural subtype is defined by the expression of genes related to neural (e.g., *ASCL1*, *OLIG2*) and glioma-CpG island methylator phenotype (Noushmehr *et al.*, 2010), frequently associated to *TP53* mutation. Interestingly, proneural subgroup comprises *IDH1/2* mutated GBMs, concomitantly with significantly better prognosis and younger age (Yan *et al.*, 2009). In contrast, the gene signatures of both classical and mesenchymal subtypes are both associated with poorer outcome and older age. The classical subtype is characterized by high frequency of both *EGFR* gene amplification and/or EGFRvIII mutations, which also correlates with poorer outcome (Verhaak *et al.*, 2010), but these patients might strongly benefit from metronomic temozolomide (TMZ) administration, with additional advantage if carrying PTEN loss (Cominelli *et al.*, 2015). Also, homozygous deletion of 9p21.3 (*CDKN2A* locus), lack of *TP53* mutations and RB pathways alteration are also frequent (Verhaak *et al.*, 2010). Finally, the mesenchymal subtype is characterized by high expression of YKL40, MET and CD44, frequent deletion at 17q11.2 (containing the *NF1* gene), chromosomal

aberrations in *CDK6*, *CDKN2A* and *RB1* and activation of the NF-kB pathway (Q. Wang *et al.*, 2017). Interestingly, recurrences are frequently associated with a phenotypic shift into the mesenchymal subtype, suggesting that glioma progression may proceed from proneural or classical into the mesenchymal phenotype (Wood *et al.*, 2016).

Recently, since the complicated molecular profile between these subtypes, a diagnostic algorithm has been proposed, which aims to classify GBM tumors into the proneural, classical or mesenchymal subtypes based on the analysis of paraffin-embedded samples. This approach results to easier application into the clinical routine, and can also preserve the morphological aspects of the tumor, that would be lost in case of homogenization of the tissue for transcriptional analyses (Orzan *et al.*, 2020).

Moreover, a rare GBM variant, named glioblastoma with primitive neuronal component (GBM-PNC), has been recognized in 2016 by the World Health Organization as a distinct entity (Louis *et al.*, 2016). These tumors are characterized by the presence of two distinct histological architectures, that are the conventional GBM areas (in which high expression of glial fibrillary acidic protein, or GFAP, can be observed) and, secondly, the regions containing well-demarcated nodules, composed by primitive cells displaying neuronal differentiation (typical of primitive neuroectodermal tumors, or PNET), which result GFAP-negative. Based on these differences, the two components are considered as separate entities, with different biological behaviors and, more importantly, with different response to therapies (Perry *et al.*, 2009). Additional molecular alterations have been identified in GBM-PNCs, the most representatives being frequent mutations on *TP53*, *PTEN* and *RB1* genes, amplification of *MYC* and *MYCN* genes, along with TERT promoter mutations and highly elevated Ki-67 proliferative index (Perry *et al.*, 2009; Xu, Zheng and Li, 2019; Suwala *et al.*, 2021).

Accounting for only the 0.5% of the total cases, GBM-PNC tumors are usually described singularly in case-report studies (Karsy *et al.*, 2012), and, due to their extreme rarity, no standard therapeutic regimen has been universally validated for the treatment of GBM-PNCs. However, it is reported that the addition of platinum-based chemotherapy (typically used for the treatment of PNET tumors) to the conventional treatment used for GBMs (which is based on irradiation and the use of the alkylating agent temozolomide, as explained in the following paragraph) seems to prevent dissemination of the disease through the cerebrospinal fluid and may increase patient survival in some cases (O'Leary *et*

*al.*, 2016; Prelaj *et al.*, 2018). The treatment of this rare GBM variant remains challenging and minimal progress has been achieved in the treatment of these aggressive tumors. However, the therapeutic strategy for glioblastomas remains common for all the identified entities.

## *Treatment and managing of glioblastoma*

The standard therapeutic protocol for GBM is a multimodal approach that combines surgery, radiotherapy, and adjuvant chemotherapy with temozolomide (TMZ), a DNA alkylating agent (Stupp, Hegi et al. 2009). Surgery represents the first-line intervention, with the current standard of surgical care being the complete safe resection. The removal of more than 98% of the tumoral mass has been correlated with a significant increase of the prognostic value (Lacroix *et al.*, 2001).

Moreover, due to the extreme infiltrative and invasive nature of glioblastoma, the concept of supratotal resection is emerging, which consists in a resection beyond the tumor area, as well as the use of fluorescent labelling of the cancerous mass with 5-aminolevulinic acid (5-ALA) or the implantation of wafers containing carmustine, in order to maximize the effectiveness of the surgery (Brown *et al.*, 2016; Eyüpoglu *et al.*, 2016; Khasraw *et al.*, 2022).

After tumor mass reduction, a combination of radio- and chemotherapy is used. The combination of the two strategies has been reported to increase the survival of patients, but fails to be curative (Stupp *et al.*, 2005; Yang, Zhou and Lin, 2014; Parisi *et al.*, 2015). Although, nowadays, temozolomide (TMZ) is administered to all patients regardless of their *MGMT* gene methylation status, it has been confirmed the greater efficacy of the treatment in the case of methylated *MGMT* (Stupp *et al.*, 2009).

Combination treatment of TMZ and lomustine (an alkylating nitrosourea similar to carmustine), has been recently explored, suggesting that this combination can improve the overall survival of patients affected from glioblastoma with methylated *MGMT* gene (Herrlinger *et al.*, 2019).

Also, the use of the anti-VEGF antibody bevacizumab has been FDA-approved in 2009 for recurrent glioblastoma. Unfortunately, the combined treatment of radiotherapy, TMZ and bevacizumab failed to improve the survival of patient compared to the combination of radiotherapy and TMZ (Chinot *et al.*, 2014; Gilbert *et al.*, 2014).

Despite all the aggressive therapeutic regimens used and all the efforts on finding alternative strategies, the median overall survival of GBM patients after treatment remains low (from 12 to 15 months) (Khasraw *et al.*, 2022). Hence, the urge to find new therapeutic targets to counter glioblastoma recurrence and progression. Recently, the high tumor recurrence after treatment, which is peculiar to GBM, has been linked to the presence of cancer stem-like cells.

### *Glioblastoma cancer stem cells*

Recently, a staminal component has been identified in GBM tumors, accounting for about 0.1-10% of the total GBM tumor (Bao *et al.*, 2006; Yan *et al.*, 2014). This cell population, named glioblastoma cancer stem cells (GBM-CSCs), is characterized by self-renewal and by the capacity of reproduce a secondary tumor which has the characteristics of the original tumor (Mitchell *et al.*, 2021).

Further analyses of these cells revealed the expression of both cell surface markers and of intracellular markers typical of a staminal cell, such as the activation of the Notch, the sonic hedgehog and the Wnt/β-catenin signaling pathways, which are involved in embryonal neurogenesis and in the physiological maintenance of adult neural stem cells (Sanai, Alvarez-Buylla and Berger, 2005; Garnier *et al.*, 2019; Loras *et al.*, 2023). As a consequence, these cells have been demonstrated able to maintain themselves through serial steps of *in vitro* dilutions and of *in vivo* transplantation (Galli *et al.*, 2004). Therefore, GBM-CSCs constitute a component of glioblastoma tumors characterized by self-renewal capabilities.

Also, many studies on GBM-CSCs revealed the coexistence of a number of different subpopulations, each conferring unique characteristics to the tumor (Dirkse *et al.*, 2019; Gupta *et al.*, 2019; Suvà and Tirosh, 2020). Moreover, when orthotopically injected *in vivo*, each subclone has been demonstrated able to reproduce only a specific characteristic of the original biopsy (Reinartz *et al.*, 2017), and the injection of patient-derived GBM-CSCs in immunodeficient mice is able to reproduce the phenotype of the original tumor (Meyer *et al.*, 2015; Lan *et al.*, 2017), confirming that the high heterogeneity observed in GBM tumors is caused by the simultaneous presence of multiple subpopulations, which contribute to the final tumor phenotype.

GBM-CSCs are also characterized by high resistance to conventional treatments. It has been proved that, after irradiation, these cells can activate various checkpoint proteins in

response to DNA damage, such as ataxia-telangiectasia-mutated (ATM), Rad17, Chk1 and Chk2, thus contributing to tumor repopulation after ionizing radiation exposure (Bao *et al.*, 2006). Resistance to TMZ and to other chemotherapeutic agents in these cells has been linked to the expression of MGMT and of the ATP-binding cassette transporter protein BCRP1, which can respectively neutralize the DNA damage caused by alkylating agents and favor the efflux of these drugs from the cell (Hirschmann-Jax *et al.*, 2004; Liu *et al.*, 2006). The reduced sensitivity to treatments is also caused by the high heterogeneity of the subpopulations that are present in the tumor, which, after the exposure to treatment, can undergo selective proliferation and give rise to even more aggressive tumors (Sottoriva *et al.*, 2013; Xie *et al.*, 2022).

Moreover, GBM-CSCs are characterized by plasticity, that is, the ability of reverting their phenotype to a less differentiated and more staminal one, in response to external stimuli (Gimple *et al.*, 2022). It has been observed that the exposure to TMZ can cause differentiated GBM cells to revert to GBM-CSCs (Auffinger *et al.*, 2014; Adamski *et al.*, 2017). These cancer stem-like cells, when compared to the cells that constitute the tumor bulk, are characterized by a more quiescent cell state and, consequently, by inferior sensitivity to treatments (Safa *et al.*, 2015). As a result, the persistence of this staminal component is responsible for tumor recidivation after therapy, which, also, causes the selective proliferation of the most treatment-resistant subpopulations, thereby increasing the aggressiveness of secondary tumors (Kim *et al.*, 2015; Wang *et al.*, 2016).

Given all these characteristics, the discovery of new therapeutical targets in GBM-CSCs could improve the treatment of glioblastoma. To this purpose, since GBM-CSC *in vitro* lines can reproduce with high fidelity the characteristics of the original tumor and its heterogeneity, this model is a powerful tool in giving meaningful insights into resistance to treatment and tumor relapse in glioblastoma patients. In this context, since many previously published works suggest the sensitivity of GBMs to ferroptosis inducers, this study investigated whether the induction of this new type of cell death could be effective in reducing the progression of this treatment-resistant component of GBMs.

## *Ferroptosis in glioblastoma*

Analogously to other tumor types, GBM has been reported to highly depend on iron. Comparing to normal brain tissue, increased expression of TfR1 has been reported in GBM

samples (Recht *et al.*, 1990), along with higher levels of both FtH and FtL (Jaksch-Bogensperger *et al.*, 2020) suggesting higher dependency on iron and, potentially, sensitivity to ferroptosis. Moreover, TfR1, FtL and FtH overexpression have been reported also in GBM-CSC lines, along with active production and secretion of transferrin in order to ensure increased iron intake (Schonberg *et al.*, 2015). These studies confirm iron addiction as a characteristic of GBM and, more interestingly, also of the staminal component of GBM responsible for tumor relapse. Moreover, also high levels of transferrin receptor 2 (TfR2) have been detected in GBMs, inversely correlating with patient prognosis (Calzolari *et al.*, 2010). This receptor, rather than in iron uptake, is more involved in intracellular signaling, mediating the activation of MAPK pathway and, in turn, hepcidin expression, ultimately decreasing FPN-mediated iron efflux (Brown *et al.*, 2020).

Also, supplementation with iron increased the efficacy of radiotherapy in reducing the growth of nitrosoethylurea-induced gliomas in Wistar rats (Ivanov *et al.*, 2015), suggesting that the exposure to ionizing radiations synergized with iron-dependent lipid peroxidation in inducing GBM cell death by ferroptosis, as already reported elsewhere (L. F. Ye *et al.*, 2020; Lei *et al.*, 2020).

Moreover, increased activity of the system $X_c^-$ antiporter seems to be involved in the onset of epileptic seizures caused by GBMs, which is a common event in patients, both before and after diagnosis and treatment of the tumor (Davis, 2016). Indeed, this symptom has been linked with induction of excitotoxicity in normal brain cells due to the release of glutamate from GBM cells (Buckingham *et al.*, 2011). On the other hand, extracellular glutamate acts on ionotropic receptors, thereby promoting the growth and the migratory activity of these cells (Takano *et al.*, 2001; Lyons *et al.*, 2007).

The increase of glutamate in the peritumoral zone has been also correlated to the increased uptake of cystine necessary for glutathione synthesis (Savaskan and Eyüpoglu, 2010) to counteract increased oxidative stress levels in GBM cells (Kim *et al.*, 2001). Moreover, increased glutathione levels in tumors have been correlated to decreased sensitivity to TMZ regimens and to poorer prognosis (Zhu *et al.*, 2018). Accordingly, the overexpression of xCT has been reported to increase the *in vitro* resistance of glioma cells to TMZ (Sehm, Rauh, *et al.*, 2016) and these data have been confirmed in patients, where increased xCT levels positively correlated with poorer patient prognosis (Takeuchi *et al.*, 2013; Robert *et al.*, 2015) and with decreased sensitivity to chemotherapeutic agents (Huang *et al.*, 2005). Thus the

increased metabolic needs of GBM cells induce the increased import of cystine needed for GSH synthesis, causing the collateral death of surrounding healthy nervous cells by exposure to excessively high concentrations of glutamate, which also stimulates the growth of GBM cells (Ye and Sontheimer, 1999; Conrad and Sato, 2012; Robert and Sontheimer, 2014). Therefore, the blockade of system $X_c^-$ could both prevent the further destruction of brain parenchyma and, at the same time, reduce GBM progression by the deprivation of glutathione, essential for tumor growth.

In this context, the xCT inhibitor erastin has been observed to decrease cell viability of glioma cell lines via ferroptosis induction, as demonstrated by the increase of lipid peroxide content in treated cells (Fan *et al.*, 2017). Ulteriorly, the simultaneous inhibition of both xCT and cystathionine γ-lyase (which is involved in GSH synthesis via the transsulfuration pathway) expression using silencing RNAs led to a significant decrease of cell viability after TMZ treatment, suggesting that the reduction of GSH in glioma cells could be an effective strategy for the sensitization of TMZ-resistant gliomas (Chen *et al.*, 2015).

Moreover, the FDA-approved xCT inhibitor sulfasalazine has been observed to increase the efficacy of TMZ in U251 glioma cells (Polewski *et al.*, 2016). Also, a clinical trial for the evaluation of sulfasalazine toxicity in recurrent GBM patients had been conducted, but, unfortunately, half of the patients experienced significant brain edema due to sulfasalazine treatment, while no reduction of tumor volume was noticed, leading to early termination of the study (Robe *et al.*, 2009). Interestingly, these last results are in contrast with a more recent work, which claims that sulfasalazine is able to reduce peritumoral edema (Sehm, Fan, *et al.*, 2016). So, the inhibition of xCT seems to be an effective strategy for the management of gliomas, and the discordance between these two studies could be caused by the advanced status of the disease in the patients enrolled in the clinical trial.

Finally, also RSL3 has been tested on glioblastoma cells, where it has been reported to decrease GPX4 levels and to increase the amount of membrane lipid peroxides (Li *et al.*, 2021). Furthermore, RSL3 has been demonstrated effective also *in vivo*, where it significantly reduced the proliferation of glioma cells in mice (Wang *et al.*, 2019). A comparative immunohistochemical analysis between primary and their correspondent recurrent GBM tumors has shown a significant decrease in GPX4 protein content and a correspondent increase in ACSL4 expression, suggesting that recurrent tumors are characterized by increased sensitivity to ferroptosis (Kram *et al.*, 2022).

GBM is an aggressive CNS tumor that often develops resistance to current therapies leading to the tumor relapse, caused by a staminal component due to its extremely heterogeneous composition. Thus, new therapeutic strategies are required and, in this context, ferroptosis induction could be a valid strategy for the treatment of glioblastoma.

# Materials and methods

## *Antibodies and Chemicals*

Erastin was purchased from Selleckchem (cat. no. S7242) and resuspended in DMSO at the concentration of 10 mM. RSL3 was purchased from Sigma Aldrich (cat. no. SML2234) and resuspended in DMSO at the concentration of 4.5 mM. ML162 was purchased from Sigma Aldrich (cat. no. SML2561) and resuspended in DMSO at the concentration of 10 mM. Temozolomide (TMZ) was purchased from Cayman Chemicals (cat. no. 14163) and resuspended in DMSO at the concentration of 5 mg/mL. Ferrostatin-1 (Fer-1) was purchased from Sigma Aldrich (cat. no. SML0583) and resuspended in DMSO at the concentration of 10 mM. Deferrioxamine (DFO) was purchased from Sigma Aldrich (cat. no. D9533) and fresh 20 mM stock solutions were made in sterile dd$H_2O$ prior use. The antibodies used in this study were anti-TfR1 (cat. no. 136800, Thermo Scientific, Waltham, MA, USA), anti-Ferroportin (cat. no. NBP1-21502, Novus Biologicals, Centennial, CO, USA), anti-FSP1 (cat. no. sc-377120, Santa Cruz Biotechnology, Dallas, TX, USA), anti-ACSL4 (cat. no. sc-271800, Santa Cruz Biotechnology, Dallas, TX, USA), anti-tubulin (cat. no. T5168, Sigma-Aldrich, Saint Louis, MO, USA). HRP-conjugated secondary antibodies used were anti-mouse (cat. no. sc-516102, Santa Cruz Biotechnology, Dallas, TX, USA) and anti-rabbit (cat. no. sc-2357, Santa Cruz Biotechnology, Dallas, TX, USA). C11-BODIPY$^{581/591}$ probe was purchased from Thermo Scientific (cat. no. D-3861) and resuspended in DMSO at a concentration of 2.5 mM.

## *Glioblastoma cell lines*

Human GBM cell lines BT302 (mesenchymal subtype, conventional GBM), BT334 (classical subtype, conventional GBM) and CT014 ϕ (GBM with a primitive neuronal component) were obtained from Prof. Poliani's group (Pathology Unit, Department of Molecular and Translational Medicine, University of Brescia). The cells were cultured in medium composed of Dulbecco's Modified Eagle Medium (DMEM, EuroClone, Pero, MI, Italy) and Ham's F12 Medium (EuroClone, Pero, MI, Italy) mixed in a 1:1 ratio and supplemented with 2% B27 Supplement (Gibco, Life Technologies, Grand Island, NY, USA), 100 U/mL/100 mg/L Penicillin-Streptomycin (EuroClone, Pero, MI, Italy), and 2mM L-glutamine (EuroClone, Pero, MI, Italy). Moreover, BT302 and BT334 cells were cultured in the presence of recombinant human epidermal growth factor (EGF) and recombinant human fibroblast growth factor 2

(FGF) (PeproTech, Westlake Village, CA, USA), both at the concentration of 20 ng/mL, while CT014 cells were cultured in absence of growth factors to maintain PNC phenotype, and therefore are referred to as "CT014 Φ". Cells were maintained at 37°C in a humidified atmosphere with 5% $CO_2$. To expand cultures, neurospheres were pelleted by centrifugation at 300 rcf for 3 minutes, then, after supernatant removal, spheres were mechanically dissociated, counted with trypan blue to evaluate the number of live cells, and then re-plated as single cells at clonal density (6,000 cells/$cm^2$ for BT302 and 10,000 cells/$cm^2$ for BT334 and CT014 Φ) in complete fresh medium.

### *Cell treatments and cell viability assay*

For the time-course experiments, the cells were seeded in 96-well white plates (at a density of 2.500 cells/well for all the cell lines) in a volume of 90 µL. Then, 24 hours after seeding, the cells were incubated for 1 hour at 37°C with 45 µL of medium containing the RealTime-Glo Mix 4X (RealTime-Glo™ MT Cell Viability Assay, cat. n. G9713, Promega Corporation, Madison, WI, USA), and then medium containing various concentrations of either erastin, RSL3, ML162 or temozolomide were added, to reach a final concentration of 1X of both RealTime-Glo Mix and of the tested compound in a volume of 180 µL. Then, the luminescence signal, produced by the conversion of the MT Cell Viability Substrate, was measured after 24, 48 and 72 hours after the treatment using a plate reader for luminescence (EnSight Multimode plate reader; Perkin Elmer), following the manufacturer's instructions. The percentage of cell viability at each concentration was calculated using Microsoft Excel 2016 software.

### *Lactate dehydrogenase (LDH) cytotoxicity assay*

The cell cytotoxicity during time-course experiments was evaluated using the LDH Cytotoxicity Assay Kit (cat. n. 197004, Abcam, Cambridge, UK). The cells were seeded in 96-well plates (at a density of 10,000 cells/well for BT302 cells and of 5,000 cells/well for both BT334 and CT014 Φ cells) in a volume of 90 µL. Then, 24 hours after seeding, 90 µL of treatment-containing complete culture medium were added, to reach a final concentration in a volume of 180 µL, and cell cytotoxicity was assessed after 24, 48 and 72 hours of treatment for BT302 and BT334, and after 1 week of treatment for CT014 Φ.

Briefly, in this assay, LDH enzyme released from cells converts lactate and $NAD^+$ to pyruvate and NADH, which reduces the proprietary PicoProbe to an intensely fluorescent product.

As a result, the amount of fluorescence is directly proportional to the damaged cells. Culture medium alone was used as a negative control (blank), while a standard of LDH diluted in culture medium was also added as an internal positive control. The supernatant of lysed cells (not treated) was used for the determination of total LDH cells content. To this aim, 18 µL of Cell Lysis buffer (provided by the kit) were added to untreated cells, followed by 30 minutes of incubation at 37°C. The plates were centrifuged at 700 rcf for 5 minutes to sediment cells and cell debris. Then, 9 µL of supernatant from each well were transferred to a white 96-well plate. According to the manufacturer's instructions, 95 µL of a Reaction Mix (composed by 2 µL of LDH substrate mix, 4 µL of PicoProbe and 89 µL of LDH assay buffer) were added to each well of the white plate (including both test samples and controls). The plate was incubated at room temperature for 15 minutes, and fluorescence was then detected using an EnSight plate reader (Perkin Elmer) at Ex/Em = 535/587 nm. Results were calculated by subtracting the fluorescent value of the negative control (blank) from each sample, then LDH release was calculated using Microsoft Excel 2016 software and expressed as a percentage of tested sample/lysed cells (considering the fluorescent values of lysed cells as 100% of LDH release).

### *RNA-Seq analysis*

For the RNA-Seq data analysis, formalin-fixed paraffin-embedded patient-derived GBM samples were histologically classified as conventional glioblastomas (GBM, further subdivided into the classical, proneural and mesenchymal subtypes) (Verhaak *et al.*, 2010; Orzan *et al.*, 2020), primitive neuroectodermal tumors (PNET) (Sturm *et al.*, 2016), or glioblastomas with primitive neuronal component (GBM-PNC, for which the GBM component was separated from the PNC component and analyzed separately) (Perry *et al.*, 2009; Louis *et al.*, 2021; Suwala *et al.*, 2021). Then, RNA was extracted from each sample, total mRNA was sequenced, and data were available from Prof. Poliani's group (Pathology Unit, Department of Molecular and Translational Medicine, University of Brescia). The expression level of the considered genes was compared between the four groups (conventional GBMs vs. PNET vs. GBM component vs. PNC component) and between the three subtypes of the GBM group (classical vs. proneural vs. mesenchymal).

## *RNA extraction and gene expression analysis using qPCR*

RNA was obtained with TRI Reagent (Sigma-Aldrich) and cDNA was generated using ImProm-II™ Reverse-Transcription System kit (Promega, Madison, WI) according to the manufacturer's instructions. Real time qPCR was performed using SsoAdvanced Universal SYBR Green Supermix (cat. no. 1725274, BioRad, Hercules, CA, USA), according to the manufacturer's instructions, for ACSL3, ACSL4, NFE2L2, SLC7A11, HMOX1, CHAC1, NQO1, PTGS2, GPX4, AIFM2, TFRC, SLC40A1, FTH, FTL mRNA detection, normalized to TBP based on the analyzed cell line, and expressed as $2^{-\Delta Ct}$.The sequences of the forward and reverse primers used for the amplification of targets are the following:

| | | |
|---|---|---|
| Hs TBP | Hs TBP F | GAACATCATGGATCAGAACAACA |
| | Hs TBP R | ATAGGGATTCCGGGAGTCAT |
| Hs NFE2L2 | Hs NFE2L2 F | CACATCCAGTCAGAAACCAGTGG |
| | Hs NFE2L2 R | GGAATGTCTGCGCCAAAAGCTG |
| Hs SLC7A11 | Hs SLC7A11 F | TCTCCAAAGGAGGTTACCTGC |
| | Hs SLC7A11 R | AGACTCCCCTCAGTAAAGTGAC |
| Hs NQO1 | Hs NQO1 F | CCTGCCATTCTGAAAGGCTGGT |
| | Hs NQO1 R | GTGGTGATGGAAAGCACTGCCT |
| Hs ACSL3 | Hs ACSL3 F | GGCGTAGCGGTTTTGACA |
| | Hs ACSL3 R | CCAGTCCTTCCCAACAACGA |
| Hs ACSL4 | Hs ACSL4 F | ACTGGCCGACCTAAGGGAG |
| | Hs ACSL4 R | GCCAAAGGCAAGTAGCCAATA |
| Hs GPX4 | Hs GPX4 F | GCCATCAAGTGGAACTTCAAC |
| | Hs GPX4 R | CTTCTCTATCACCAGGGGCTC |
| Hs AIFM2 | Hs AIFM2 F | ATGGTTCGGCTGACCAAGAG |
| | Hs AIFM2 R | GCCACCACATCATTGGCATC |
| Hs HMOX1 | Hs HO-1 F | GCTGTAGGGCTTTATGCCATGT |
| | Hs HO-1 R | GGCTCCTTCCTCCTTTCCAGAG |
| Hs CHAC1 | Hs CHAC1 F | CCTGAAGTACCTGAATGTGCGAGA |
| | Hs CHAC1 R | GCAGCAAGTATTCAAGGTTGTGGC |
| Hs PTGS2 | Hs PTGS2 F | ATGCTGACTATGGCTACAAAAGC |
| | Hs PTGS2 R | TCGGGCAATCATCAGGCAC |
| Hs TFRC | Hs TFRC F | TTTCCACCATCTCGGTCATC |
| | Hs TFRC R | GGGACAGTCTCCTTCCATATTC |
| Hs SLC40A1 | Hs SLC40A1 F | ATCCATGTGCGTGGAGTACG |
| | Hs SLC40A1 R | AGGGGTTTTGGCTCAGTATCTTT |
| Hs FTH1 | Hs FTH1 F | AGAGGGAACATGCTGAGAAAC |
| | Hs FTH1 R | CACACTCCATTGCATTCAGC |
| Hs FTL | Hs FTL F | CCTAGATGAGGAAGTGAAGCTT |
| | Hs FTL R | AGAGATACTCGCCCAGCCC |

**Table 3.2. Primers sequences.**

## Protein Extraction

Cells extracts were prepared using an ice-cold lysis buffer composed of 200 mM Tris-HCl pH 8, 100 mM NaCl, 1 mM EDTA, 0.5% NP-40, 10% glycerol, 1 mM sodium fluoride, 1 mM sodium orthovanadate and Complete Protease Inhibitor Cocktail (Sigma-Aldrich) and stored at -20°C until analysis. Protein concentration was quantified using the Bicinchoninic Acid Kit for Protein Determination (Sigma-Aldrich, Saint Louis, MO, USA) and used for different analysis by western blotting and ELISA assays.

## Western Blot Assay

Western blot was used to analyze protein expression. In brief, after extraction, protein homogenates (30-60 µg) were boiled at 99°C for 5 minutes before separation by SDS–polyacrylamide gel electrophoresis and transferred to a 0.45 µM pore-sized nitrocellulose membrane (Sartorius AG, Hottingen, Germany). Membranes were incubated for 1 hour at RT with Blocking solution (Tris-buffered saline + 0,1% Tween-20 (TBS-T) with 2% milk) and incubated overnight at 4°C (or 2 hours at 37°C) with primary antibodies (reported in the "Antibodies and chemicals" paragraph). Following three TBS-T washings, membranes were incubated with HRP-conjugated secondary antibodies for 2 hours at RT. Membranes were washed again in TBS-T prior to signal visualization using enhanced chemiluminescence (PDS kit, Protein Detection System, GeneSpin, Milan, Italy). The signal was visualized with a LI-COR Odyssey (LI-COR Biosciences GmbH, Bad Homburg, Germany) or by the exposure onto CL-XPosure Film (Thermo Scientific), and densitometric analysis was performed using Image Studio Lite TM Software (LI-COR Biosciences GmbH, Bad Homburg, Germany), normalized against tubulin as a loading control and expressed as fold change over the control untreated cells.

## ELISA Assay for FtH analysis

Ninety-six-well plates were coated with 0.1 mL of primary antibody against H-ferritin (RH02) at the concentration of 10 µg/mL diluted in 50 mM carbonate buffer pH 9.6 for 18 hours at 4°C. After three washes with PBS-T (phosphate buffer saline with 0,1% Tween20), wells were over-coated by adding 0.1 mL of 3% bovine serum albumin (BSA) diluted in PBS for 1 hour at 37°C. After three washes with PBS-T, protein extracts (15 µg for BT302 and BT334, and 2 µg for CT014 ϕ) were analyzed in duplicate, diluted in 1% BSA-PBS-T and incubated at 37°C for 2 hours. A standard curve using recombinant human H-ferritin was used as calibrator.

After three washings in PBS-T, 0.1 mL of HRP-labelled anti-H-ferritin antibody (diluted 1:500 in 1% BSA-PBS-T) were added and plate incubated for 1 hour at 37°C. After three washings in PBS-T, HRP activity was detected using 1 mg/mL 3,3',5,5'-tetramethylbenzidine (TMB) dissolved in dimethyl sulfoxide (DMSO) and diluted 1:10 in phosphate-citrate buffer pH 5 (added with fresh hydrogen peroxide to a final concentration of 0,006%) and the absorbance of the solution was read at 620 nm with a Multiskan©EX plate reader until signal development. Then, the reaction was stopped by adding 0.1 mL of 1 N sulfuric acid, and the absorbance was measured at 405 nm. The concentration of H-ferritin was extrapolated from the calibrator curve and expressed as ng of ferritin/mg of protein extract.

## *Lipid ROS staining with C11-BODIPY$^{581/591}$ probe*

For the lipid ROS detection after treatment with both ferroptosis inducers and inhibitors, BT302 were seeded in 6-well plates (at a density of 200,000 cells/well and in a volume of 1.5 mL) and, after 24 hours from seeding, 500 µL of treatment-containing complete culture medium were added, to reach a final concentration in a volume of 2 mL. After 24 hours of treatment, cells were collected and centrifuged at 300 rcf for 3 minutes at RT. Then, supernatant was discarded, and the pellet was resuspended in 500 µL of 5 µM C11-BODIPY$^{581/591}$ probe and incubated for 30 minutes at 37°C, with 5% $CO_2$. Then, cells were collected and centrifuged at 300 rcf for 3 minutes at RT. Supernatant was discarded, cells were resuspended in 200 µL of PBS 1X, and centrifuged on polarized glass slides at 700 rcf with a cytocentrifuge for 6 minutes at RT for the thin-layer preparation. Then, cells were fixed with 4% paraformaldehyde (PFA) for 15 minutes at RT, and, after three washes in dd$H_2O$, cells were counterstained with 0.1 µg/mL DAPI for 5 minutes at RT. Then, coverslips were mounted over the fixed cells, and images were taken using a Zeiss Axiovert microscope and SensiCam-PCO Optics (GmbH, Germany) with 63× magnification (with immersion) using FITC, RHOD and DAPI filters to visualize, respectively, the oxidized probe, total probe, and the nuclei.

## *Statistical Analysis*

Data are presented as mean ± standard deviation (SD). Statistical significance was assessed by Student's t-test, by one-way ANOVA or by two-way ANOVA (as reported in figure legends), which were performed by GraphPad Prism 8 software (GraphPad Software Inc., La Jolla, CA). p-values lower than 0.05 were considered significant.

# Results

Glioblastoma is the most frequent malignant tumor of the central nervous system with still poor prognosis, despite multimodal therapy and novel therapeutic approaches emerged in the recent years (Khasraw *et al.*, 2022). Therapy resistance and tumor recurrence are very frequent in GBM and have been found to be rendered by the staminal component of the tumor, also called glioblastoma cancer stem cells (GBM-CSCs) (Xie *et al.*, 2022). These cells, due to their plasticity, contribute to tumor heterogeneity and can easily adapt to unfavorable conditions, acquiring therapy resistance (Kim *et al.*, 2015; Wang *et al.*, 2016). Ferroptosis, a type of regulated cell death, has been found to overcome CSCs-mediated persistence in many types of cancer, making it a promising anticancer strategy (Xu *et al.*, 2019; Rodriguez, Schreiber and Conrad, 2021).

## *Primary GBM samples express differential levels of iron- and ferroptosis-related proteins*

Since there is evidence that GBM cells are sensitive to ferroptosis, both *in vitro* and *in vivo* (Wang *et al.*, 2019; Li *et al.*, 2021), the study compared the expression levels of ferroptosis- and iron metabolism-related genes using data derived from the RNA sequencing of patient-derived GBM samples, which were classified based on their histology. Briefly, conventional GBMs were considered entirely or further subdivided into the classical, proneural and mesenchymal subtypes (Verhaak *et al.*, 2010; Orzan *et al.*, 2020). Glioblastoma with Primitive Neuronal Component (GBM-PNC), a rare and aggressive GBM variant, is a biphasic neoplasm displaying a malignant glial component with classical GBM features (GBM component) along with nodules composed of immature cells displaying primitive neuroectodermal features and early neuronal differentiation (PNC component) (Perry *et al.*, 2009). These two components of the tumor, GBM and PNC, were analyzed separately. Since PNC component partially shares a similar immunophenotype with primitive neuroectodermal tumors (PNET) (Sturm *et al.*, 2016), we also included the gene expression analysis of this type of CNS tumor.

Regarding the first comparison (Figure 3.2), we found significantly higher expression of *NFE2L2* in conventional GBMs and both GBM and PNC components compared to PNET tumors by 3.2-fold, 2.4-fold, and 2.7-fold, respectively. This gene encodes for the protein Nrf2, a master regulator of antioxidant response that is known to induce the expression of

both ferritin subunits (light, FtL, and heavy, FtH, which are involved, respectively, in the storage of iron and in its neutralization to a non-toxic $Fe^{3+}$ form), of the iron exporter ferroportin (FPN) and of the lipid peroxide-neutralizing enzyme GPX4 (Dodson, Castro-Portuguez and Zhang, 2019). Interestingly, the expression of the genes encoding for these four proteins were also upregulated in GBMs (conventional and GBM-PNC) comparing to PNET tumors. These data suggest a higher activation of the antioxidant machinery controlled by Nrf2, and therefore a higher protection in GBMs from ferroptotic cell death. Also, a significant higher expression of *HIF1A* (encoding for the protein Hypoxia Inducible Factor 1 α, also named HIF-1α) was found, which has been observed to promote iron accumulation in cancer (Torti and Torti, 2013), coherently with the increased gene expression of both ferritin subunits in conventional GBMs.

Moreover, the study found a higher expression of *ACSL3* in conventional GBMs compared to the other tumors, by 1.8-fold to the GBM component, by 2-fold to the PNC component, and by 4-fold to PNET. This gene encodes for the protein long-chain-fatty-acid-CoA ligase 3 (ACSL3), which is specifically responsible for the insertion in cell membranes of monounsaturated fatty acids (MUFAs). Increased MUFA content in the cell membrane in turn decreases the relative amount of polyunsaturated fatty acids (PUFAs), which are the final target of lipid peroxidation (Magtanong *et al.*, 2019). Therefore, this difference suggests that conventional GBMs could be more protected from ferroptosis.

On the other hand, PNET tumors express higher levels of *AIFM2*, which encodes for the protein FSP1, involved in the regeneration of the antioxidant molecule coenzyme $Q_{10}$, a feature that could suggest higher protection from the accumulation of polyunsaturated fatty acids lipid peroxides. Unfortunately, since no primary cell line derived from PNET tumors has been established yet, these differences cannot be verified with *in vitro* studies, and these findings remain speculative.

These results did not indicate an evident difference in gene expression between conventional GBMs and GBM-PNC that would suggest a susceptibility to ferroptosis. Moreover, the two components of GBM-PNC shared the same expression pattern that was more similar to the one of conventional GBM than of PNET.

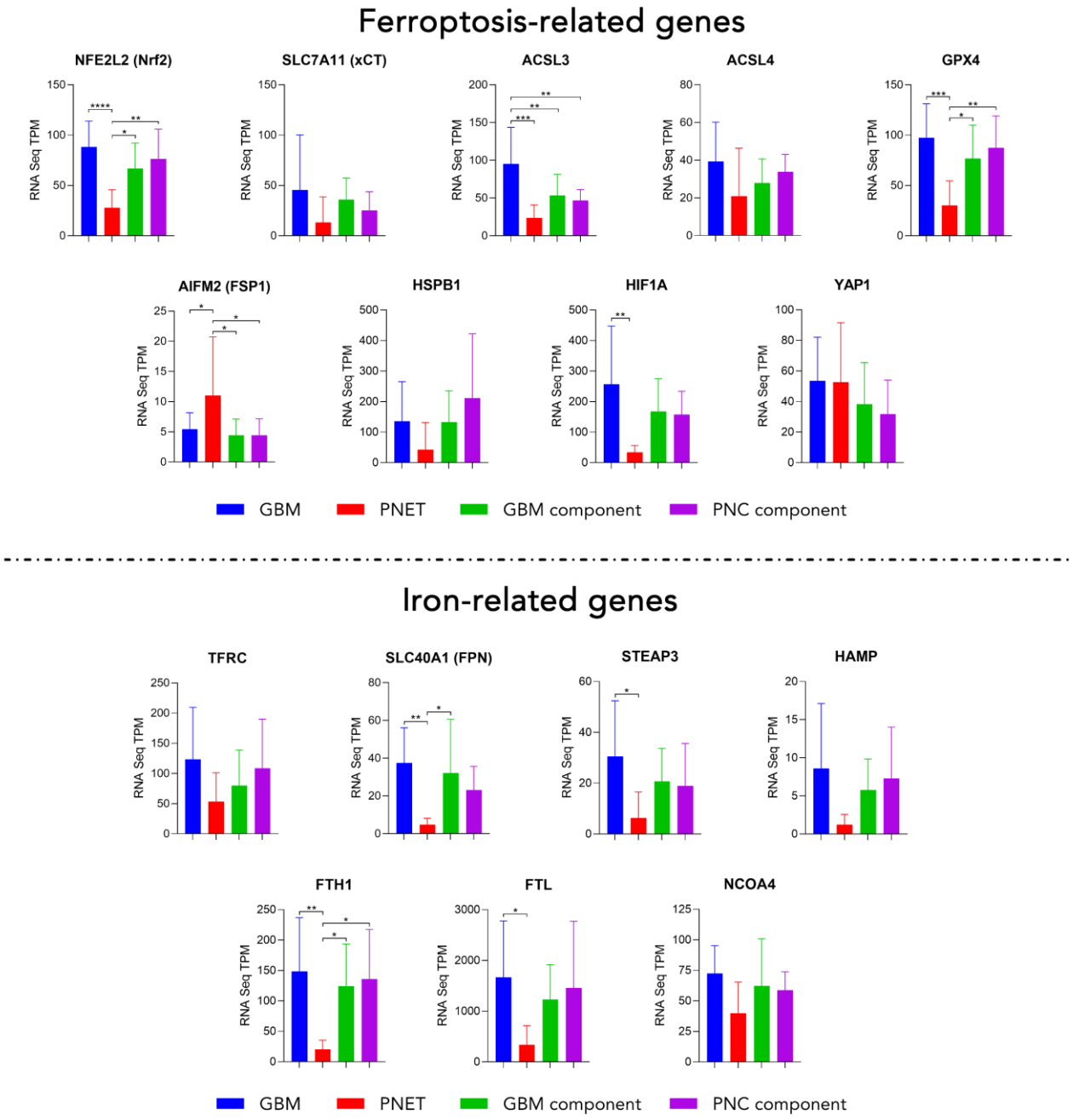


**Figure 3.2 – RNAseq data on patient-derived GBM samples regarding ferroptosis- and iron-related genes.** The samples were classified basing on their histology in conventional glioblastomas (GBM; n=15), primitive neuroectodermal tumors (PNET; n=6), and glioblastomas with primitive neuronal component (GBM-PNC, for which the GBM component [n=14] was separated from the PNC component [n=13] and analyzed separately). Then, the expression level of the considered genes was compared between the four groups (conventional GBMs vs. PNET vs. GBM component vs. PNC component). The statistical analysis was performed with ordinary one-way ANOVA, using Tukey's method for statistical hypothesis testing (* $p < 0.05$; ** $p < 0.01$; *** $p < 0.001$; **** $p < 0.0001$).

Regarding the comparison of conventional GBM subtypes (Figure 3.3), we found significantly 3-fold higher *ACSL3* mRNA levels in classical GBMs compared to the proneural subtype, suggesting increased protection from ferroptosis. The YAP1 mRNA expression was increased in mesenchymal GBMs by 1.5-fold to the classical subtype and by 3.8-fold to the

proneural one. The encoded protein Yes-associated protein 1 (YAP1) is a transcriptional factor that has been found to promote the expression of ACSL4 and TfR1 (Yang and Chi, 2020). However, no statistically significant increase in the expression level of *ACSL4* and *TfR1* mRNAs in mesenchymal GBMs compared to the other subtypes was observed. Moreover, mesenchymal tumors also showed the upregulation of *HSBP1* (by 3.9-fold and by 3.7-fold compared to the classical and proneural subtypes, respectively), whose protein product, Heat Shock Binding Protein 1, has a role in the antioxidant response and has been observed to decrease intracellular iron levels (Bogdan *et al.*, 2016). Finally, also found was a significant increase in the mRNA levels of *FTH* and *FTL* in the mesenchymal subtype compared to the classical one by 2.7-fold and 3.4-fold, respectively, suggesting increased protection from iron accumulation and increased iron storage capacity.

According to the results obtained, none of the conventional GBM subtypes presented a pro-ferroptotic gene expression profile.

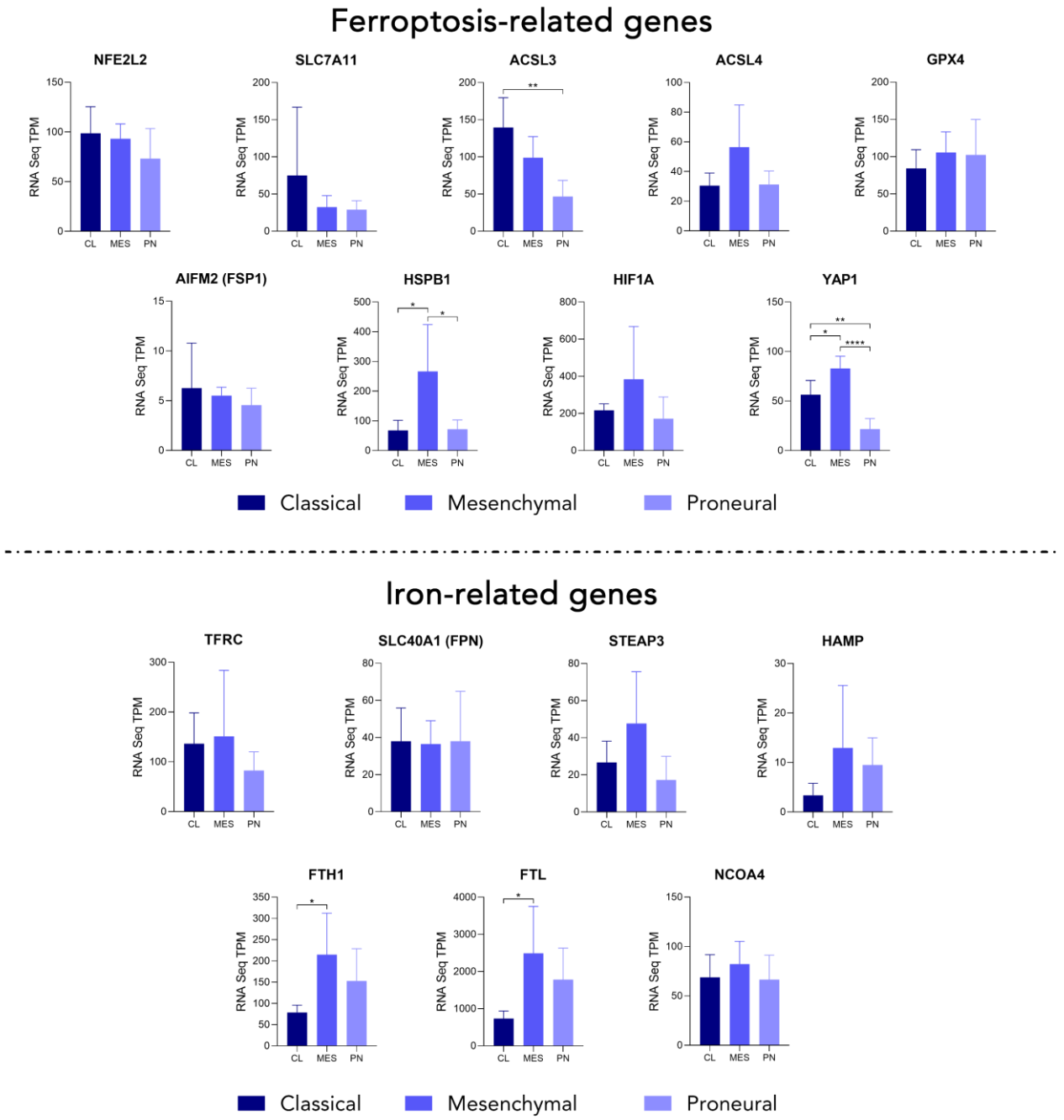


**Figure 3.3 – RNAseq data on patient-derived GBM samples regarding ferroptosis- and iron-related genes.** The samples classified as conventional glioblastomas (GBM) were ulteriorly subdivided into the classical (n=5), mesenchymal (n=5) and proneural (n=5) subtypes, and the expression level of the considered genes was compared between the three groups (classical vs. mesenchymal vs. proneural). The statistical analysis was performed with ordinary one-way ANOVA, using Tukey's method for statistical hypothesis testing (* $p < 0.05$; ** $p < 0.01$; *** $p < 0.001$; **** $p < 0.0001$).

## *Characterization of the used GBM-CSC lines*

For the *in vitro* experiments, three cell lines of GBM stem cells, representative of three different subtypes of GBM, were used. BT302 and BT334 cell lines were isolated from conventional GBM of, respectively, the mesenchymal and classical subtype, while CT014 ϕ represents GBM tumors with a primitive neuronal component (GBM-PNC). Moreover, these

three cell lines differ in the deletion of chromosome arm 1p (BT302 are 1p-deleted, while BT334 and CT014 ϕ are not), a genetic alteration found in some GBM cases. This karyotypic alteration could be of interest because, among the genes located in this region, the one encoding cystathionine gamma-lyase (CTH) is involved in the transsulfuration pathway, whose downregulation may lead to the glutathione depletion, thus potentially promoting ferroptosis. If so, chromosome 1p deletion could be considered as a marker of cell sensitivity to ferroptosis.

As first step, the cell lines were characterized for the main ferroptosis- and iron-related mRNAs and proteins. Among antioxidant genes, *NFE2L2* mRNA was more expressed in BT334 cells by 2.2-fold than BT302 and by 3.3-fold than CT014 ϕ (Figure 3.4 A). Significantly lower levels of *SLC7A11* in BT302 cells were also detected (Figure 3.4 B), while there was a higher expression of *NQO1* in CT014 ϕ cells by about 4-fold compared to the conventional GBM-CSC lines (Figure 3.4 C). Next, we analyzed the expression of *ACSL3* and *ACSL4,* encoding two members of ACSL enzyme family that suppresses or promotes ferroptosis, respectively. The mRNA level of both *ACSL3* and *ACSL4* (Figure 3.4 D-E) was significantly lower in CT014 ϕ than in conventional GBM-CSC lines (ACSL3 mRNA by 7-fold compared to two other cell lines and ACSL4 mRNA by 2-fold compared to BT302). On the other hand, the expression of *GPX4* mRNA, encoding the main enzyme detoxifying lipid peroxides, was significantly higher in BT334 cells by 1.8-fold and 2.2-fold compared to BT302 and CT014 ϕ, respectively (Figure 3.4 F). The expression levels of *AIFM2*, *HMOX1*, *CHAC1* and *PTGS2* mRNAs were variable and did not show statistically significant differences (Figure 3.4 G-J). Regarding protein expression, ACSL4 was expressed at comparable level in all analyzed GBM-CSC lines, while FSP1 was detectable only in BT302 and CT014 ϕ (Figure 3.4 K).

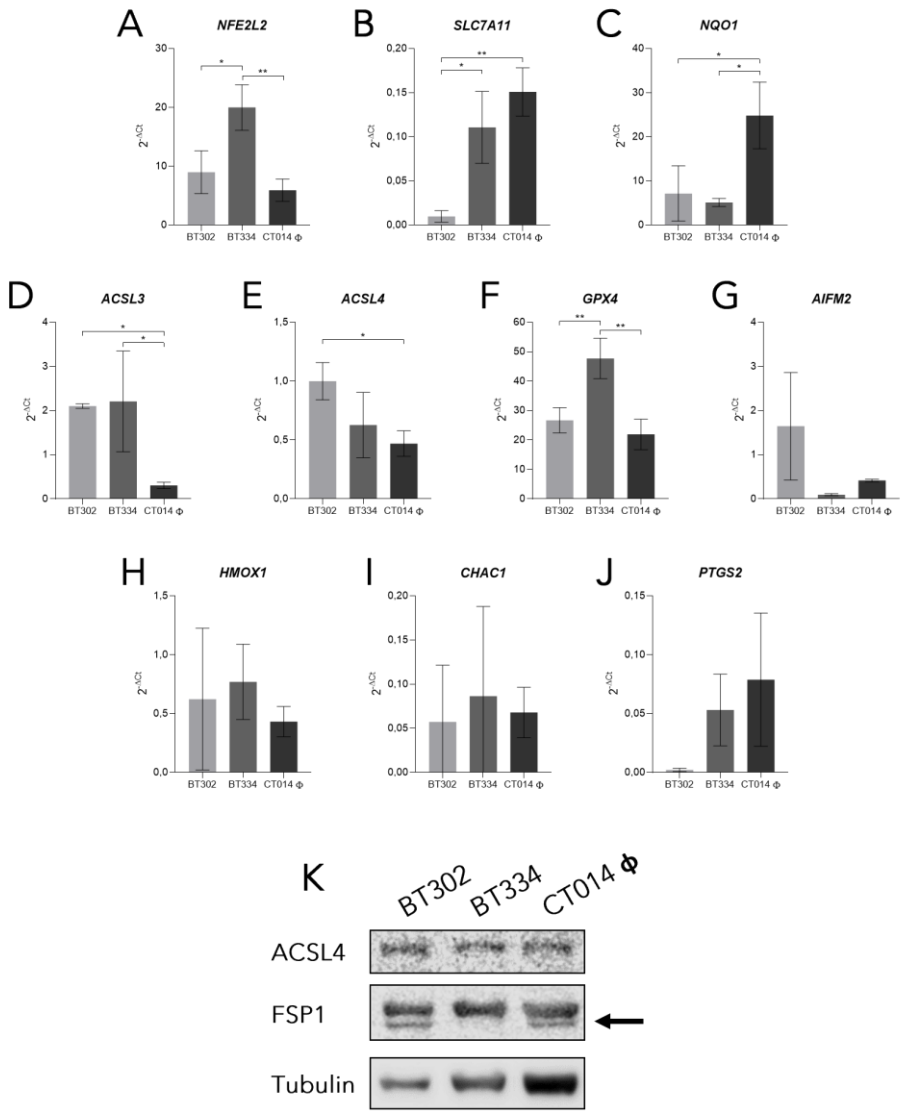


**Figure 3.4 – Characterization of the used GBM-CSC lines for ferroptosis-related genes and proteins.** Primary GBM-CSCs lines BT302 (representative of the mesenchymal subtype of conventional GBM), BT334 (representative of the classical subtype of conventional GBM) and CT014 Φ (representative of GBM with primitive neuronal component, or GBM-PNC) were analyzed for the mRNA expression of NFE2L2 (A), SLC7A11 (B), NQO1 (C), ACSL3 (D), ACSL4 (E), GPX4 (F), AIFM2 (G), HMOX1 (H), CHAC1 (I) and PTGS2 (J) by quantitative RT-PCR, and data were expressed as $2^{-\Delta Ct}$. Statistical analyses were performed with one-way ANOVA, using Tukey's method for statistical hypothesis testing (* $p < 0.05$; ** $p < 0.01$; *** $p < 0.001$; **** $p < 0.0001$). The protein expression of ACSL4 and FSP1 was analyzed by western blot, using β-tubulin as loading control (K).

Next, the study analyzed the expression of mRNAs and proteins of TfR1, FPN and Ferritin, involved in iron uptake, export and storage, respectively. The expression of *TFRC* mRNA did not differ significantly between the cell lines (Figure 3.5A), while FPN transcript (*SLC40A1*) level was higher in BT334 cells by 73-fold compared to BT302 and by 4.6-fold to CT014 ϕ (Figure 3.5 B). However, these transcript levels did not correspond to the protein level, TfR1 protein was expressed by all cell lines (at higher level in BT334 cells), while FPN was expressed in BT302 and scarcely detectable in BT334 and CT014 ϕ (Figure 3.5 E). The expression of mRNAs encoding ferritin subunits, FTL and FTH, was detectable in all cell lines

at different levels. The FTL transcript was significantly lower in CT014 ϕ cells by 6.6-fold and 9.5-fold than in BT302 and BT334, respectively. On the other hand, the same cell line (CT014 ϕ) was characterized by significantly higher FTH expression at mRNA (by 2.8-fold than BT334) and protein (by 2.2-fold and 2.8-fold than BT302 and BT334, respectively) levels (Figure 3.5 C-D, F), suggesting increased iron storage capability.

Altogether, these data do not allow the discrimination, as in primary tumor analysis, of a GBM-CSC line that could be sensitive or resistant to ferroptosis based on the specific gene and protein expression.

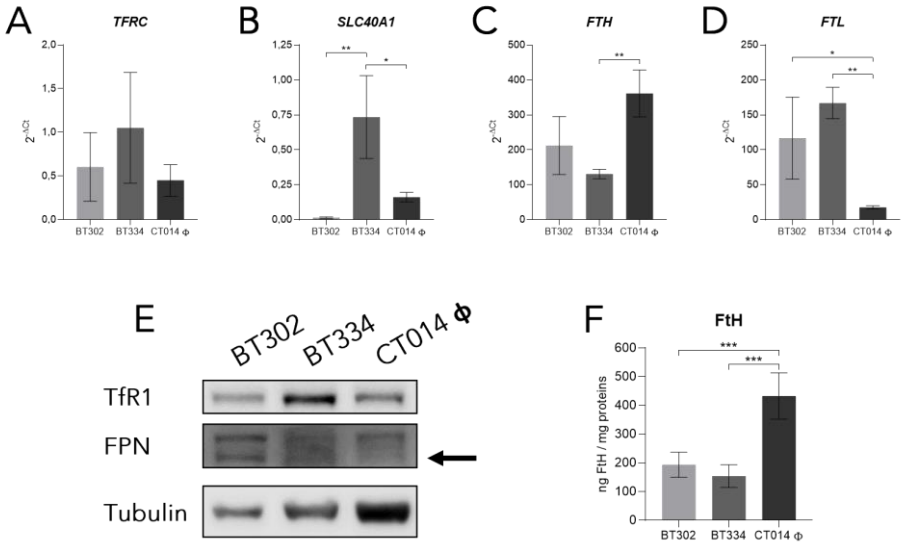


**Figure 3.5 – Characterization of the used GBM-CSC lines for iron-related genes and proteins.** Primary GBM-CSCs lines BT302 (representative of the mesenchymal subtype of conventional GBM), BT334 (representativeof the classical subtype of conventional GBM) and CT014 Φ (representative of GBM with primitive neuronal component, or GBM-PNC) were analyzed for the mRNA expression of TFRC (A), SLC40A1 (B), FTH (C) and FTL (D) by quantitative RT-PCR, and data were expressed as $2^{-\Delta Ct}$. The protein expression of TfR1 and FPN was analyzed by western blot, using β-tubulin as loading control (E). the protein content of H-ferritin was evaluated by ELISA assay (F). Statistical analyses were performed with one-way ANOVA, using Tukey's method for statistical hypothesis testing (* $p < 0.05$; ** $p < 0.01$; *** $p < 0.001$; **** $p < 0.0001$).

## *GBM-CSCs are sensitive to ferroptosis inducers*

To assess the effects of ferroptosis inducers on the cell viability of primary GBM-CSCs, cells were incubated with increasing doses of the system $X_c^-$ inhibitor erastin or of the GPX4 inhibitors RSL3 or ML162, and cell viability was assessed after 24, 48 and 72 hours of treatment. We found that all three cell lines showed a dose-dependent decrease of cell viability after the treatment with all the considered compounds. The treatment with erastin (Figure 3.6 A, D, G) caused a maximal reduction of cell viability to 50% at the dose of 40 μM, while significantly lower doses of RSL3 (Figure 3.6 B, E, H) and ML162 (Figure 3.6 C, F, I) were sufficient to reduce cell viability. BT302 cells were the most sensitive ones showing the

reduction of cell viability by about 50% after 24 h at 5 μM RSL3 (Figure 3.6 B) and 4.5 μM ML162 (Figure 3.6 C), BT334 at 8 μM RSL3 (Figure 3.6 E) and 5 μM ML162 (Figure 3.6 F), while CT014 ϕ cells at 9 μM RSL3 (Figure 3.6 H) and 5 μM ML162 (Figure 3.6 I). Moreover, while erastin reduced cell viability only in a dose-dependent manner, also a time-dependent effect on cell viability could be seen after the treatment with GPX4 inhibitors.

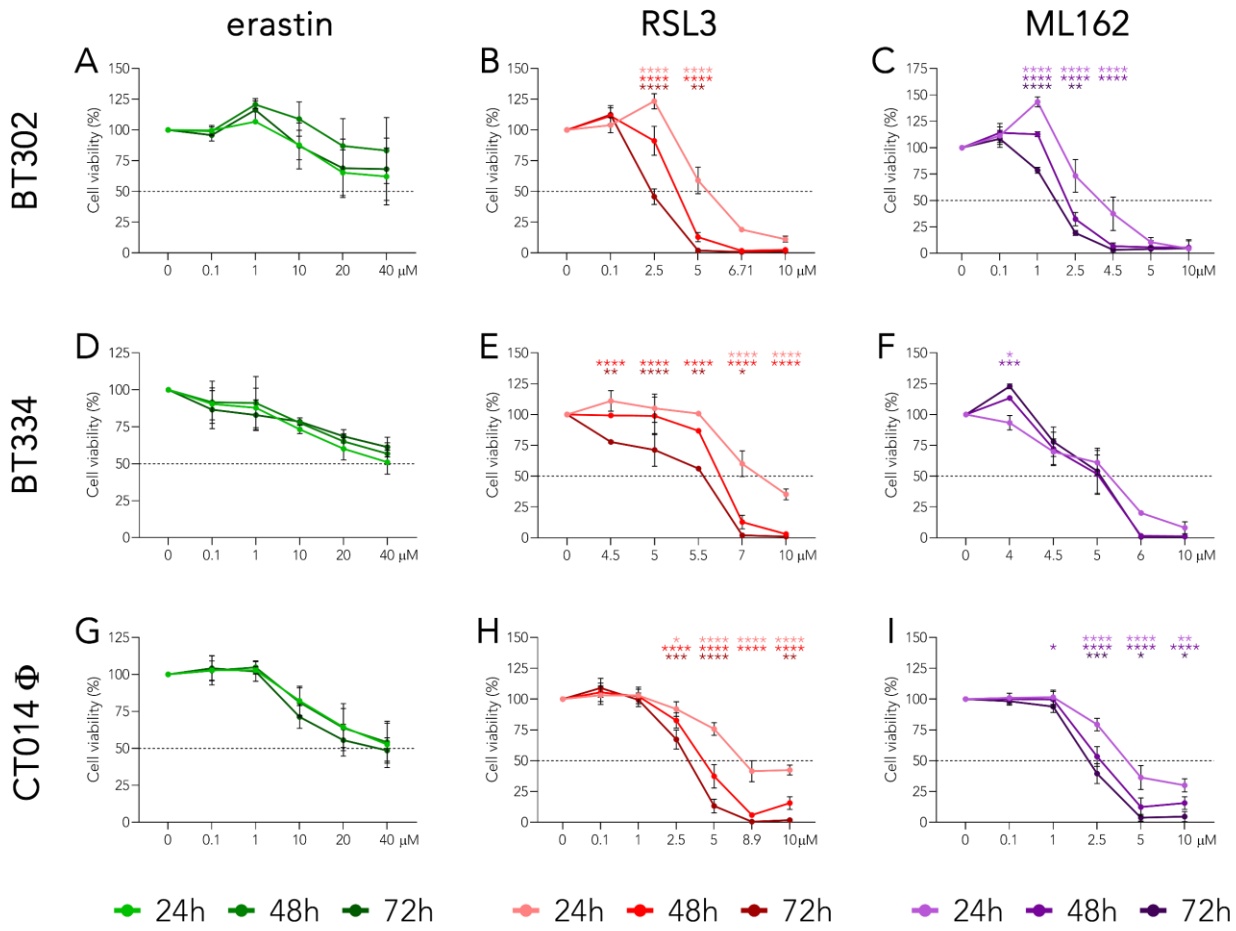


**Figure 3.6 – The viability of primary GBM-CSCs lines is reduced after a treatment with ferroptosis inducers.** BT302 (A-C), BT334 (D-F) and CT014 Φ cells (G-I) were treated with increasing concentrations of erastin (A, D, G), RSL3 (B, E, H) and ML162 (C, F, I) for 24, 48 and 72 hours. The cell viability was analyzed using RealTime-Glo™ MT Cell Viability Assay. The values are expressed as percentage of viable cells over the not treated cells at the indicated time points. The statistical analysis was performed with two-way ANOVA, using Tukey's method for statistical hypothesis testing; the light-colored stars correspond to the comparison between 24 h and 48 h, the medium-colored stars between 24 h and 72 h and the dark-colored stars between 48 h and 72 h (* $p < 0.05$; ** $p < 0.01$; *** $p < 0.001$; **** $p < 0.0001$).

Then, the study verified the cytotoxic effects of ferroptosis inducers on GBM-CSC lines by measuring the release in the culture medium of lactate dehydrogenase (LDH), caused by cell membrane rupture. The three analyzed cell lines were incubated with increasing doses of erastin, RSL3 or ML162, and then, the amount of LDH released in the medium was quantified after different times: for the conventional GBM cell lines BT302 and BT334, the measure of LDH release was performed after 24, 48 and 72 hour of treatment, while the

release of LDH from the GBM-PNC cell line CT014 ϕ was assessed after one week of treatment, since no significant variations were found after the aforementioned timepoints. We found that, in all the cell lines, the treatment with erastin did not cause cytotoxic effects, even at high concentration of 40 μM (Figure 3.7 A, D, G), while both GPX4 inhibitors RSL3 and ML162 were effective in increasing the release of LDH from cells in a dose-dependent manner at considerably lower doses (respectively, Figure 3.7 B, E, H and C, F, I). In details, BT302 cell line showed increased LDH release at doses 2.5-10 μM of RSL3 (Figure 3.7 B) and ML162 (Figure 3.7 C), BT334 cells demonstrated a trend (not statistically significant) at 10 μM RSL3 (Figure 3.7 E) and 5-10 μM ML162 (Figure 3.7 F), while CT014 ϕ at 5 μM RSL3 (Figure 3.7 H) and 5-10 μM ML162 (Figure 3.7 I).

Also, since GBM-CSCs lines grow in suspension forming the so-called neurospheres, and since the cytotoxic effects of chemical agents is reported to impair the formation of spheres in culture (Galli, 2019), we monitored the morphological changes that cells underwent after 72 hours of treatment with ferroptosis inducers for BT302 and BT334 and after 1 week of treatment for CT014 ϕ cells. It was observed that increasing concentrations of erastin were able to reduce the formation of neurospheres, while increasing the presence of single cells in all analyzed GBM-CSC lines (Figure 3.7 J). On the other hand, the same effect was observed only after lower doses of RSL3 and ML162, while at higher concentrations the cells demonstrated morphological changes, such as shrinkage and visible cell debris (Figure 3.7K, L), suggesting the cell death.

These data confirm that GPX4 inhibitors caused the reduction of cell viability due to the cytotoxicity and as a result the cell death, while the inhibition of the system $X_c^-$ antiporter channel had rather a cytostatic effect.

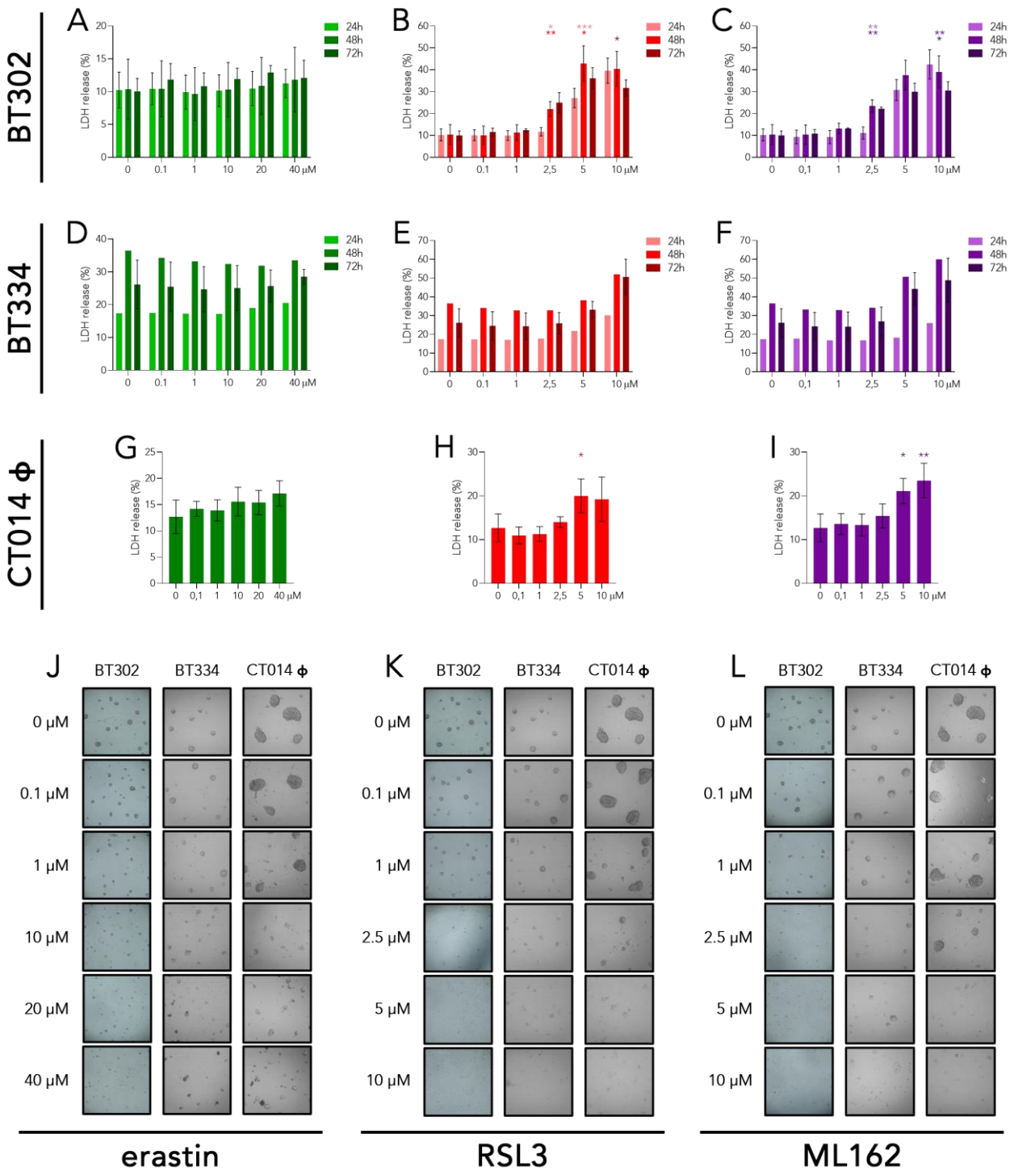


**Figure 3.7 – Ferroptosis inducers have cytotoxic effects on GBM-CSCs lines, impeding the normal formation of neurospheres.** BT302 (A, D, G), BT334 (B, E, H) and CT014 Φ cells (C, F, I) were treated with increasing concentrations of erastin, RSL3, and ML162, for 24, 48 and 72 hours for BT302 and BT334, and for 7 days for CT014 Φ cells. LDH release (A-I) was analyzed using the LDH Cytotoxicity Assay Kit. The values are expressed as percentage of LDH released in tested sample over lysed cells at the indicated time points. The statistical analysis was performed with two-way ANOVA, using Tukey's method for statistical hypothesis testing; the light-colored stars correspond to the comparison between 24 h and 48 h, the medium-colored stars between 24 h and 72 h and the dark-colored stars between 48 h and 72 h (* $p < 0.05$; ** $p < 0.01$; *** $p < 0.001$; **** $p < 0.0001$). The images for macroscopic analysis (J, K, L) were taken after 72 hours of the treatment for BT302 and BT334, and after 7 days for CT014 Φ cells.

## *Ferroptosis is partially involved in FINs-mediated cell death of GBM-CSCs*

To verify if the type of cell death induced by GPX4 inhibitors was ferroptosis, all three cell lines were co-treated with the ferroptosis inducers RSL3 (at the concentration of 5 μM for BT302, 7 μM for BT334, and 8.9 μM for CT014 ϕ) or ML162 (at the concentration of 4.5 μM for BT302, 5 μM for BT334, and 5 μM for CT014 ϕ) and with the ferroptosis inhibitors 100 μM DFO or 10 μM ferrostatin-1 (Fer-1) for 24 hours. The study found that ferroptosis inhibitors could only partially rescue FINs-induced cell mortality in BT302 by 15-25% in RSL3-treated cells (Figure 3.8 A) and by 25-35% in the ML162-treated ones (Figure 3.8 D), and in CT014 ϕ cells by 20% for ML162-DFO co-treated cells (Figure 3.8 E), while the study could not detect differences between treated and co-treated cells in BT334 (Figure 3.8 C, F) and RSL3-treated CT014 ϕ cells (Figure 3.8 B).

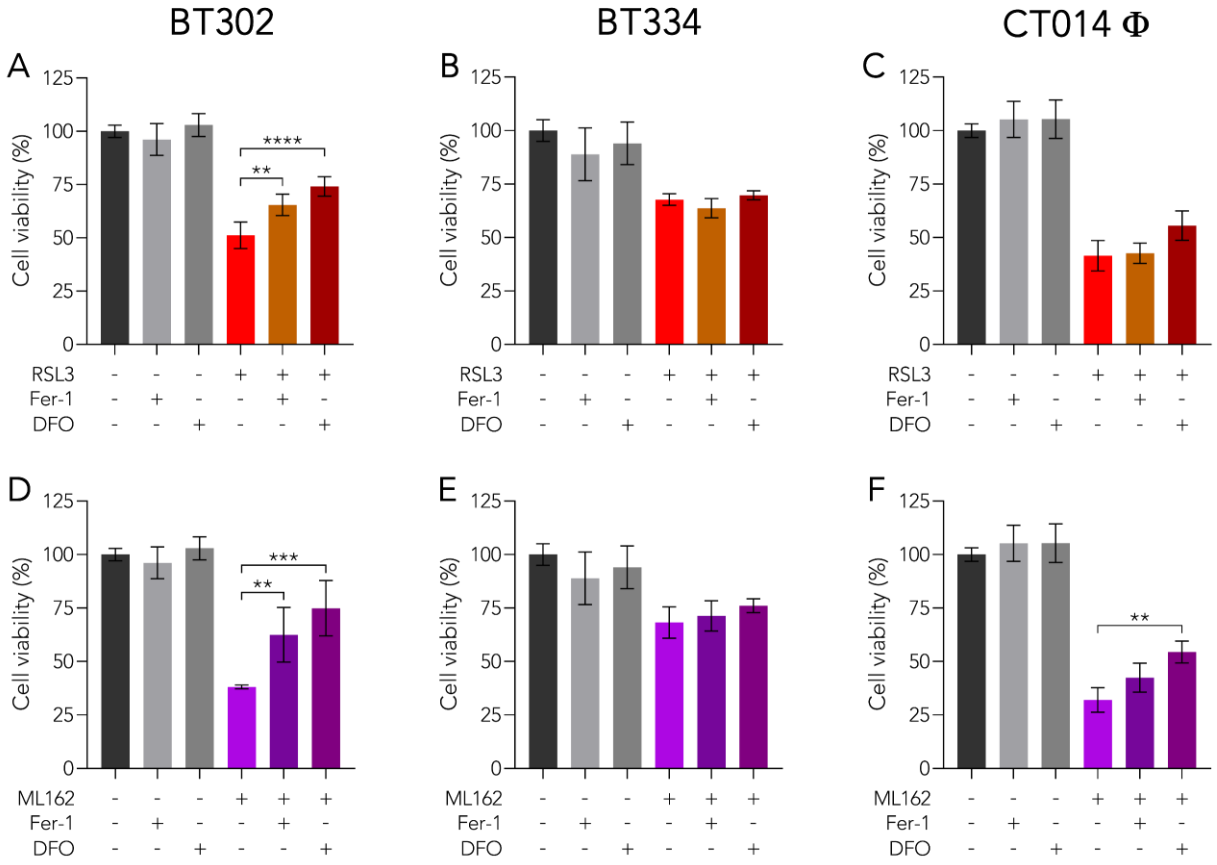


**Figure 3.8 – The co-treatment with FINs and ferroptosis inhibitors partially rescues the cell viability of GBM-CSCs lines.** BT302, BT334 and CT014 Φ cells were co-treated with RSL3 (at the concentration of 5 μM for BT302, 7 μM for BT334, and 8.9 μM for CT014 Φ, shown respectively in A, B and C) or ML162 (at the concentration of 4.5 μM for BT302, 5 μM for BT334, and 5 μM for CT014 Φ, shown respectively in D, E and F) and with the ferroptosis inhibitors 100 μM DFO or 10 μM ferrostatin-1, Fer-1) for 24 hours. The cell viability was analyzed using RealTime-Glo™ MT Cell Viability Assay. The values are expressed as percentage of viable cells over the not treated cells at the indicated time points. The statistical analysis was performed with ordinary one-way ANOVA, using Tukey's method for statistical hypothesis testing (* $p < 0.05$; ** $p < 0.01$; *** $p < 0.001$; **** $p < 0.0001$).

To further confirm ferroptosis induction after the treatment with FINs, BT302 cells were treated with sublethal doses of RSL3 (2.5 μM) or ML162 (1 μM) in presence or absence of both ferroptosis inhibitors 100 μM DFO) and 10 μM Fer-1. Then, after 24 hours of treatment, lipid peroxidation was analyzed using C11/BODIPY$^{581/591}$ probe. Treatment with ferroptosis inducers alone increased the amount of lipid peroxides, while the co-treatment with ferroptosis inhibitors significantly countered lipid ROS generation in these cells (Figure 3.9), thus confirming ferroptosis as one of the types of cell death involved.

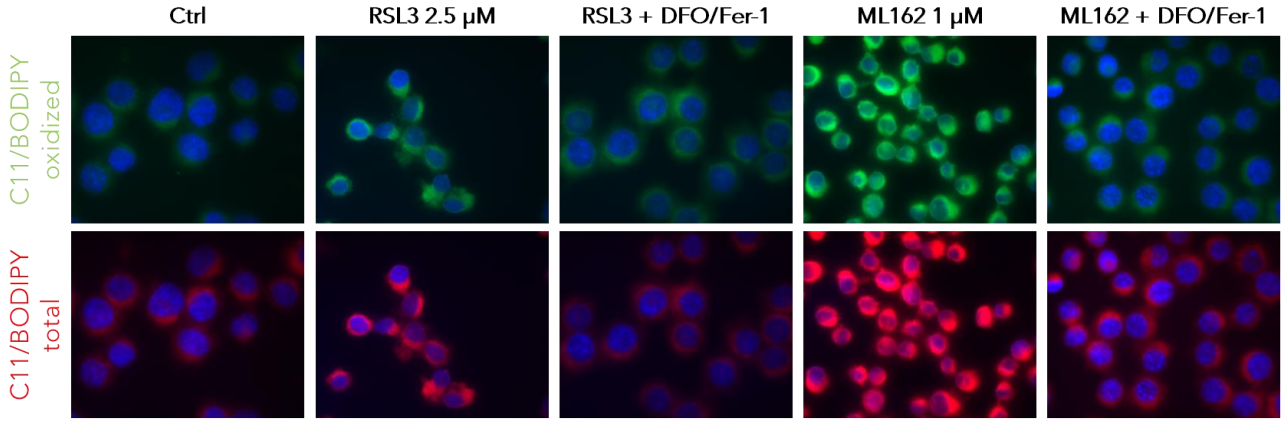


**Figure 3.9 – BT302 cells show increased lipid peroxide content after both RSL3 and ML162 treatment.** BT302 cells were treated with 2.5 μM RSL3 or 1 μM ML162 in presence or in absence of both ferroptosis inhibitors 100 μM DFO and 10 μM Fer-1 for 24 hours. For the lipid ROS analysis, cells were stained with C11/BODIPY$^{581/591}$ and counterstained with DAPI. Images were obtained by fluorescent microscopy using a 63x magnification (with immersion) using the FITC, RHOD and DAPI filters to visualize, respectively, the oxidized probe, the total probe, and the nuclei.

## *BT302 cells are sensitive to the combined effect of TMZ and FINs*

Since the use of the alkylating agent temozolomide (TMZ) is the current gold standard in systemic treatment of GBM, we wanted to test our cell lines for their sensitivity to this molecule. Therefore, cells were incubated with increasing doses of TMZ, and cell viability was assessed after 24, 48 and 72 hours of treatment. The study found that only BT302 cells showed a dose- and time-dependent reduction of cell viability after the treatment (Figure 3.10 A). Contrarily, the viability of BT334 cells was not affected by TMZ, even at the dose of 1 mM (Figure 3.10 B), while minor effect could be seen in CT014 ϕ cells at the highest doses and after 72 hours of treatment (Figure 3.10 C). Since BT302 showed greater sensitivity to TMZ treatment comparing to the other cell lines, and since GSH availability in GBM has been inversely correlated to their TMZ response (Chen *et al.*, 2015), the study sought if TMZ could also alter the lipid peroxide content, whose neutralization is also dependent on GSH utilization by GPX4. It was found that a 24-hours exposure to 100 μM TMZ (a condition that resulted non-toxic in this cell line) increased lipid peroxidation in BT302 cells (Figure 3.10

D). These data suggest that, in addition to the canonical induction of apoptosis, also ferroptotic cell death could be involved in TMZ-mediated cytotoxicity.

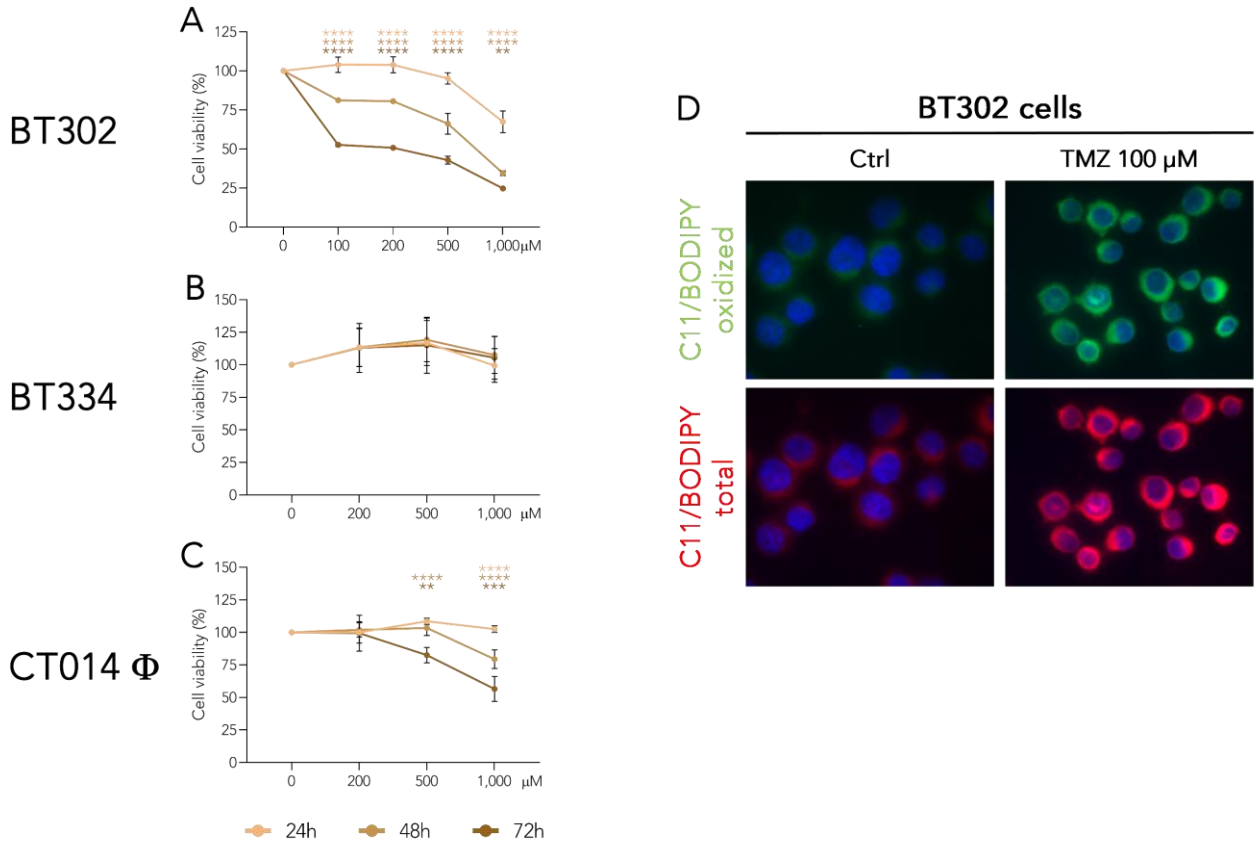


**Figure 3.10 – TMZ reduces only the cell viability of BT302 cells, in which also increases the lipid peroxide content.** For the cell viability experiments, BT302 (A), BT334 (B) and CT014 Φ cells (C) were treated with increasing doses of TMZ for 24, 48 and 72 hours. The cell viability was analyzed using RealTime-Glo™ MT Cell Viability Assay. The values are expressed as percentage of viable cells over the not treated cells at the indicated time points. The statistical analysis was performed with two-way ANOVA, using Tukey's method for statistical hypothesis testing; the light-gold stars correspond to the comparison between 24h and 48h, the gold stars between 24h and 72h and the dark-gold stars between 48h and 72 h (* $p < 0.05$; ** $p < 0.01$; *** $p < 0.001$; **** $p < 0.0001$). For the lipid ROS analysis (D), BT302 were treated with 100 µM TMZ for 24 hours. Then, cells were stained with C11/BODIPY$^{581/591}$ and counterstained with DAPI. Images were obtained by fluorescent microscopy using a 63x magnification (with immersion) using the FITC, RHOD and DAPI filters to visualize, respectively, the oxidized probe, the total probe, and the nuclei.

Finally, studies were aimed to test if the ferroptosis inducers would sensitize GBM-CSCs to TMZ. Therefore, the three cell lines were treated with sublethal doses of TMZ (100 µM for BT302, 1000 µM for BT334, and 500 µM for CT014 ϕ) and RSL3 (2.5 µM for BT302, 4.5 µM for BT334, and 2.5 µM for CT014 ϕ), alone or in combination, and cell viability was assessed after 24, 48 and 72 hours of treatment. Surprisingly, the combination of the two agents effectively reduced cell viability only in BT302 cells by about 30-40% (Figure 3.11 A), while no effect could be observed in BT334 (Figure 3.11 B) nor in CT014 ϕ cells (Figure 3.11 C).

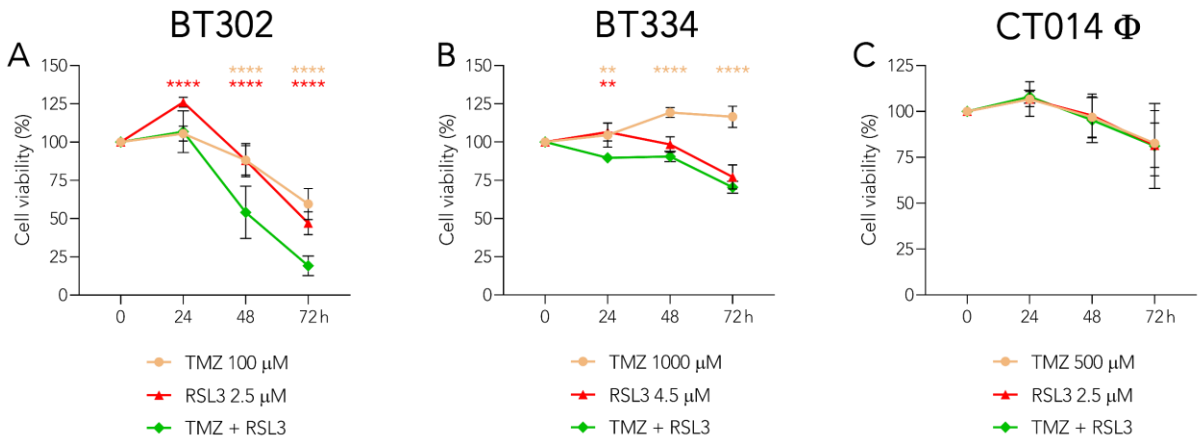


**Figure 3.11 – RSL3 increases the efficacy of TMZ in BT302 cells but not in BT334 nor CT014 Φ cells.** BT302 (A), BT334 (B) and CT014 Φ cells (C) were treated with sublethal doses of TMZ (100 µM for BT302, 1000 µM for BT334, and 500 µM for CT014 Φ) and RSL3 (2.5 µM for BT302, 4.5 µM for BT334, and 2.5 µM for CT014 Φ), alone or in combination, for 24, 48 and 72 hours. The cell viability was analyzed using RealTime-Glo™ MT Cell Viability Assay. The values are expressed as percentage of viable cells over the not treated cells at the indicated time points. The statistical analysis was performed with two-way ANOVA, using Tukey's method for statistical hypothesis testing; the gold stars correspond to the comparison between the TMZ-RSL3 combined treatment and the TMZ-alone treatment, while the red stars correspond to the comparison between the TMZ-RSL3 combined treatment and the RSL3-alone treatment (* $p < 0.05$; ** $p < 0.01$; *** $p < 0.001$; **** $p < 0.0001$).

Altogether, these data show that BT302 cells are the most susceptible ones to the ferroptosis inducers RSL3 and ML162, that can also sensitize these cells to TMZ, the chemotherapeutic agent currently used for GBM treatment.

# Discussion

Glioblastoma (GBM), the most frequent tumor of the central nervous system, is a devastating disease that is still characterized by poor patient prognosis (Ostrom *et al.*, 2022). Despite the profound efforts that have been made in the finding of new therapeutic strategies, tumor recurrence is still frequent, along with resistance to current therapies (Thakur *et al.*, 2022). The presence in GBM of a staminal component, referred to as glioblastoma cancer stem cells (GBM-CSCs), which is less sensitive to the commonly used antitumor strategies, have been identified as responsible for tumor relapse, giving rise to secondary and more aggressive tumors (Liu *et al.*, 2006; Xie *et al.*, 2022). Ferroptosis is characterized by increased levels of intracellular iron and reduced antioxidant defense, which promote excessive lipid peroxide accumulation in cell membranes, thus leading to cell death (Stockwell, 2022). The use of ferroptosis-inducing agents (FINs) has been demonstrated to be effective in reducing tumor progression, targeting the antiporter channel system $X_c^-$ (which mediates the import of cystine, used for the synthesis of glutathione) and the selenoenzyme GPX4 (which, using glutathione as a cofactor, neutralizes lipid peroxides) (Stockwell and Jiang, 2020). Interestingly, ferroptosis-inducing agents (FINs) have been demonstrated effective in reducing, both *in vitro* and *in vivo*, the proliferation of GBM cell lines (Wang *et al.*, 2019; Li *et al.*, 2021).

The current study aimed to assess the sensitivity to ferroptosis inducers in GBM cancer stem cells (GBM-CSCs), and to test their effect in combination with temozolomide (TMZ), the chemotherapeutic agent currently approved for the treatment of glioblastoma. To this aim, three primary GBM-CSC lines were used, namely BT302 (derived from mesenchymal subtype of conventional GBM, characterized by chromosome 1p deletion), BT334 (representative of the classical subtype of conventional GBM) and CT014 ϕ cells (representative of GBM with primitive neuronal component, or GBM-PNC).

Firstly, the study analyzed RNA sequencing data of patient-derived GBM samples. The study did not find any gene expression pattern that could suggest higher sensitivity or resistance to ferroptosis of a specific GBM subtype. Likewise, the characterization of the three cell lines for the expression of iron- and ferroptosis-related mRNAs and proteins did not indicate the GBM-CSC lines as potentially susceptible to ferroptosis. Although GBM-CSC lines are valuable and reliable *in vitro* models to study GBM, they do not fully recapitulate the

conditions and the microenvironment of the tumor, thus there can be some slight discrepancy between the gene expression in the patient-derived GBM samples regarding their representative cell lines.

Next, studies analyzed the GBM-CSC sensitivity to class I (erastin) and class II (RSL3, ML162) FINs. The cell viability of all analyzed cell lines was suppressed by FINs, with the class II (GPX4 inhibitors) showing distinctly higher efficiency. The occurrence of ferroptosis, as one of the cytotoxic mechanisms involved, was confirmed by the lipid ROS accumulation after a treatment with GPX4 inhibitors and the cell viability rescue after co-treatment with ferroptosis inhibitors, Fer-1 and DFO. Among the GBM-CSC lines, BT302 cells seem to be the most sensitive for RSL3- and ML162-induced ferroptosis. On the other hand, erastin had rather cytostatic effect on GBM-CSC lines as shown by cell viability, LDH release and macroscopic analyses. These results suggest that, in GBM-CSC lines, the inhibition of GPX4 has greater impact on cell viability than the impairment of glutathione synthesis.

Since GBM-CSCs are characterized by chemoresistance (Beier, Schulz and Beier, 2011; Singh *et al.*, 2021), the three cell lines were analyzed for the cell sensitivity to the gold-standard chemotherapeutic agent temozolomide. Only BT302 cells showed dose- and time-dependent reduction of cell viability, even if at high dosages, while BT334 and CT014 ϕ cells showed minor or no sensitivity to TMZ. Also, this difference was observed between the cell lines after a combined treatment with TMZ and the ferroptosis inducer RSL3, which showed synergistic effect in reducing the cell viability only in BT302 cells. The chromosome arm 1p deletion, occurring in the BT302 cell line, causes the absence of the gene encoding for the enzyme cystathionine γ-lyase, involved in the production of cysteine from the transsulfuration pathway, which in turn sustains glutathione synthesis (Sbodio, Snyder and Paul, 2019). Also, higher glutathione levels in glioma samples have been correlated with resistance to TMZ and poorer prognosis in patients (Zhu *et al.*, 2018), and TMZ has been observed to cause, among the others, also cell death by ferroptosis (Buccarelli *et al.*, 2018). Thus, BT302 cells may be more sensitive to temozolomide and ferroptosis due to reduced glutathione content, and the ferroptosis-inducing properties of TMZ could contribute to the increased sensitivity of BT302 cells to ferroptosis; in addition, chromosome 1p deletion could become a predictive marker of sensitivity to ferroptosis in GBM. Although it has been demonstrated that GBM-CSCs with EGFR overexpression are more sensitive to TMZ treatment (Cominelli *et al.*, 2015), the BT334 cell line representing the classical GBM subtype

with *EGFR* amplification did not show any changes in the cell viability after the treatment. However, in the current study used different technique for the cell viability analysis and different conditions. The strongest effect of TMZ treatment is observed after 7-10 days, while at 72 h (as the last time point) the TMZ did not significantly affect cell viability (Cominelli *et al.*, 2015). On the other hand, TMZ resistance was confirmed in CT014 ϕ cells, representing PNC component of rare and aggressive GBM-PNC variant (Perry *et al.*, 2009; Prelaj *et al.*, 2018).

In conclusion, the data demonstrated that the use of ferroptosis inducers represents a promising new therapeutical strategy for the treatment of GBM and for counteracting GBM recurrence caused by cancer stem cells. However, this antitumor strategy requires further studies to confirm its efficiency against all GBM subtypes to ascertain or define specificity or selectivity based on the genotype and molecular profiles of the different GBM subtypes.

# 4- Rhabdomyosarcoma, iron and ferroptosis

# Introduction

## *Clinical features*

Rhabdomyosarcoma (RMS) is a high-grade, malignant neoplasm deriving from mesenchymal cells that failed to undergo myogenic differentiation. It is the most common soft tissue sarcoma in children, accounting approximately for 3.5% of pediatric cancers (Agaram, 2022). Globally, it has a frequency of 4.5 patients per million individuals and it has been reported that RMS occurs predominantly in young children from birth to 4 years and in adolescents between 15 and 19 years (Van Gaal *et al.*, 2012). However, due to the rarity of the disease, both the epidemiology and the classification of RMS remain uncertain (Skapek *et al.*, 2019).

Independently from the primary site of development, four subtypes of RMS can be distinguished, namely, embryonal RMS (ERMS), alveolar RMS (ARMS), pleomorphic RMS (PRMS, occurring typically in adults) and spindle cell/sclerosing RMS (ScRMS, a variant that occurs only in children).

Embryonal and alveolar RMS, the two subtypes object of the current research of this thesis, are the most represented among pediatric RMS, with ERMS occurring 3 times more frequently than ARMS (60% of RMS cases are reported to be ERMS, while 20% of the total are classified as ARMS), with a better prognosis, while the alveolar subtype is more aggressive. (Skapek *et al.*, 2019; Ramadan *et al.*, 2020). Morphologically, ERMS cells resemble immature skeletal myoblasts (Patton and Horn, 1962), while ARMS cells appear distributed around an open central space (Enterline and Horn, 1958). RMS can arise in a variety of sites throughout the body, the most frequent being the head and neck region (35%) and the genitourinary tract (24%), and extremity sites (19%). Being highly aggressive, metastases in lung, bone and bone marrow are very frequent and already present in non-detectable sizes in all new diagnoses, constituting the main reason of therapy failure (Van Gaal *et al.*, 2012; Skapek *et al.*, 2019).

## *Molecular alterations*

The main molecular alterations observed in ERMS are reported to be various point mutations and karyotypic alterations, which lead to activation of extracellular regulated kinases 1 and 2 (ERK1/2) and phosphatidylinositol-4,5-bisphosphate 3-kinase (PI3K)

signaling pathways, and to the inactivation of the tumor suppressor gene p53 pathway (Monti and Fanzani, 2016).

In contrast, the major molecular alteration detected in ARMS are related to the chromosomal translocation involving the fusion of the Pair Box (PAX) gene with the transactivation domain of FOXO genes, leading to the formation of the PAX-FOXO oncoprotein (Ramadan *et al.*, 2020). The most frequent fusion genes are PAX3-FOXO1 or, less frequently, PAX7-FOXO1 fusion genes due to chromosomal translocations involving chromosomes 2 (on which PAX3 is located), or chromosome 1 (containing PAX7), and chromosome 13 (containing FOXO1, also named FKHR), which are referred to as t(2;13) and t(1;13), respectively (Shern *et al.*, 2014; Skapek *et al.*, 2019).

The formation of a fusion gene does not occur in all ARMS tumors, since it has been found in about 80% of the total cases of the ARMS (60% of the total cases characterized by PAX3-FOXO1 and in the other 20% characterized by PAX7-FOXO1), giving this subgroup the name "fusion-positive RMS" (FPRMS, or also FP). The remaining 20% of ARMS cases is called "fusion-negative RMS" (FNRMS, or FN), and shares morphological and molecular features with ERMS. It has been reported that this new proposed classification in FP- and FN-tumors could better subdivide RMS in subtypes characterized by, respectively, poorer and more favorable prognosis (Skapek *et al.*, 2019), indicating that this criterion could contribute to the risk stratification and the choice of the therapeutic strategy (Williamson *et al.*, 2010). More precisely, the presence of PAX3-FOXO1 identifies the group with the highest aggressiveness, while the prognosis of other FP-tumors (comprising PAX7-FOXO1 and other minorly represented, recently discovered fusion genes like PAX3-NCOA1, PAX3-NCOA2 and PAX3-INO80D) is more favorable and similar to the one of FN-tumors (Missiaglia *et al.*, 2012). Figure 4.1 schematizes the main differences between the embryonal and the alveolar subtypes of RMS.

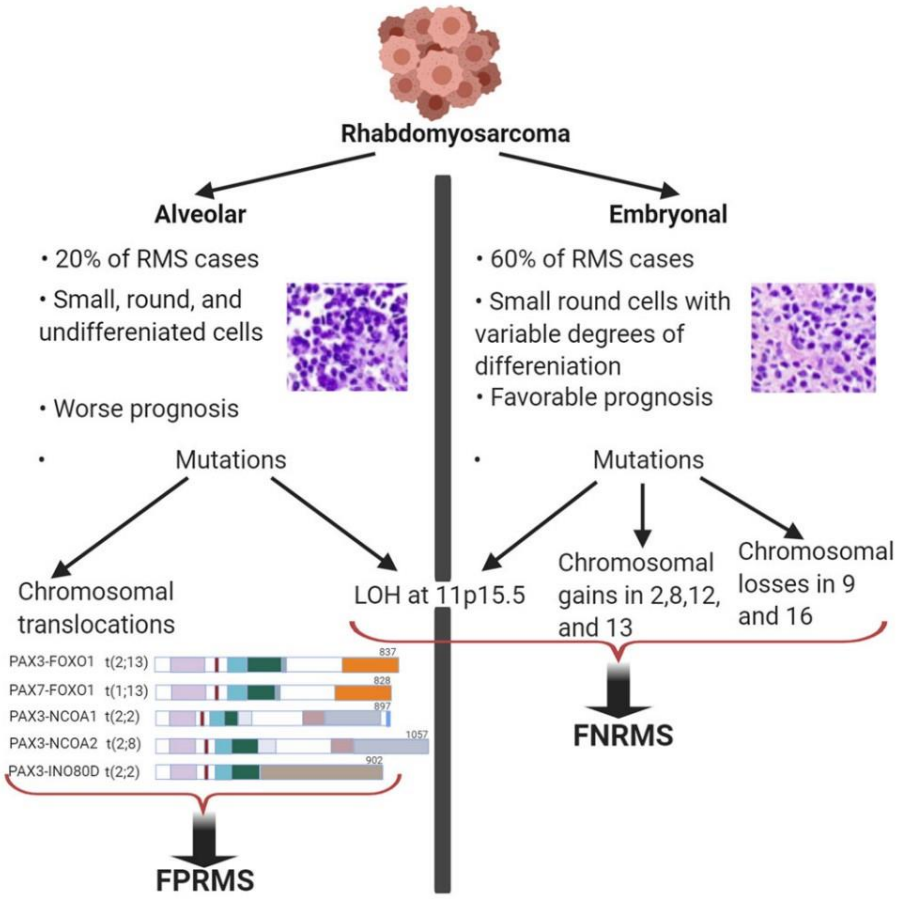


Figure 4.1 – Schematization of alveolar (ARMS) and embryonal (ERMS) rhabdomyosarcoma frequency and their main molecular alterations. Among all cases of rhabdomyosarcoma (RMS), the 60% are classified as ERMS, of which 20% is caused by the more aggressive ARMS. However, a more precise classification has been proposed, dividing RMS in fusion-positive (FP-) and fusion-negative (FN-) RMS. The first is distinguished by the presence of fusion genes, the most frequent being PAX3-FOXO1 and PAX7-FOXO1, while the second is characterized by a wider mutational burden, such as loss of the region 11p15.5, whole chromosome gains and losses and a series of point mutations. In terms of prognosis, this new division fits better with prognostic values, with the PAX3-FOXO1 mutated tumors having the worst prognosis, while the other FP-tumors are characterized by a higher survival expectancy, together with all FN-tumors, with which prognostic resemblance occurs (Ramadan *et al.*, 2020).

## *RMS and Caveolin-1*

In addition to the molecular alteration observed in RMS reported above, another class of proteins, caveolins, have been shown to be altered in RMS, having a role in its invasiveness and metastatic potential. This family of proteins is composed by three members, caveolin-1, -2 and -3, which are required for the formation of caveolae (invaginations of the cell membrane enriched for several signal transduction mediators), but also for the regulation of a plethora of signal transduction mediators and scaffolding proteins on the cell membrane. In normal conditions, Cav-1 and Cav-2 are expressed ubiquitously in the body, while Cav-3 selectively marks differentiated myofibers (Rossi, Poliani, Missale, *et al.*, 2011). Contrarily, in muscular tissue, Cav-1 has been reported to be expressed only in satellite cells,

which are responsible for muscle repair after damage, maintaining them in a quiescence status that is abolished after tissue injury, where a switch of expression from Cav-1 to Cav-3 has been reported (Volonte, Liu and Galbiati, 2005).

In particular, Cav-1 has been identified as a key protein in maintaining energy homeostasis by regulating energy metabolism and contributing to the signal transduction of glucose and lipid metabolism-related pathways (Baudrand *et al.*, 2016). Cav-1 has been reported to act as a docking site on the cell membrane for glycolytic enzymes such as phosphofructose kinase and aldolase, along with promoting GLUT4-mediated glucose uptake, thus increasing the glycolytic activity of cells (Yuan *et al.*, 2007; Nwosu *et al.*, 2016). Also, increased Cav-1 levels have been reported to stabilize the electron transport chain complexes in mitochondria, stabilizing mitochondrial function and protecting cells from apoptosis (Fridolfsson *et al.*, 2012; Volonte *et al.*, 2016; Raudenska *et al.*, 2020).

Also, Cav-1 is involved in both the initial formation of lipid droplets in the endoplasmic reticulum (Pezeshkian, Chevrot and Khandelia, 2018) and in the decoration of lipid droplets surface (Robenek *et al.*, 2004). Moreover, Cav-1 can directly interact with fatty acids (Trigatti, Anderson and Gerber, 1999), and has a high affinity for cholesterol (Murata *et al.*, 1995), and contributes to both its transport to the cell membrane, to its localization for caveolae formation from lipid rafts, and to its distribution throughout the cell (Smart *et al.*, 1996; Gokani and Bhatt, 2022). Interestingly, among the others, Cav-1 has been demonstrated to interact with fatty acid translocase (FAT, or CD36), promoting its translocation to caveolae and FAT-mediated uptake of long-chain fatty acids (Ring *et al.*, 2006).

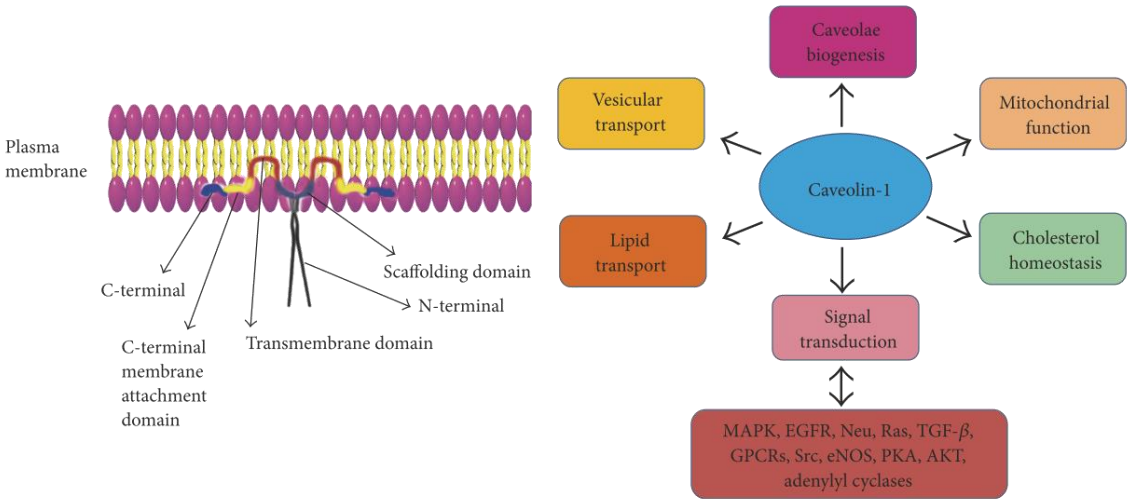


**Figure 4.2 – An overview of the roles of caveolin-1 in cellular signaling.** Caveolin-1 is an integral membrane protein with a hairpin-like conformation that is found in caveolae as a homodimer. The N-terminal domain of caveolin-1 extrudes into the cytoplasm, and can interact with various intracellular messengers that in turn modulate various biological processes (such as mitochondrial function, lipid transport and cholesterol homeostasis) and numerous signaling pathways (such as the MAPK cascade and the TGF-β signaling) (modified from Wang *et al.*, 2017).

The exact role of Cav-1 in cancer progression has not been fully elucidated yet, as both tumor-promoting and tumor-suppressing roles have been reported, depending on different cancer types and on cell differentiation status (Raudenska *et al.*, 2020). In RMS, Cav-1, which is mainly expressed in ERMS cell lines, correlates with immature phenotype, while Cav-3, more strongly expressed in ARMS cells, is indicative of a more differentiated phenotype and also in ERMS subtypes with a higher degree of differentiation, downregulation of Cav-1 in favor of an increase in Cav-3 expression can be observed, mimicking the differential expression reported in normal tissues (Rossi, Poliani, Missale, *et al.*, 2011). Therefore, due to its correlation with poor differentiation, the role of Cav-1 has been studied in RMS, revealing that its expression in tumor cells causes both activation or repression of genes and proteins of the MEK/ERK signaling. This ambiguous behavior suggests that, in normal conditions, Cav-1 expression has an anti-carcinogenic role, while, during tumor progression, Cav-1 switches its function to being a tumor promoter, thereby leading to aggressive cell behavior and tumor metastasis (Rossi, Poliani, Cominelli, *et al.*, 2011; Ketteler and Klein, 2018).

In both ERMS and ARMS cell lines, Cav-1 has been reported to be constitutively phosphorylated on tyrosine 14 (pCav-1) by Src kinase. In addition, the overexpression of Cav-1 led to the enhanced activation state of ERK kinase in the RD cell line (representative of ERMS) and of AKT kinase in the RH30 cell line (representative of ARMS), thus increasing cell proliferation, migration, invasiveness and chemoresistance and reducing apoptosis. This

was also confirmed with the silencing of Cav-1 or the inhibition of its phosphorylation, which reduced the proliferation and the aggressiveness of both RMS cell lines, thus confirming the pivotal role of Cav-1 in tumor progression (Faggi *et al.*, 2014). Moreover, recently it has been reported that Cav-1-overezpressing RMS cell lines showed increased radioresistance, with enhanced DNA repair and protection against cellular senescence and apoptosis from oxidative stress (Codenotti *et al.*, 2021).

*In vivo*, the injection both subcutaneously and in the tail vein of NOD/SCID mice with Cav-1-overexpressing RD cells was shown to promote, respectively, faster tumor growth and the formation of a higher number of pulmonary metastases compared to control RD cells. Then, cells derived from metastases were isolated, cultured *in vitro* and re-injected into the mice. This procedure was repeated twice, to obtain respectively $RD^{F1}$ and $RD^{F2}$ derived cell lines, which were confirmed to have an even more aggressive phenotype than the previous generation $RD^{F0}$, with a progressive increase of lung metastases number (Codenotti *et al.*, 2019).

All the three derived RD cell lines overexpressing Cav-1 ($RD^{F0}$, $RD^{F1}$ and $RD^{F2}$) were characterized by higher levels of ERK1/2 phosphorylation, along with decreased levels of marker of myogenic differentiations such as MyoD, MHC and myogenin, higher capacity of wound healing and ever-increasing sprouting ability compared to the control cells $RD^{ctrl}$, confirming the aggressive phenotype observed *in vivo* (Codenotti *et al.*, 2019).

## *Treatment and management of rhabdomyosarcoma*

The first-line intervention for RMS is the surgical resection of the identified tissue mass, and then, the adoption of two alternative chemotherapeutic strategies. The US guidelines recommend aggressive treatments with the combination of high doses of vincristine, actinomycin D and cyclophosphamide (commonly named "VAC") in order to inhibit the formation and the progression of metastases, while the European mindset suggests a milder approach with the association of lower dosages of ifosfamide, vincristine and actinomycin D (known as "IVA") to avoid subsequent side effects and improve the quality of life in case of remission, with the possibility of dosage increase in case of poor clinical response (Miwa *et al.*, 2020). However, it has been reported that both approaches obtained similar responses on tumor reduction, with the only difference of being the side effects observed. Nowadays, in addition to the attempts at further increasing the overall survival rates of

patients using the conventional therapy, significant attention is also paid to the improvement of the quality of life after disease remission (Van Gaal *et al.*, 2012; Skapek *et al.*, 2019).

Among the treatment modalities, ionizing radiation (IR) therapy is also used as a standard strategy to decrease tumor recurrence, above all when the complete resection of the mass is not possible, particularly for the advanced-state RMS (Kaseb, Kuhn and Babiker, 2021). Radiotherapy is recommended for the treatment of RMS at all stages (except for localized ERMS tumors staged in a low-risk class), and receiving a radiotherapeutic treatment is often correlated with a better response (Million *et al.*, 2011; Yechieli *et al.*, 2021).

Unfortunately, as reported for many tumors, RMS can frequently develop resistance to the currently used treatments, both chemotherapy and irradiation. Thus, new therapeutic approaches such as ferroptosis are required, and new targets are being investigated.

## *Iron metabolism and ferroptosis in rhabdomyosarcoma*

Iron metabolism has been poorly studied in RMS. Recent studies showed that cell lines that represented both ERMS (RD, SMS, RH36 cell lines) and ARMS (RH4, RH18, RH30 cell lines) expressed detectable levels of iron related proteins and genes such as TfR1, FPN, FTL and FTH, whose expression was affected with short-term iron supplementation or with iron chelators. These results confirmed that iron is essential for their survival and RMS cell lines are capable of maintaining the balance between the iron demand and the iron toxicity to modulate the expression of iron metabolism proteins (Asperti *et al.*, 2023).

In addition, iron chelation and supplementation were reported to reduce cell viability of both ERMS and ARMS cell lines in a dose-dependent manner, while also reducing their motility and the colony formation capability. Interestingly also, in an *in vivo* xenograft mouse model, treatment with iron loading or iron chelators both reduced the tumor mass and the expression of both the proliferative marker Ki-67 and the angiogenesis marker CD31, with the iron chelating strategy being the most effective one (Asperti *et al.*, 2023).

In this context, the use of a chemical compound that could chelate iron and at the same time inhibit the activity of an enzyme essential for cell survival such as the ribonucleotide reductase (RR), could be a promising strategy to counteract RMS's growth.

Ribonucleotide reductase (RR) is the sole enzyme in the cell capable of catalyzing the formation of deoxyribonucleotides from the corresponding ribonucleotides and it is one of the 50 most overexpressed genes in cancer (Ruskoski and Boal, 2021). The RR holoenzyme is a tetramer composed by two catalytic subunits, RRM1, containing the catalytic site, and two regulatory subunits, RRM2 or RRM2B, which contain a tyrosyl radical site essential for the reaction initiation (Foskolou *et al.*, 2017). As with many cellular enzymes (Mackenzie, Iwasaki and Tsuji, 2008; Lane *et al.*, 2015; Puig *et al.*, 2017), RR requires an iron for tyrosyl radical generation. In detail, two $Fe^{2+}$ atoms are incorporated in the subunit during the first steps of folding, then the rapid addition of one oxygen molecule and the transfer of an electron from an adjacent amino acid causes the formation of a $Fe_2^{III/IV}$ intermediate that ultimately oxidizes Tyr122 to generate the tyrosyl radical (Ruskoski and Boal, 2021). In this context, studies on human leukemia K562 cells demonstrated that iron depletion caused the reduction of RR activity, dNTPs pool, DNA synthesis and cell proliferation (Cavanaugh *et al.*, 1985; Furukawa *et al.*, 1992).

The compound didox (3,4-dihydroxybenzohydroxamic acid) is a potent synthetic inhibitor of RRM2, being about 20 times more effective and causing fewer side effects than its precursor, hydroxyurea (HU), the first RR inhibitor approved for clinical use (Elford, Wampler and Riet, 1979; Riet, Wampler and Elford, 1979; Musiałek and Rybaczek, 2021). Although didox has been already tested in various clinical studies on sarcoma, melanoma and breast cancer patients (Veale *et al.*, 1988; Carmichael *et al.*, 1990; Rubens *et al.*, 1991) causing only mild toxicities, it was found to be ineffective, therefore further studies on patients were not conducted. More recently, didox has been repurposed for combined treatments with alkylating agents. Its use with temozolomide (Figul *et al.*, 2003) or carmustine (Horvath *et al.*, 2004) in brain cancer cell lines, with doxorubicin in liver and breast cancer (Al-Abd *et al.*, 2013; Wilson *et al.*, 2021) and with tamoxifen in breast cancer (Shah *et al.*, 2015) showed a synergic effect, causing a downregulation of DNA repair mechanisms and therefore an increase in DNA damage, as well as preventing resistance mechanisms in tumor cells. From previous studies, it is known that didox is a molecule characterized by two mechanisms of action. It acts as a reversible RRM2 inhibitor, due to the radical scavenging action of the hydroxy groups on the tyrosyl radical of RRM2 (Elford, Wampler and Riet, 1979; Saban and Bujak, 2009), and as an iron chelator, due to the catechol-like moiety enabling binding of iron (Fritzer-Szekeres *et al.*, 1997; Asperti *et al.*, 2019). Since iron is an essential cofactor for

RRM2 activity, both functions of didox are responsible for RR inhibition (Elford and Van't Riet, 1985; Szekeres, Fritzer-Szekeres and Elford, 1997).

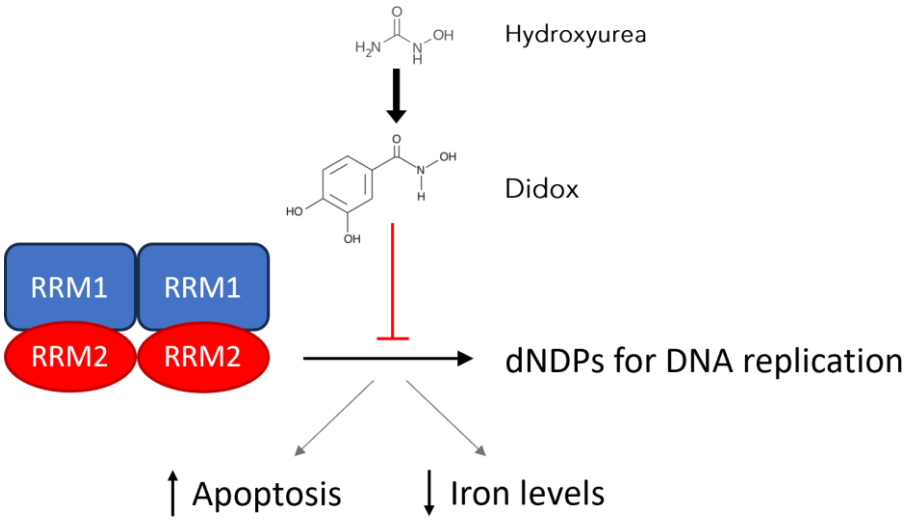


**Figure 4.3 – Brief overview of the mechanism of action of didox.** Developed based on the small molecule hydroxyurea, didox (3,4-dihydroxybenzohydroxamic acid) has been demonstrated as a potent inhibitor of RRM2. This protein is the regulatory subunit of the enzyme ribonucleotide reductase and, together with the catalytic subunit RRM1, is responsible for the rapid production of dNTPs necessary to the duplication of the genome. Also, after its first application as RRM2 inhibitor, didox has also been discovered an iron chelator, being able to reduce the amount of bioavailable iron in cancer cells.

As for iron metabolism, to date, only few works explored the ferroptotic cell death in RMS. However, in the past years, several research highlighted the strict relationship between rhabdomyosarcoma and oxidative stress (Hochwald *et al.*, 1997; Castro *et al.*, 2002; Seitz *et al.*, 2010; Zitka *et al.*, 2012). The overexpression of Nrf2 has been observed in primary RMS tumors, suggesting a strong dependence of this tumors on antioxidant pathways. Coherently, a high GSH/GSSG ratio has been found in four patient-derived RMS biopsies, indicating a great effort in maintaining oxidative stress under control (Zitka *et al.*, 2012). More interestingly, the tumors derived from patients treated with chemotherapeutic drugs were more aggressive and had a higher content of GSH than the non-treated ones, and that lower intracellular levels of GSH correlated with increased radio- and chemosensitivity and a less aggressive behavior, while higher GSH levels were observed in high-grade tumors. Moreover, it was reported that the levels of the γ-glutamyl transpeptidase (GGTP, the enzyme responsible for extracellular GSH hydrolysis), correlated with the malignant characteristics of the tumor (Hochwald *et al.*, 1997).

In addition, the combination of traditional chemotherapeutics such as vincristine, doxorubicin and topotecan with GST inhibitors potentiate the reduction of cell viability

(Seitz *et al.*, 2010). Also, GSH depletion in RMS cell lines has been reported to reduce their tumorigenicity, confirming the dependency of RMS on glutathione-dependent antioxidant mechanisms (Castro *et al.*, 2002).

To date, all the published studies regarding ferroptosis and RMS confirmed that different RMS cell lines (both representative ERMS and ARMS) are sensitive to ferroptosis inducers in a dose and time dependent manner, with RSL3 being the most potent one (Schott *et al.*, 2015; Habermann *et al.*, 2017; Codenotti *et al.*, 2018; Dächert *et al.*, 2020).

The treatment of RD cells (ERMS) and RH30 cells (ARMS) with erastin or RSL3 led to increased cell membrane permeability, ROS, and lipid peroxides levels, and to reduced intracellular GSH levels, causing ferroptotic cell death. Coherently, cell death could be rescued by antioxidant molecules (such as Fer-1, Lip-1 and α-tocopherol), iron chelators (such as DFO and bathophenanthroline sulfonate, BPS) and, in only in the case of erastin treatment, by GSH (or its precursor, N-acetylcysteine, NAC, used as an alternative cellular source of cysteine) (Schott *et al.*, 2015; Codenotti *et al.*, 2018; Dächert *et al.*, 2020).

Also, erastin and BSO have been co-administered in RD cells with the thioredoxin reductase inhibitor auranofin, resulting in the synergic induction of ferroptosis cell death (Habermann *et al.*, 2017).

Taken together, all these data seem to be promising, since both ERMS and ARMS have been shown to be sensitive to ferroptosis inducers. This could open a new prospective for new therapeutic tools for the managing or RMS in case of development of both drug and IR resistance. The current study therefore aimed to investigate the effects of the iron chelator didox on RMS progression and, separately, to examine the mechanism of ferroptosis in Cav-1-overexpressing ERMS cells.

# Materials and methods

## *Antibodies and Chemicals*

Didox was purchased by Cayman Chemicals (cat. n. 10009081) and resuspended in dimethyl sulfoxide (DMSO) at the concentration of 20 mg/mL for *in vitro* studies or at the concentration of 200 mg/mL for *in vivo* studies. Hydroxyurea (HU) was purchased by Sigma-Aldrich (cat. n. H8627) and resuspended in DMSO at the concentration of 20 mg/mL, analogously to didox.

Erastin was purchased from Selleckchem (cat. no. S7242) and resuspended in DMSO at the concentration of 10 mM. RSL3 was purchased from Sigma Aldrich (cat. no. SML2234) and resuspended in DMSO at the concentration of 4.5 mM. ML162 was purchased from Sigma Aldrich (cat. no. SML2561) and resuspended in DMSO at the concentration of 10 mM. Triacsin C was purchased from Cayman Chemicals (cat. no. 10007448) and resuspended in DMSO at the concentration of 5 mg/mL. Deferrioxamine (DFO) was purchased from Sigma Aldrich (cat. no. D9533) and fresh 20 mM stock solutions were made in sterile dd$H_2O$ prior use. Fatty acids-free bovine serum albumin (FFA-BSA, cat. no. A8806) was purchased from Sigma Aldrich, and working solutions were made by dissolving FFA-BSA in complete medium at a concentration of 333.3 µM, and the solution was then filtered using a 0.22 µm pores PES filter. Palmitic acid (cat. no. P0500), oleic acid (cat. no. O1383), linoleic acid (cat. no. L1012), α- linoleic acid (cat. no. L2376), γ-linolenic acid (cat. no. L2378) and arachidonic acid (cat. no. 10931) were all purchased from Sigma Aldrich and stocked at -20°C. Dilutions of fatty acids (FA) were made in ethanol at the concentration of 50 mM, and then stocked at -20°C up to 1 month, then fresh dilutions were reprepared. Treatment medium was prepared by dissolving the 50 mM stock dilutions of FA in complete medium containing FFA-BSA, with a FA:FFA-BSA ratio of 3:1. Then, solutions were incubated for 30 minutes at 37°C in agitation to promote FA binding to BSA before being delivered to cells.

The antibodies used in this study were anti-TfR1 (cat. no. 136800, Thermo Scientific, Waltham, MA, USA), anti-Ferroportin (cat. no. NBP1-21502, Novus Biologicals, Centennial, CO, USA), anti-FSP1 (cat. no. sc-377120, Santa Cruz Biotechnology, Dallas, TX, USA), anti-ACSL4 (cat. no. sc-271800, Santa Cruz Biotechnology, Dallas, TX, USA) and anti-tubulin (cat. no. T5168, Sigma-Aldrich, Saint Louis, MO, USA). HRP-conjugated secondary

antibodies used were anti-mouse (cat. no. sc-516102, Santa Cruz Biotechnology, Dallas, TX, USA) and anti-rabbit (cat. no. sc-2357, Santa Cruz Biotechnology, Dallas, TX, USA).

C11-BODIPY$^{581/591}$ probe was purchased from Thermo Scientific (cat. no. D-3861) and resuspended in DMSO at a concentration of 2.5 mM.

For the transient silencing of ACSL4, MISSION® esiRNA targeting human ACSL4 (cat. no. EHU087251) and EGFP (cat. no. EHUEGFP) were purchased from Sigma Aldrich and used, respectively, for ACSL4 silencing and as a negative control for transfection.

### *Rhabdomyosarcoma (RMS) cell lines*

Human embryonal rhabdomyosarcoma cell line RD and human alveolar rhabdomyosarcoma cell line RH30 were obtained from Prof. Alessandro Fanzani's group from University of Brescia (who, purchased from the European Collection of Cell Cultures, ECACC, Salisbury, UK) was cultured in Dulbecco's Modified Eagle Medium (DMEM, EuroClone, Pero, MI, Italy) supplemented with 10% endotoxin-free fetal bovine serum (Gibco, Life Technologies, Carlsbad, CA, USA), 0.04 mg/mL gentamicin sulfate (EuroClone, Pero, MI, Italy), 2mM L-glutamine (EuroClone, Pero, MI, Italy) and 1mM sodium pyruvate (EuroClone, Pero, MI, Italy). Cells were maintained at 37°C with 5% $CO_2$.

RD control cells (referred as RD mock) and RD cells overexpressing caveolin-1 (referred as RD Cav-1 F2) were generated by Prof. Alessandro Fanzani's group from University of Brescia, as described in Faggi *et al.*, 2014. Both RD mock and RD Cav-1 F2 cell lines, were cultured in complete DMEM medium and only RD Cav-1 F2 in the presence of 0.5 mg/mL geneticin, as antibiotic selection (InvivoGen, Toulouse, France) in order to maintain the stable overexpression of Cav-1, which was then removed during experiments.

### *Cell Treatments*

For the time-course experiments with didox and hydroxyurea (HU), RD and RH30 cells were seeded in a 96-wells plate (at a density of 2,500 cells/well for RD and at a density of 1,000 cells/well for RH30) and exposed to various concentrations of didox or hydroxyurea (0, 1, 10, 25, 50, 100, 200 and 500 μM) for 24, 48 and 72 hours, then cell viability was evaluated with an MTT assay.

RD mock and RD Cav-1 F2 were seeded in 96-wells plates (at a density of 3,000 and 1,000 cells/well, respectively) and, 24 hours after seeding, cells were treated with various

concentrations of triacsin C (0.25-0.5-1-2.5-5-7.5 and 10 μM) for 24 and 48 hours, then cell viability was evaluated with an MTT assay.

For the combined treatments with the pan-ACSL inhibitor triacsin C and ferroptosis inducers, RD Cav-1 F2 cells were seeded in 96-wells plates and, the day after seeding, medium was removed and 50 μL of triacsin C at sublethal concentration (0.25 μM) were added. Then, after 16 hours, 50 μL of medium were added, containing the same concentration of triacsin C plus the various ferroptosis inducers: 1 μM erastin, 1 μM RSL3 or 5 μM ML162. Then, after a 24-hours treatment, cell viability was evaluated with an MTT assay.

For the treatment with fatty acids RD Cav-1 F2 cells were seeded in 96-wells plates (at a density of 1,000 cells/well) and, the day after seeding, cells were pre-treated for 16 hours with sublethal concentrations of fatty acids: 62.5 μM palmitic:oleic (PA:OA, in a 1:2 ratio), 250 μM linoleic acid (LA), 250 μM α-linolenic acid (α-LNA), 62.5 μM γ-linolenic acid (γ-LNA), 62.5 μM arachidonic acid (AA). Then, medium was removed, and cells were exposed to 0.15 μM RSL3 (without adding the fatty acids). Then, after a 24-hours treatment, cell viability was evaluated by MTT assay.

### *Cell Viability Assay*

The cell viability was evaluated by MTT assay (3-[4,5-dimethyl-2- thiazolyl]-2,5-diphenyl-2H-tetrazolium bromide, cod. M5655, Sigma-Aldrich, Saint Louis, MO). At the indicated time points after treatments, the supernatant was removed and 100 μL of cell medium containing 0.5 mg/mL MTT were added in each well. After 3.5 hours of incubation at 37°C and 5% $CO_2$, the MTT-containing medium was removed and 75 μL of DMSO were added to each well. Plates were shaken for 15 minutes at 37°C until complete dissolution of formazan crystals and absorbance was measured at 540 nm emission wavelength using a Multiskan©EX plate reader (Thermo Scientific, Waltham, MA, USA). The percentage of cell viability at each concentration was calculated using Microsoft Excel 2016 software, and the $IC_{50}$ doses for each treatment were interpolated from the dose-response data using GraphPad Prism 8's integrated nonlinear regression tool.

### *Oil Red O staining for lipids*

For the Oil Red O staining for the lipid uptake evaluation RD Cav-1 F2 cells were seeded in 24-wells plates (at a density of 9,500 cells/well) and, 24 hours after seeding, cells were treated

with various doses of fatty acids. Then, cells were washed in PBS 1X and then fixed in 4% paraformaldehyde (PFA) for 30 minutes at 4°C. Then, fixed cells were washes again in PBS 1X, incubated in 60% isopropanol for 5 minutes at room temperature (RT) and, immediately after, stained with Oil Red O working solution for 5 minutes at RT. Then, cells were washed three times in dd$H_2O$, and, after drying, images were taken. For dye quantification, Oil Red O staining was solubilized in 100% isopropanol, and the absorbance of the resulting solution was measured at 540 nm emission wavelength using a Multiskan©EX plate reader (Thermo Scientific, Waltham, MA, USA). Then, fixed cells were washed three times in dd$H_2O$, and then stained with Crystal Violet solution (0.2% Crystal violet, 20% methanol in PBS 1X) for 15 min at RT. Then, cells were washed in dd$H_2O$, and the staining was solubilized in 10% acetic acid. The amount of Oil Red O dye internalized by cells was then normalized on the number of cells by dividing the absorbance results from Oil Red O solution by the absorbance of the Crystal violet solution, and results were expressed as percentage of internalized dye (considering the not-treated cells as 100%).

### *Silencing of ACSL4*

The transient silencing of ACSL4 was performed using esiRNA in RD Cav-1-F2 cells. Briefly, 10,000 RD Cav-1-F2 cells were seeded into 24-wells plate. After 24 hours, cells were transfected with 25 pmol esiRNA ACSL4 or EGFP as control, using RNAiMAX, following the manufacturer's instructions, in a final volume of 2 mL of media without FBS. After 6 hours from the transfection, media was changed with DMEM containing 5% FBS. The day after, a second round of transfection was performed and 6 hours after, cells were added or not with the ferroptosis inducer RSL3 at a concentration of 0.5 µM and incubated for other 24 hours. Cells were collected for protein extraction to verify the efficiency of the transfection for the analysis of ACSL4 protein by Western blot. MTT assay was performed to define the cell viability after ferroptosis inducers.

## *RNA extraction and gene expression analysis using qPCR*

RNA was obtained with TRI Reagent (Sigma-Aldrich) and cDNA was generated using ImProm-II™ Reverse-Transcription System kit (Promega, Madison, WI) according to the manufacturer's instructions. Real time qPCR was performed using SsoAdvanced Universal SYBR Green Supermix (cat. no. 1725274, BioRad, Hercules, CA, USA), according to the manufacturer's instructions, for *ACSL1*, *ACSL3*, *ACSL4*, *ACSL5*, *ACSL6*, *ACLY*, *ACACA*, *FASN*, *SCD*, *SREBP1*, *SREBP2*, *GPX4*, *HMOX1*, and *TXNR* mRNA detection, normalized to *TBP* and expressed as $2^{-\Delta Ct}$. The sequences of the forward and reverse primers used for the amplification of targets are the following:

| | | |
|---|---|---|
| Hs TBP | Hs TBP F | GAACATCATGGATCAGAACAACA |
| | Hs TBP R | ATAGGGATTCCGGGAGTCAT |
| Hs TxnR1 | Hs TxnR1 F | GGTCCAACCTTGAAGGCTTA |
| | Hs TxnR1 R | CATATTGGGCTGCCTCCTTA |
| Hs HO-1 | Hs HO-1 F | GCTGTAGGGCTTTATGCCATGT |
| | Hs HO-1 R | GGCTCCTTCCTCCTTTCCAGAG |
| Hs α-SREBP1 | Hs α-SREBP1 F | ACAGTGACTTCCCTGGCCTAT |
| | Hs α-SREBP1 R | GCATGGACGGGTACATCTTCAA |
| Hs α-SREBP2 | Hs α-SREBP2 F | CTGCAACAACAGACGGTAATGA |
| | Hs α-SREBP2 R | CCATTGGCCGTTTGTGTCAG |
| Hs α-FASN | Hs α-FASN F | AAGGACCTGTCTAGGTTTGATGC |
| | Hs α-FASN R | TGGCTTCATAGGTGACTTCCA |
| Hs α-ACACA (ACC-α) | Hs α-ACACA (ACC-α) F | ATGTCTGGCTTGCACCTAGTA |
| | Hs α-ACACA (ACC-α) R | CCCCAAAGCGAGTAACAAATTCT |
| Hs α-ACLY | Hs α-ACLY F | TCGGCCAAGGCAATTTCAGAG |
| | Hs α-ACLY R | CGAGCATACTTGAACCGATTCT |
| Hs SCD | Hs SCD F | TCTAGCTCCTATACCACCACCA |
| | Hs SCD R | TCGTCTCCAACTTATCTCCTCC |
| Hs ACSL1 | hACSL1 F | CCATGAGCTGTTCCGGTATTT |
| | hACSL1 R | CCGAAGCCCATAAGCGTGTT |
| Hs ACSL3 | Hs ACSL3 F | GGCGTAGCGGTTTTGACA |
| | Hs ACSL3 R | CCAGTCCTTCCCAACAACGA |
| Hs ACSL4 | Hs ACSL4 F | ACTGGCCGACCTAAGGGAG |
| | Hs ACSL4 R | GCCAAAGGCAAGTAGCCAATA |
| Hs ACSL5 | Hs ACSL5 F | CCCCATGTCCACTTCAGTCAT |
| | Hs ACSL5 R | GTGCATTCTGTTTGACCATAAGCT |
| Hs ACSL6 | Hs ACSL6 F | GTGTTGGCTTCTTCCAGGGAGA |
| | Hs ACSL6 R | GGTGTGTTTGCCTGGCTGAAGA |
| Hs GPX4 | Hs GPX4 F | GCCATCAAGTGGAACTTCACC |
| | Hs GPX4 R | CTTCTCTATCACCAGGGGCTC |

**Table 4.1 – Primers sequences.**

## Protein Extraction

Cells extracts were prepared using an ice-cold lysis buffer composed of 200 mM Tris-HCl pH 8, 100 mM NaCl, 1 mM EDTA, 0.5% NP-40, 10% glycerol, 1 mM sodium fluoride, 1 mM sodium orthovanadate and Complete Protease Inhibitor Cocktail (Sigma-Aldrich) and stored at -20°C until analysis. Protein concentration was quantified using the Bicinchoninic Acid Kit for Protein Determination (Sigma-Aldrich, Saint Louis, MO, USA) and used for different analysis by western blotting and ELISA assays.

## Western Blot Analysis

Western blot was used to analyze protein expression. In brief, after extraction, protein homogenates (30-60 µg) were boiled at 99°C for 5 minutes before separation by SDS-polyacrylamide gel electrophoresis and transferred to a 0.45 µM pore-sized nitrocellulose membrane (Sartorius AG, Hottingen, Germany). Membranes were incubated for 1 hour at RT with Blocking solution (Tris-buffered saline + 0.1% Tween-20 (TBS-T) with 2% milk) and incubated overnight at 4°C (or 2 hours at 37°C) with primary antibodies (reported in the "Antibodies and chemicals" paragraph). Following three TBS-T washings, membranes were incubated with HRP-conjugated secondary antibodies for 2 hours at RT. Membranes were washed again in TBS-T prior to signal visualization using enhanced chemiluminescence (PDS kit, Protein Detection System, GeneSpin, Milan, Italy). The signal was visualized with a LI-COR Odyssey (LI-COR Biosciences GmbH, Bad Homburg, Germany) or by the exposure onto CL-XPosure Film (Thermo Scientific), and densitometric analysis was performed using Image Studio Lite TM Software (LI-COR Biosciences GmbH, Bad Homburg, Germany), normalized against tubulin as a loading control and expressed as fold change over the not-treated cells.

## ELISA Assay

Ninety-six-wells plates were coated with 0.1 mL of primary antibody against H-ferritin (RH02) at the concentration of 10 µg/mL diluted in 50 mM carbonate buffer pH 9.6 for 18 hours at 4°C. After three washes with PBS-T (phosphate buffer saline with 0,1% Tween20), wells were over-coated by adding 0.1 mL of 3% bovine serum albumin (BSA) diluted in PBS for 1h at 37°C. After three washes with PBS-T, 100 µg of protein extract were rated in duplicate, diluted in 1% BSA-PBS-T and incubated at 37°C for 2 hours. A standard curve using recombinant human H-ferritin was used as calibrator. After three washings in PBS-T, 0.1 mL

of HRP-labelled anti-H-ferritin antibody (diluted 1:500 in 1% BSA-PBS-T) were added and plate incubated for 1 hour at 37°C. After three washings in PBS-T, HRP activity was detected using 1 mg/mL tetramethylbenzene (TMB) dissolved in dimethyl sulfoxide (DMSO) and diluted 1:10 in phosphate-citrate buffer pH 5 (added with fresh hydrogen peroxide to a final concentration of 0,006%) and the absorbance of the solution was read at 620 nm with a Multiskan©EX plate reader until signal development. Then, the reaction was stopped by adding 0.1 mL of 1 N sulfuric acid, and the absorbance was measured at 405 nm. The concentration of H-ferritin was extrapolated from the calibrator curve and expressed as ng of ferritin/mg of protein extract.

## *Colony Assay*

RD and RH30 cells were seeded in 12-wells plates (at the concentration of 1,000 cells/well for RD and 500 cells/well for RH30) and, after 48 hours from the seeding, were treated with didox at the concentrations of 0, 1, 10, 25, 50 and 100 μM. After 48 hours, the treatment was removed and cells were left in culture medium until the formation of colonies (one week for RD and four days for RH30), then colonies were fixed in 4% PFA and stained with crystal violet solution.

RD mock and RD Cav-1 F2 cells were seeded in 6-wells plates (at the concentration of 1,000 and 500 cells/well, respectively). 48 hours after seeding, cells were treated with different concentrations of triacsin C (0.25-0.5-1- 2.5-5 μM), and after 24 hours of treatment, media was replaced with fresh one. Cells were then cultured until well-defined colonies had formed (3 days for RD Cav-1 F2 and 6 days for RD mock), and then colonies were washed in PBS 1X, fixed in 4% PFA for 15 minutes at RT, and stained with Crystal Violet solution (0.2% Crystal violet, 20% methanol in PBS 1X) for 15 min at RT. The dishes were washed with deionized water and representative pictures of the colonies were taken.

The clonogenic capability of cells was evaluated by dissolving the coloration with 1% SDS in PBS 1X and by measuring the absorbance at 540 nm of the resulting solution using a Multiskan©EX plate reader (Thermo Scientific, Waltham, MA). The graphed data derive from the normalization of each value over the absorbance of the not-treated cells.

## Cell Motility Assay

RD and RH30 cells were seeded in 6-wells plates at a concentration of 200,000 cells/well and, when 90% confluence was reached, were pre-treated overnight with sublethal doses of didox (respectively, with 120 and 35 μM). Then, the monolayer was interrupted using a pipette tip, and medium was changed with the same fresh treatment medium used for the pre-treatment.

RD mock and RD Cav-1 F2 cells were seeded in 6-wells plates (at the concentration of 400,000 and 150,000 cells/well, respectively) and, when 90% confluence was reached, the monolayer was interrupted using a pipette tip, and fresh media, containing triacsin C at the concentrations of 2.5, 5 and 10 μM, was added.

Then, after 10 hours treatment, cells were fixed in 3% glutaraldehyde and stained with 0.1% Crystal Violet. The extent of wound repair was calculated using the "MRI Wound Healing tool" for ImageJ (NIH, Bethesda, MD, USA). The percentage of wound closure was calculated by subtracting the value of the measured area to the value of the area of the wound at time zero and by expressing it as a percentage over the value of the area of the wound at time zero. Each value derives from four measurements made on two different wounds in the same well, and p-values were obtained with T-Test, comparing the treatment over the not-treated cells.

## Annexin V/Propidium Iodide Assay

RD and RH30 cells were seeded in six-well plates (150,000 cells/well) and, 24 hours after the seeding, were treated with didox (50 and 150 μM); then, the apoptotic cell death was analyzed after 24, 48 and 72 hours using the commercial kit AnnexinV-FITC Apoptosis Detection (Immunostep) and following the manufacturer's instructions. Briefly, cells were harvested, washed with 1X PBS and resuspended in 1X Annexin-binding buffer, then, 5 μL of AnnexinV-FITC and 5 μL of propidium iodide (PI) were added, and cells were incubated at RT for 15 minutes in darkness. After the incubation, 400 μL of 1X Annexin-binding buffer was added, and cells were analyzed by flow cytometry within one hour, using the MACSQuant Analyzer (Miltenyi Biotec). Analysis of apoptosis was performed by considering the cells that were simultaneously stained with AnnexinV-FITC and PI in order to discriminate intact cells (AnnexinV-FITC- and PI-negative) from cells in an early apoptotic state (AnnexinV-FITC-positive and PI-negative) and in a late apoptotic state (AnnexinV-FITC- and

PI-positive). The percentage of cells positive to each dye was represented in the plot, whereas the histogram showed the cells positive to AnnexinV-FITC (the sum of the percentage of cells in early and late apoptosis).

### *MitoSOX™ Red Mitochondrial Superoxide Indicator Assay*

RD and RH30 cells were seeded in 12-wells plates (50,000 cells/well for RD and 3,000 cells/well for RH30) and, after reaching 50% confluence, were treated with didox (50 or 150 µM). After 24, 48 and 72 hours of treatment, cells were stained with 1 µM MitoSOX™ Red (Invitrogen) for 10 minutes at 37°C for mitochondrial superoxide revelation, then were fixed in 4% PFA for 15 minutes at RT and counterstained with 0.01 µg/mL DAPI dye for 5 minutes at RT for nuclei identification. Images were collected using Zeiss fluorescence Axiovert microscope with a CCD black-and-white TV camera (SensiCam-PCO Computer Optics GmbH, Germany) Image quantification was performed using ImageJ software (NIH, Bethesda, MD, USA) and the total signal of the MitoSOX™ Red probe was normalized for the number of cells in the capture field.

### *Lipid ROS staining with C11-BODIPY$^{581/591}$ probe*

For the lipid ROS detection at basal level, 50,000 RD mock and RD Cav-1-F2 cells were seeded on coverslips in 12-wells plates, and, after 48 hours from seeding, cells were incubated with 2.5 µM C11-BODIPY$^{581/591}$ probe for 30 minutes at 37°C, with 5% $CO_2$, protected from direct sunlight to prevent bleaching of the probe. Then, cells were fixed with 4% PFA for 15 minutes at RT, and, after three washes in dd$H_2O$, cells were counterstained with 0.1 µg/mL DAPI for 5 minutes at RT. Finally, coverslips were mounted on glass slides, and images were taken using a Zeiss Axiovert microscope and SensiCam-PCO Optics (GmbH, Germany) with 63× magnification (with immersion) using FITC, RHOD and DAPI filters to visualize, respectively, the oxidized probe, total probe, and the nuclei.

### *Xenograft studies and immunohistochemical analyses*

Five million RH30 cells were resuspended in a volume of 100 µL of PBS 1X and subcutaneously injected into the flank of 9-11 weeks-old NOD/SCID mice (2 injections per mice). The growth of tumors was assessed twice a week using a digital caliper. For injections, didox was resuspended in DMSO at a stock concentration of 200 mg/mL, then, fresh dilutions in PBS 1X to a final concentration of 40 mg/mL were made each day prior injection,

according to manufacturer's instructions. Didox was administered intraperitoneally 3 times a week at a dose of 200 mg/kg for 3 weeks, then mice were sacrificed and livers, spleens, blood samples and tumor masses were collected and kept at -20°C for further analyses. Serum iron was determined spectrophotometrically using a commercial kit, according to manufacturer's instructions (Randox Laboratories, cod. SI257), whereas non-heme iron content in livers and spleens was measured by spectrophotometric assay using the bathophenanthroline sulphonate assay as indicated (Roetto et al., 2010). The study was approved by the Institutional Animal Care and Use Committee of the University of Brescia, Italy.

For immunohistochemical studies, tumor samples were fixed in 10% buffered formalin, and four-micron thick tissue sections were used for immunohistochemical staining. After antigen retrieval sections were incubated with anti-PECAM-1 (goat, clone M-20, rabbit polyclonal, diluted 1:200 from Santa Cruz Biotechnology) and anti-Ki-67 (rabbit, clone 30-9, ready to use from Ventana). Reactions were revealed using Goat-on-Rodent-HRP- Polymer (BIOCARE) or EnVision + System HRP Labelled polymer anti-Rabbit (Dako, Agilent) followed by DAB. Slides were digitalized using ScanScope CS Slide Scanner (Aperio Technologies, Leica) at 20X magnification and analyzed by ImageScope. PECAM and Ki-67 analysis were obtained using Positive Pixel count V9 and Nuclear algorithm, respectively.

## *Statistical Analysis*

Data are presented as mean ± standard deviation (SD). Statistical significance was assessed by Student's t-test, by one-way ANOVA or by two-way ANOVA (as reported in figure legends), which were performed by GraphPad Prism 8 software (GraphPad Software Inc., La Jolla, CA). p-values lower than 0.05 were considered significant.

# Results

Rhabdomyosarcoma (RMS) is an aggressive rare pediatric neoplasm derived from mesenchymal cells, that frequently develops resistance to the current therapies. Among the new therapeutic strategies, here the current study investigated the efficacy of didox, a compound with iron chelating properties and with a great inhibitory activity on RRM2 enzyme, that is essential for the rapid *de novo* synthesis of deoxyribonucleotides.

On the other hand, in collaboration with Prof. Fanzani's group, it was observed that RMS cells that overexpress caveolin-1, a protein involved in different metabolic and signaling pathways (S. Wang *et al.*, 2017), were highly sensitive to ferroptosis inducers (Codenotti *et al.*, 2018). Thus, we investigated the reason of this sensitivity, focusing on the link between ferroptosis, the antioxidant response and lipid metabolism of Cav-1-overexpressing RD cells.

# Results, Part 1 – The RRM2 inhibitor didox counteracts the *in vitro* and *in vivo* growth of rhabdomyosarcoma cell lines

## *Didox suppresses the viability of both ERMS and ARMS cell lines*

Rhabdomyosarcoma cell lines RD and RH30 were considered to study the effects of didox on cell viability. The two cell lines are representative of the most frequent embryonal subtype and of the most aggressive alveolar subtype. Cells were treated with different concentrations of didox (1-10-25-50-100-200-500 μM), and cell viability was assessed by MTT assay after 24, 48 and 72 hours of treatment. Didox effectively reduced cell viability in a dose- and time-dependent manner in both cell lines, with increased potency using a long-term exposure (Figure 4.3).

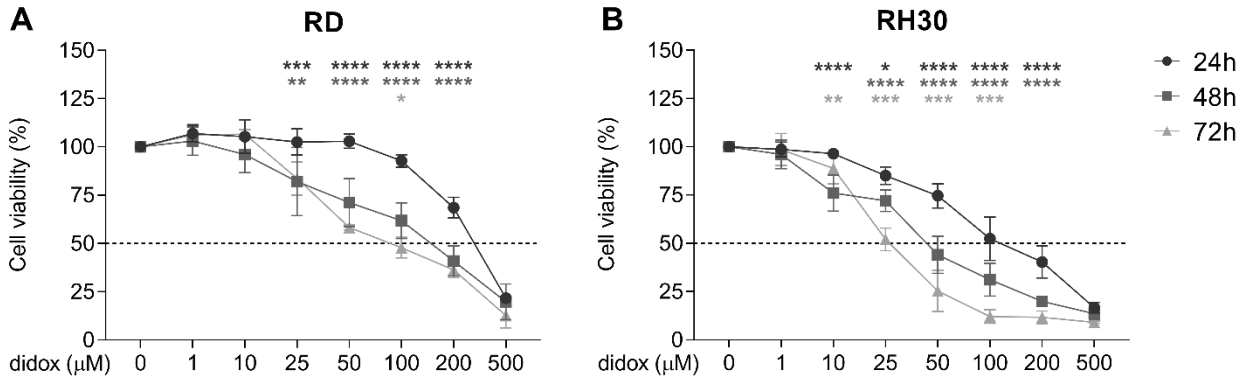


**Figure 4.3 – Didox reduces cell viability in RMS cell lines in a time- and dose-dependent manner.** RD (A) and RH30 (B) cell lines (representing embryonal and alveolar RMS, respectively) were treated with 0-1-10-25-50-500-200-500 μM didox for 24, 48 and 72 hours; then, MTT assay was performed to verify cell viability after treatment. The values are expressed as percentage of viable cells over the not treated cells at the indicated time points. The black dotted line is drawn in correspondence to the half maximal inhibitory dose ($IC_{50}$). The graph represents the means of three independent experiments (N = 3) with three internal values for each experiment. The statistical analysis was performed with two-way ANOVA, using Tukey's method for statistical hypothesis testing; the black stars correspond to the comparison between 24h and 48h, the grey stars between 24h and 72h and the light grey stars between 48h and 72 h. * $p < 0.05$; ** $p < 0.01$; *** $p < 0.001$; **** $p < 0.0001$.

Also, as a comparison, cells were treated with the same doses of hydroxyurea (HU), the precursor of didox and the first RR inhibitor approved for clinical use, and cell viability was assessed after 24, 48 and 72h hours of treatment. We observed a dose- and time-dependent reduction of cell viability, which was markedly less effective than the treatment with didox (Figure 4.4).

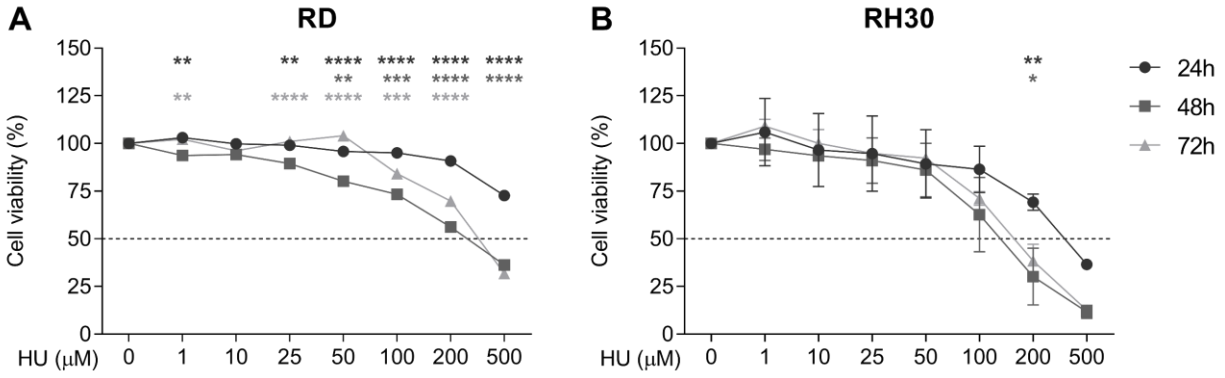


**Figure 4.4 – Hydroxyurea reduces cell viability in RMS cell lines in a time- and dose-dependent manner.** RD (A) and RH30 (B) cell lines (representing embryonal and alveolar RMS, respectively) were treated with 0-1-10-25-50-500-200-500 μM hydroxyurea (HU) for 24, 48 and 72 hours; then, MTT assay was performed to verify cell viability after treatment. The values are expressed as percentage of viable cells over the untreated cells at the indicated time points. The black dotted line is drawn in correspondence to the half maximal inhibitory dose (IC50). The graph represents the means of three independent experiments (N = 3) with three internal values for each experiment. The statistical analysis was performed with two-way ANOVA, using Tukey's method for statistical hypothesis testing; the black stars correspond to the comparison between 24h and 48h, the grey stars between 24h and 72h and the light grey stars between 48h and 72 h. * $p < 0.05$; ** $p < 0.01$; *** $p < 0.001$; **** $p < 0.0001$.

The half maximal inhibitory doses ($IC_{50}$) values of the drugs (both didox and hydroxyurea) for the considered timepoints were interpolated from the dose-response data using GraphPad Prism 8's integrated nonlinear regression tool. At the 24h, 48h and 72h timepoints, the $IC_{50}$ values of didox for RD cells were 331.83 μM, 135.58 μM and 97.34 μM respectively, while for the RH30 cell line were 129.57 μM, 43.25 μM and 29.17 μM respectively, showing higher efficacy of didox on the ARMS subtype (Table 4.2). The $IC_{50}$ values of HU for both cell lines were sensibly increased compared to the values obtained from the treatment with didox, as reported in Table 4.2.

| | Didox | | Hydroxyurea | |
|---|---|---|---|---|
| $IC_{50}$ (μM) | RD | RH30 | RD | RH30 |
| 24h (μM) | 331.83 | 129.57 | --- | 361.79 |
| 48h (μM) | 135.58 | 43.25 | 504.65 | 145.34 |
| 72h (μM) | 97.34 | 29.17 | 349.31 | 178.56 |

**Table 4.2 – Calculation of $IC_{50}$ values after a treatment with didox and hydroxyurea.** The $IC_{50}$ values (corresponding to the dose that reduced cell viability by 50%) for the treatment with didox and hydroxyurea for both RD and RH30 cells were interpolated from the data reported in Figure 1 and Figure 2 respectively, using GraphPad Prism 8's integrated nonlinear regression tool and are the mean of three independent experiments.

## *Didox induces apoptotic cell death and increases mitochondrial ROS*

Since didox has been reported to cause cell death by apoptosis in various tumor types (Grusch *et al.*, 2001; Raje *et al.*, 2006), performed the Annexin-V/PI assay was performed to determine if this observation was similar also in RMS cell lines. RD and RH30 cells were treated with sublethal doses of didox (50-150 μM and 25-50 μM respectively) and their positivity to either annexin-V or PI was evaluated with a cytofluorimeter after 24, 48 and 72 hours. It was found that didox induces an increase in annexin-V-positive cells in a dose- and time-dependent manner, with no significant differences between the 48 hours and the 72 hours timepoints. Thus, didox induces an apoptotic cell death also in RMS cell lines (Figure 4.5).

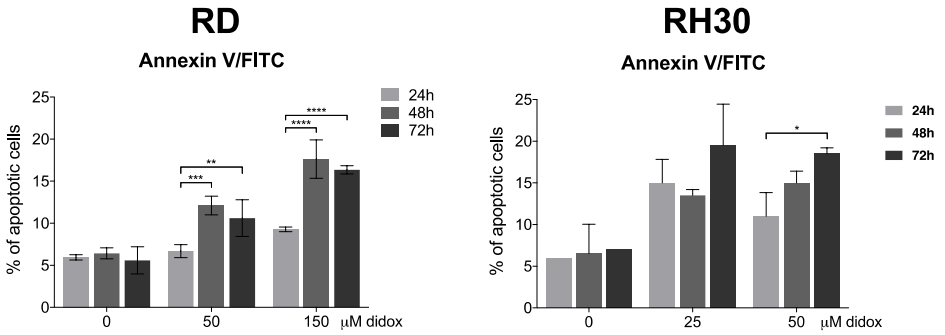


**Figure 4.5 – Didox causes cell death by apoptosis RD and RH30 cell lines.** For apoptosis detection, RD cells (representative of embryonal RMS) were treated with 50 and 150 μM didox and RH30 cells (representative of alveolar RMS) with 25 and 50 μM didox, for 24, 48 and 72 hours. Then cells were stained with Annexin V-FITC and propidium iodide (PI) and signals were detected by flow cytometry. The histograms show the percentage of apoptotic cells (FITC-positive cells) relatively to the entire population at each time point. The statistical analyses were performed with two-way ANOVA, using Tukey's method for statistical hypothesis testing. * $p < 0.05$; ** $p < 0.01$; *** $p < 0.001$; **** $p < 0.0001$.

Moreover, to verify if didox can increase mitochondrial oxidative stress, RD and RH30 cells were treated with sublethal doses of didox respectively, 50 and 150 μM for RD and 25 and 50 μM for RH30) and, after 24, 48 and 72 hours, were stained with the mitochondrial specific fluorescent probe MitoSOX™ Red; then, the superoxide accumulation in mitochondria was observed by fluorescent microscopy. It was found that didox induces a dose- and time-dependent increase of superoxide content in the mitochondria of RD cells, with significant differences after 48 and 72 hours of treatment (Figure 4.6 A, C), while, in RH30 cells, a significant increase in mitochondrial ROS could be seen only after 72h hours of treatment at the highest dose (Figure 4.6 B, D).

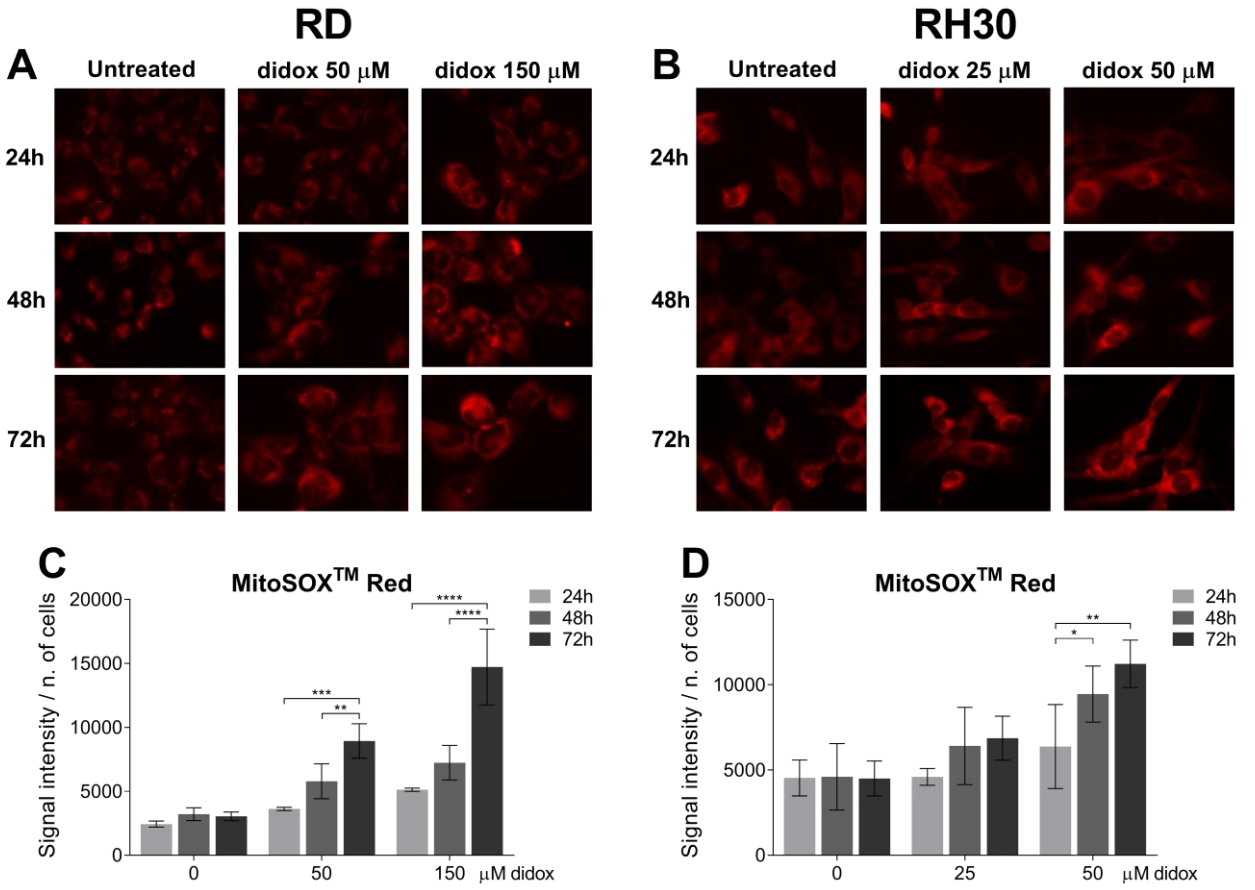


**Figure 4.6 – Didox increases mitochondrial oxidative stress in RD and RH30 cell lines.** For mitochondrial superoxide detection, RD cells were treated with 50 and 150 μM didox and with 25 and 50 μM didox, for 24, 48 and 72 hours. Then, cells were stained with MitoSOX™ Red, fixed in 4% PFA, and images were obtained by fluorescent microscopy using a 63x magnification (with immersion) using the rhodamine filter (B). The histograms in D show the signal intensity of the probe normalized for the number of cells in the considered field. The statistical analyses were performed with two-way ANOVA, using Tukey's method for statistical hypothesis testing. * $p < 0.05$; ** $p < 0.01$; *** $p < 0.001$; **** $p < 0.0001$.

## *Didox decreases the motility and the clonogenic capability of RMS cells*

Since didox reduces RMS cell viability, it was sought whether lower concentrations exposures to the drug were effective in altering the motility of both RD and RH30 cells. Cells were pre-treated overnight with sublethal doses of didox (120 μM and 35 μM), then, the monolayer was interrupted, and wound repair was measured after 10 hours of treatment. Although the behavior of the two cell lines was comparable in normal conditions, the motility of RD cells was reduced up to 50%, while RH30 cells showed lower sensitivity to the treatment (Figure 4.7 A-C). Moreover, to verify the effects on the clonogenicity, RD and RH30 cells were treated with increasing doses of didox (0-1-10-25-50-100 μM) for 48h, and then media was changed with fresh one without didox. Both RD and RH30 cells showed a dose-dependent reduction of the clonogenic capability (Figure 4.7 D-E). The decrease in

colony formation was evident with a dose of 50 μM, with a 25% reduction of the colonies, for both cell lines. Moreover, RH30 cells needed shorter time to develop colonies (4 days) compared to RD cells (7 days) also after a treatment with didox, therefore confirming the greater aggressiveness of the alveolar subtype.

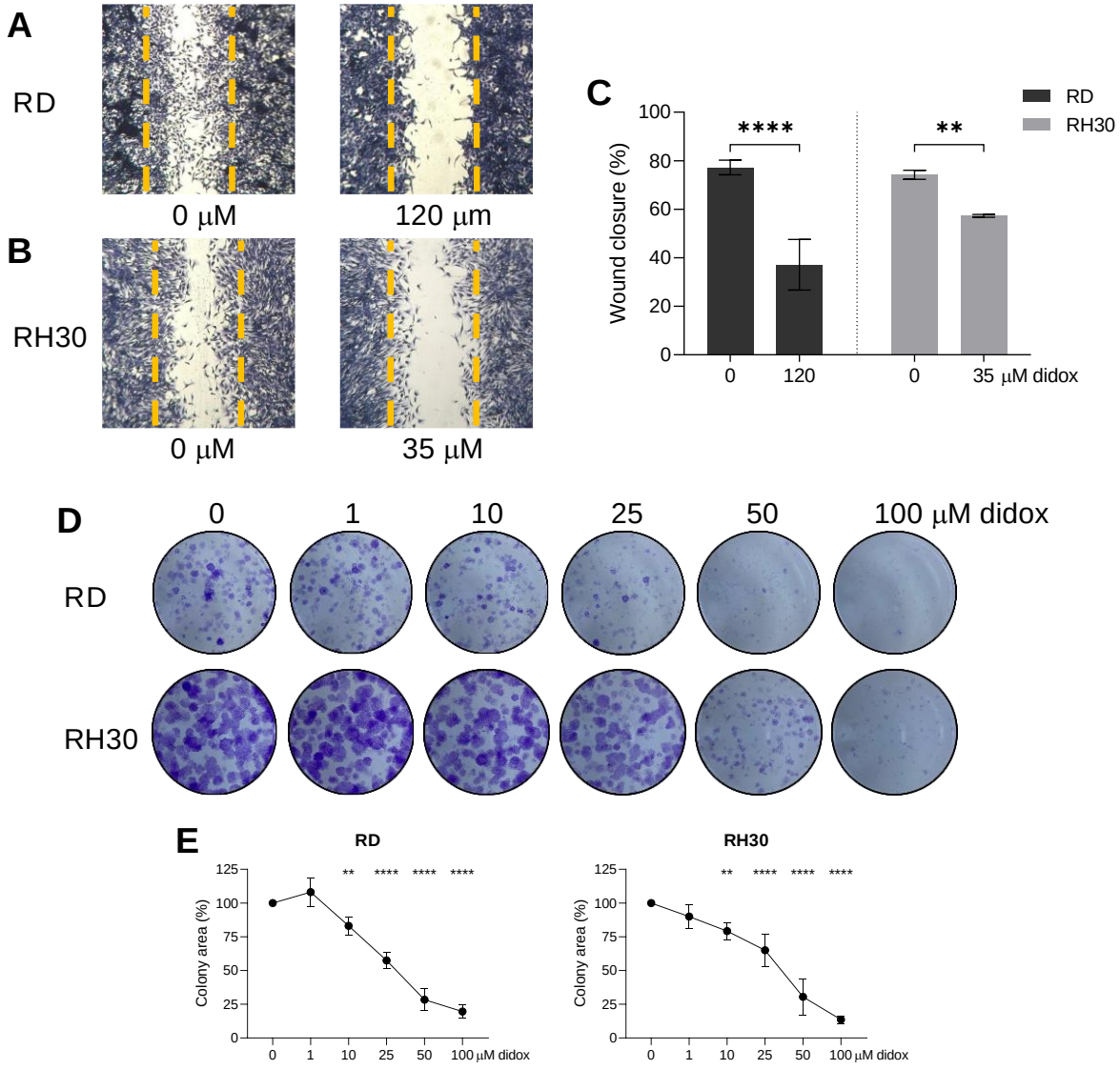


**Figure 4.7 – Didox decreases cellular motility of both embryonal and alveolar RMS subtypes and reduces their clonogenic capability in a dose-dependent manner.** For the motility assay (A-C), RD (representative of embryonal RMS; A) and RH30 (representative of alveolar RMS; B) cells were seeded in 6-wells plates and, at 90% confluence, were pre-treated overnight with sublethal doses of didox (respectively, with 120 and 35 μM); then, the monolayer was interrupted using a pipette tip, and culture medium was changed with a fresh one containing the same concentrations of didox used for the pre-treatment. The graph shows the percentage of wound closure, considering the width of a fresh wound as 100%. Each value derives from four measurements made on two different wounds in the same well, and statistical analyses were performed with two-way ANOVA, using Sidak's method for statistical hypothesis testing. For the clonogenic assay (D-E), 1000 RD and 500 RH30 cells (D) were seeded in Φ 3,5 cm dishes and, after respectively 48- and 24-hours post-seeding, were treated with 0-1-10-25-50-100 μM didox for 48 hours. Then, the medium was changed with fresh one and, after respectively 7 and 4 days, cells were fixed in 3% PFA and stained with 0,1% Crystal Violet. The clonogenic capability of cells was evaluated by dissolving the coloration with 1% SDS in PBS 1X and by measuring the absorbance at 540 nm of the resulting solution. The graphed data derive from the normalization of each value over the

absorbance of the not-treated cells, and statistical analyses were performed with one-way ANOVA, using Dunnett's method for statistical hypothesis testing. * $p < 0.05$; ** $p < 0.01$; *** $p < 0.001$; **** $p < 0.0001$.

## *Didox alters the iron status of RMS cell lines*

Our previous work demonstrated that didox, in addition to its RRM2 inhibiting activity, is also an iron chelator (Asperti *et al.*, 2019). Therefore, both RD and RH30 cells were treated with sublethal concentrations of didox and analyzed the iron status of cells analyzed afterwards. We did not find any significant alteration in the levels of transferrin receptor 1 protein (TfR1, Figure 4.8 A), whereas H-ferritin (FtH) protein levels were decreased in RH30 cells treated with didox 25 μM and in RD cells treated with didox 100 μM was found, while we only found a trend in the decrease of FtH expression in RH30 cells treated with didox 100 μM (Figure 4.8 B). Interestingly, the intracellular levels of iron were increased in both cell lines after the treatment with didox 25 μM, while there was no significant alterations of the labile in iron pool content of the cells treated with didox 100 μM (Figure 4.8 C), These data suggest that, at low concentrations, didox increases the import of iron, a behavior that is similar to other iron chelators such as catechols, which are structurally similar to didox (Torti *et al.*, 2018; Asperti *et al.*, 2019).

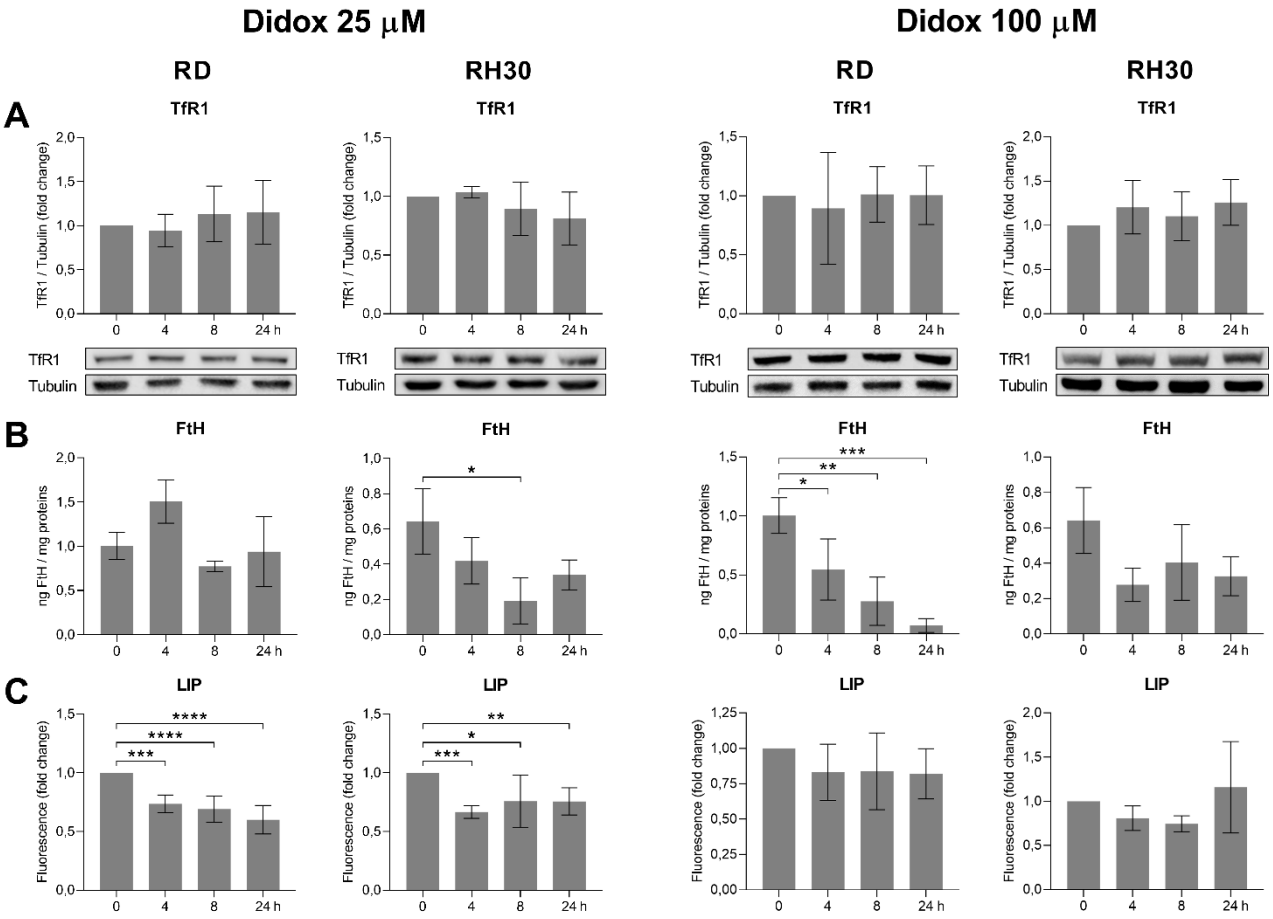


**Figure 4.8 – Didox affects iron-related proteins (TfR1 and H-ferritin) in RMS cell lines, acting as an iron chelator.** RMS cells at 80% confluence were treated with sublethal doses of didox (25 and 100 μM) for 48 hours and analyzed for transferrin receptor 1 (TfR1) with immunoblot assay (A). Tubulin was used as loading control. Densitometry was performed using Image Studio Lite TM software and the values were normalized to tubulin as indicated. The expression of heavy subunits of ferritin (FtH) was analyzed by ELISA assay (B), and the labile iron pool was measured with the Calcein-AM assay (C). Statistical analyses were performed with two-tailed t-Test, using Holm-Sidak's method for statistical hypothesis testing. * $p < 0.05$; ** $p < 0.01$; *** $p < 0.001$; **** $p < 0.0001$.

## *Didox inhibits the in vivo growth of RH30 cells*

Since didox influences *in vitro* properties of RMS cells, then further studies were conducted to test its *in vivo* effects on RH30 cells (the most aggressive cell line) in mouse xenograft. Five million RH30 cells were injected subcutaneously in the flanks of 9-11 weeks-old NOD/SCID mice and, after the development of a measurable tumor mass, mice were treated with either vehicle (DMSO) or 200 mg/kg didox three times a week for three weeks, and time-course tumor growth was determined with time course measurements using a caliper. As shown in Figure 4.9 A, didox potently reduced the growth of RH30 cells, since the tumor volume was lower compared to the control treated mice for the entire experiment. In fact, at the end of the experiment, tumor treated with didox showed around 200 $mm^3$ of volume versus 600 $mm^3$ of tumors treated with DMSO (Figure 4.9 A). These

findings were accompanied by a decrease of both tumor weight (Figure 7B) and dimensions (Figure 4.9 C) after didox treatment at the end of the experiment, while it did not affect the content of iron in liver, spleen, or serum (Figure 4.9 D-F). Finally, the treatment with didox reduced the number of cells positive to the proliferation marker Ki-67, suggesting a decrease in the proliferation rate of these tumors, while only a trend in the reduction of the cell adhesion protein CD31 and in the increase of the apoptosis marker caspase-3 (Figure 4.9 G-H) were detected.

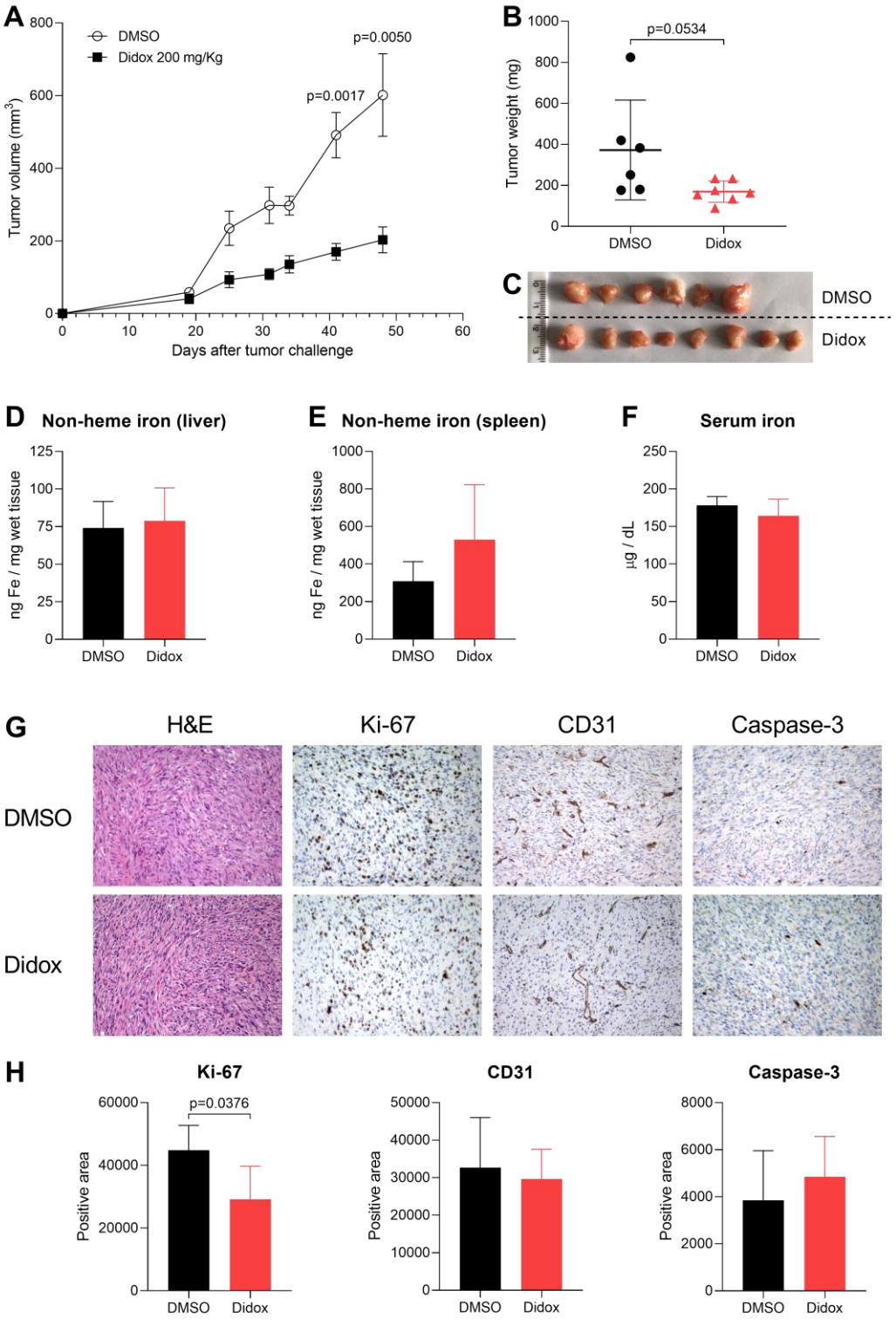


**Figure 4.9 – Didox effectively inhibits the *in vivo* growth of RH30 cells in NOD-SCID mice.** 5x10$^6$ RH30 cells were injected subcutaneously in the flanks of 9-11 weeks-old NOD-SCID mice (2 plugs per mice). After assessment of tumor growth, mice were given intraperitoneal injections of vehicle or didox (200 mg/kg) three times a week for three weeks, and tumor growth was monitored during time (A). At the experimental timepoint, mice were sacrificed, and tumors, livers, spleens, and blood samples were harvested. Tumors were weighted (B) and fixed in 10% buffered formalin (C), while livers and spleen were either fixed in 10% buffered formalin and snap-frozen for further analyses. Non-heme iron content (D-E) of both organs and serum iron levels (F) were assessed, and immunohistochemical analyses for Ki-67, CD31 and caspase-3 were conducted (G-H).

# Results, Part 2 – Rhabdomyosarcoma, fatty acid metabolism and ferroptosis

## *RD cells overexpressing Cav-1 are characterized by altered iron-related proteins, antioxidant compartment and lipid metabolism*

As already mentioned, in collaboration with Prof. Alessandro Fanzani's group at the University of Brescia, we found that caveolin-1-overexpressing RD cells (referred to as "RD Cav-1 F2") are more sensitive than control RD cells (referred as "RD mock") to ferroptosis inducers (Codenotti *et al.*, 2018). Since Cav-1 is a protein involved in the regulation of many cellular pathways as well as in lipid metabolism (Luo *et al.*, 2021), we aimed to define if there could be a possible link among ferroptosis sensitiveness and iron-metabolism, antioxidant compartment and fatty acid metabolism in Cav-1-overexpressing RD cells.

Control and Cav-1-overexpressing RD cells were analyzed for some iron-related proteins such as Transferrin Receptor 1 (TfR1, involved in the cellular iron uptake), ferroportin (FPN, the sole cellular iron exporter known) and ferritin (in particular, the H-subunit, FtH, a protein which stores iron in a non-toxic form for the cells). As shown in Figure 4.10, RD Cav-1 F2 cells expressed lower levels of TfR1 protein (2.5-fold less), almost undetectable levels of FPN (Figure 4.10 A) and significantly lower levels of FtH (10-fold less) than RD mock cells (Figure 4.10 B). These data showed that Cav-1-overexpressing cells are characterized by an alteration of iron-related proteins, suggesting that these cells could not be able to properly handle iron dysregulation, and, likely, that an increased iron content could be detrimental.

In addition, the mRNA expression of some important genes related to ferroptosis and to the antioxidant compartment, such as GPX4 (which is involved in lipid peroxides neutralization), heme oxygenase 1 and thioredoxin 1 (respectively, HMOX1 and TXNR, which are involved in the handling of cellular ROS) was analyzed. We found that the expression of these three enzymes is significantly lower in Cav-1-overexpressing cells, with 40-fold lower expression of GPX4 mRNA (Figure 4.10 C) and undetectable mRNA levels for HMOX1 and TXNR (Figure 4.10 D-E). Moreover, Ferroptosis Suppressor Protein 1 (FSP1, involved in the inhibition of lipid peroxidation by regenerating ubiquinol and suppressing ferroptosis without the requirement of GSH or GPX4) is expressed at lower level in Cav-1-overexpressing cells, than control cells (Figure 4.10 F). Finally, we also found that Cav-1-overexpressing cells are characterized by a higher lipid ROS content (Figure 4.10 G).

All these features suggest that Cav-1-overexpressing cells are characterized by a decreased capability of lipid peroxide neutralization and of ROS detoxification.

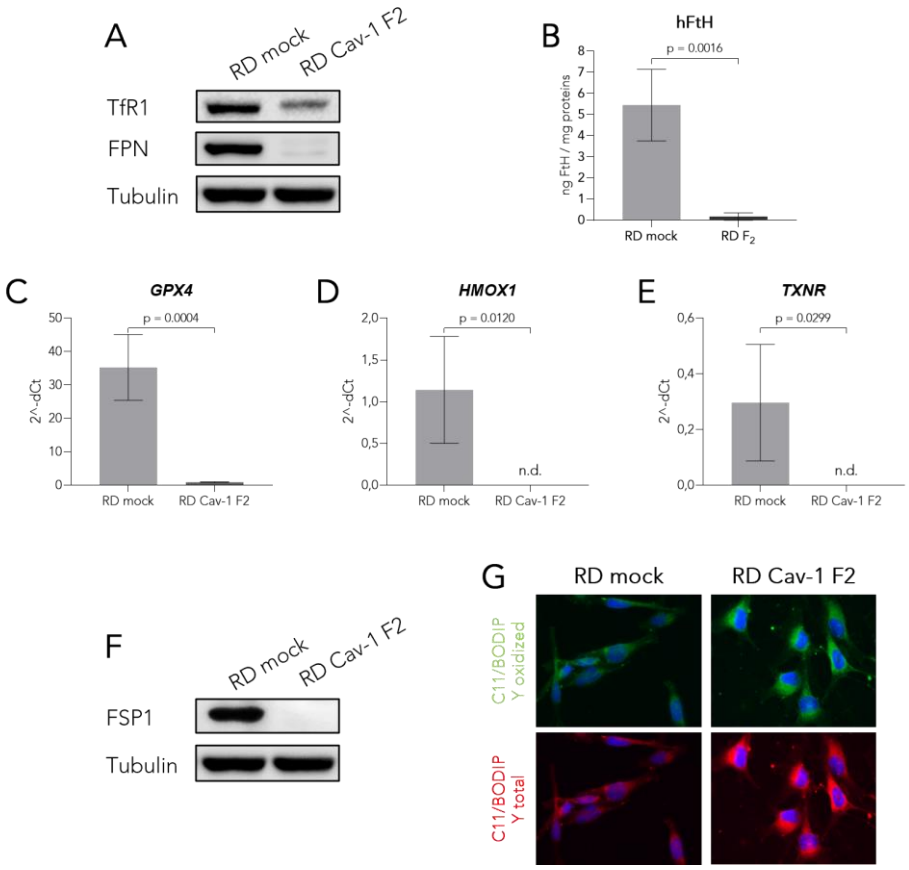


**Figure 4.10 – Characterization of control and Cav-1-overexpressing cells at basal level for iron-related proteins, ferroptosis related genes, proteins, and lipid ROS.** Western blot analysis for TfR1, FPN (A) and FSP1 (F) was performed, and tubulin was used as loading control. ELISA assay for ferritin-H (hFtH) protein content was performed and data were expressed as ng of FtH/ mg total protein content (B). For the analysis of mRNA expression (A), control and Cav-1-overexpressing cells (referred as RD mock and RD Cav-1 F2 respectively) were analyzed by qRT-PCR for the following genes: *GPX4*, *HMOX1*, *TXNR*. Data are expressed as $2^{-\Delta Ct}$, and statistical analyses were performed with two-tailed unpaired t-test (* $p < 0.05$; ** $p < 0.01$; *** $p < 0.001$; **** $p < 0.0001$). For the lipid ROS analysis (C), control and Cav-1-overexpressing cells were stained with C11/BODIPY$^{581/591}$ and counterstained with DAPI. Images were obtained by fluorescent microscopy using a 63x magnification (with immersion) using the FITC, RHOD and DAPI filters to visualize, respectively, the oxidized probe, the total probe, and the nuclei.

Among the enzymes involved in lipid metabolism, long-chain-fatty-acid-CoA ligase 4 (ACSL4, the enzyme that catalyze the conjugation of polyunsaturated fatty acids chains, or PUFAs, to coenzyme-A, activating them for their insertion in the cell membrane) was strictly correlated to ferroptosis sensitivity (Doll *et al.*, 2017). Thus, we verified the protein level of ACSL4 in control and Cav-1-overexpressing RD cells and interestingly an increased protein levels of this enzyme in Cav-1-overexpressing RD cells (Figure 4.11 A).

Also, the study analyzed the mRNA expression of all ACSL enzymes and found that RD control cells expressed detectable mRNA levels of all ACSLs, with *ACSL3* (involved in the

insertion of monounsaturated fatty acids, or MUFAs, in the cell membrane) the most expressed one, followed by *ACSL4* mRNA. In Cav-1-overexpressing cells, *ACSL1* and *ACSL3* mRNA were not detectable, whereas *ACSL4*, *ACSL5*, *ACSL6* were expressed at detectable levels, with *ACSL4* being the most expressed one (Figure 4.11 B-F).

A further characterization verified the expression of other genes linked to lipid metabolism, such as the sterol regulatory element binding protein 1 and 2 (SREBP1 and 2, the two regulatory transcription factors which regulate the expression of downstream genes involved in lipid metabolism), of ATP-citrate lyase (ACLY, which generates acetyl-CoA from citrate), of acetyl-CoA carboxylase α (ACACA, which produces malonyl-CoA from acetyl-CoA), of fatty acid synthase (FASN, which condensates acetyl-CoA with malonyl-CoA to form palmitic acid) and of stearoyl-CoA desaturase (SCD, which is involved in the production of monounsaturated fatty acids, or MUFAs). Comparing to control cells, we found that, in Cav-1-overexpressing cells, the expression of *ACACA* was increased (Figure 4.11 L), while the levels of all the other mRNAs were markedly reduced (Figure 4.11 G-I, M-N). This could indicate a deregulation of fatty acids synthesis, as indicated by the reduced levels of *SREBP1*, *SREBP2*, *ACLY* and *FASN*. Moreover, the decreased expression of *SCD* could suggest that Cav-1-overexpressing cells are able to synthetize a lower amount of MUFAs, that could protect cells from ferroptosis, thus increasing the sensitivity to ferroptosis inducers of these cells.

Finally, the lipid content between the two cell lines were analyzed by Oil Red O staining (which specifically stains non-polar lipids, contained mostly in lipid droplets), and it was found that Cav-1-overexpressing cells showed increased accumulation of intracellular non-polar lipids (Figure 4.11 O). This could indicate a higher need of fatty acids in Cav-1-overexpressing cells, possibly due to their higher proliferation rate and the increased need of building blocks for cell division. Thus, these data suggest that Cav-1-overexpressing cells are characterized by an impaired lipid metabolism.

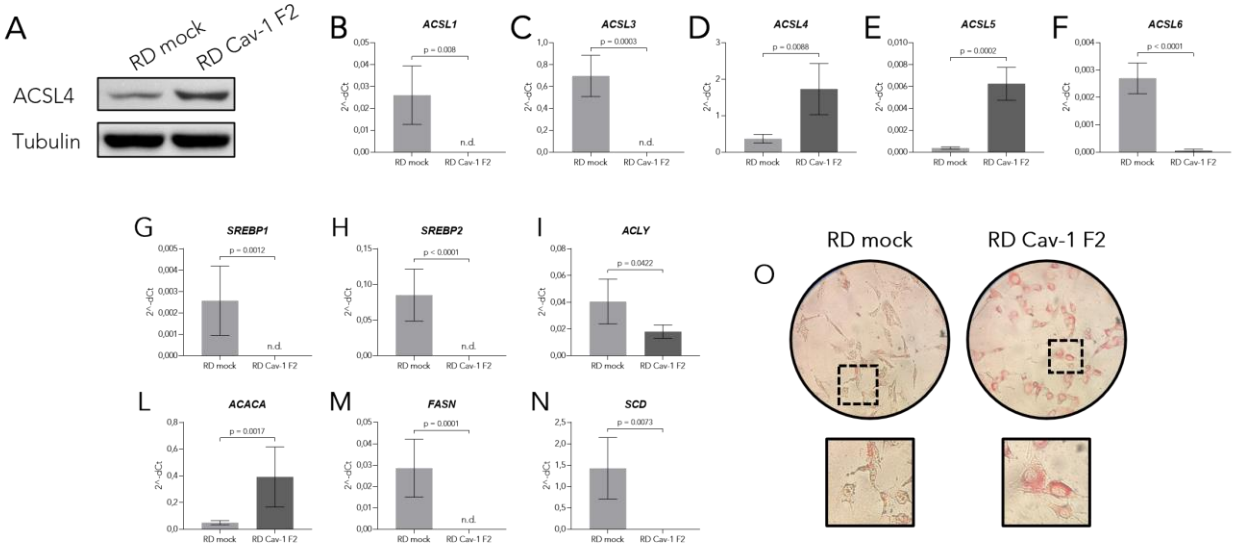


**Figure 4.11 – Characterization of control and Cav-1-overexpressing cells at basal level lipid metabolism compartment.** Western blot analysis for ACSL4 (A) was performed, and tubulin was used as loading control. For the analysis of mRNA expression (B-N), control and Cav-1-overexpressing cells (referred as RD mock and RD Cav-1 F2 respectively) were analyzed by qRT-PCR for the following genes: *ACSL1* (B), *ACSL3* (C), *ACSL4* (D), *ACSL5* (E), *ACSL6* (F), *SREBP1* (G), *SREBP2* (H), *ACLY* (I), *ACACA* (L), *FASN* (M) and *SCD* (N). Data are expressed as $2^{-\Delta Ct}$, and statistical analyses were performed with two-tailed unpaired t-test (* $p < 0.05$; ** $p < 0.01$; *** $p < 0.001$; **** $p < 0.0001$). For the lipid content analysis (O), control and Cav-1-overexpressing cells were stained with Oil Red O. Images were taken using a 40X magnification.

Altogether, these data suggest that the increased sensitivity of Cav-1-overexpressing cells to ferroptosis inducers could be due to the alteration of proteins involved in iron metabolism, to the alteration of lipid metabolism and to an imbalanced antioxidant/detoxification compartment.

## *Cav-1 overexpression sensitizes cells to the ACSL inhibitor triacsin C*

Since Cav-1-overexpressing cells showed a high expression of ACSL4, it was sought to determine if this enzyme could play a role in the increased sensitivity to ferroptosis of these cells. To verify this, we chemically inhibited the activity of ACSL4 using triacsin C, a pan-ACSL inhibitor. Also, since we verified that ACSL4 is the most expressed isoform of this family of enzymes in Cav-1-overexpressing cells, we assumed that the effect of triacsin C (which is a pan-ACSL inhibitor) in these cells would mainly inhibit ACSL4.

As first approach, we assessed the effects of triacsin C on the viability of RD cell lines were assessed. To do so, control and Cav-1-overexpressing RD cells were treated with increasing concentrations of triacsin C, and cell viability was assessed after 24 and 48 hours. It was found that triacsin C decreased the cell viability in a dose-dependent manner in both cell lines, with Cav-1-overexpressing cells being the most sensitive ones (Figure 4.12 A-B). In

fact, the IC50 was about 7.5 μM at 24h and 1 μM at 48h in control cells, whereas it was about 0.5 μM both at 24 and 48h in Cav-1-overexpressing cells. Thus, a time-dependent response in terms of cell viability, was observed in control cells where the 48 hours-treatment further increased the cytotoxic effect of triacsin C (Figure 4.12 A), no time-dependent effect was observable in Cav-1-overexpressing cells (Figure 4.12 B). Then, to investigate the effects of triacsin C on cell motility, both control and Cav-1-overexpressing cells were grown to confluence, then the monolayer was interrupted, and cells were allowed to repair the wound in presence of triacsin C. It was found that the motility of control RD cells was not affected by the inhibitor, while the wound repair capability of Cav-1-overexpressing cells was significantly reduced in a dose-dependent manner, with a 50% reduction at the highest dose of 10 μM (Figure 4.12 C, D). Finally, to assess the effects of triacsin C on the clonogenic capability of the two cell lines, both control and Cav-1-overexpressing cells were seeded at low density and exposed to triacsin C for 24 hours, and then cells were allowed to form colonies in the absence of treatment. In this case, we found that triacsin C effectively inhibited the clonogenic capability of both cell lines, with greater potency in Cav-1-overexpressing cells, where the same percentage of residual clonogenicity observed in control cells could be reached with a 20-fold lower dose (Figure 4.12 E, F).

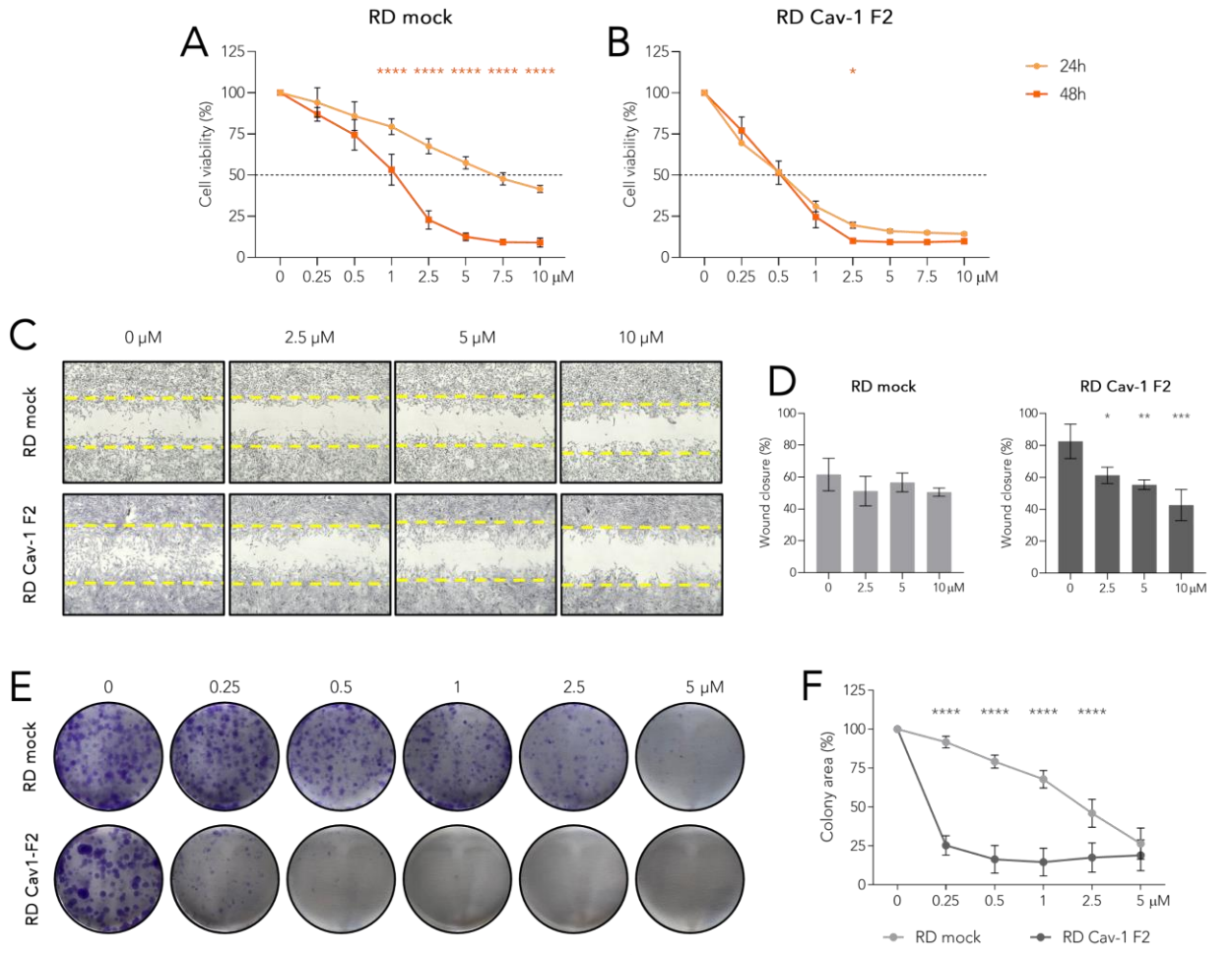


**Figure 4.12 – Cav-1-overexpressing cells are more sensitive to triacsin C, in terms of cell viability, cell motility and clonogenicity.** Control (RD mock, A) and Cav-1-overexpressing RD cells (RD Cav-1 F2, B) were treated with 0-0.25-0.5-1-2.5-5-7.5-10 µM triacsin C for 24 and 48 hours; then, MTT assay was performed to verify cell viability. The values are expressed as percentage of viable cells over the untreated cells at the indicated time points. The black dotted line is drawn in correspondence to the half maximal inhibitory dose ($IC_{50}$). The statistical analysis was performed with two-way ANOVA, comparing the 24h and the 48h treatment and using Tukey's method for statistical hypothesis testing (* $p < 0.05$; ** $p < 0.01$; *** $p < 0.001$; **** $p < 0.0001$). The motility assay (wound healing assay) was performed for both control and Cav-1-overexpressing RD cells. The cells were allowed to repair the wound in the presence of increasing concentrations of triacsin C for 10 hours, then cells were stained with Crystal Violet, and images were taken (C). The graphs (D) show the percentage of wound closure. The statistical analyses were performed with ordinary one-way ANOVA, using Dunnett's method for statistical hypothesis testing (* $p < 0.05$; ** $p < 0.01$; *** $p < 0.001$; **** $p < 0.0001$). For the clonogenic assay, RD mock and RD Cav-1 F2 were treated with increasing concentrations of triacsin C for 24 hours. Then, the medium was changed with fresh one and, after, respectively, 6 and 3 days, cells were stained with Crystal Violet and images were taken (E). The graphed data (F) derive from the normalization of each value over the absorbance of the not-treated cells, and statistical analysis was performed with two-way ANOVA, using Sidak's method for statistical hypothesis testing (* $p < 0.05$; ** $p < 0.01$; *** $p < 0.001$; **** $p < 0.0001$).

Altogether, these data showed that Cav-1-overexpressing cells are more sensitive to the inhibition of ACSL enzyme and, in particular, of ACSL4, probably due to the high demand of PUFA synthesis and insertion to the cell membranes, essential for their high proliferative rate.

## *Triacsin C fails to revert FINs-induced cytotoxicity in Cav-1-overexpressing RD cells*

As mentioned before, Cav-1-overexpressing RD cells are more sensitive to ferroptosis inducers than control cells. Since an increase in both mRNA and protein levels of ACSL4 in Cav-1-overexpressing RD cells was observed, it was sought to determine if the increased levels of ACSL4 could be directly linked to the higher ferroptosis sensitivity of these cells.

To this aim, the study verified if a pre-treatment with the ACSL inhibitor triacsin C could revert the sensitivity of Cav-1-overexpressing cells to ferroptosis inducers. Thus, Cav-1-overexpressing RD cells were pre-treated for 16 hours with 0.25 μM triacsin C (a concentration that resulted sublethal in the previous time-course experiments), and then treated for 24 hours with cytotoxic concentrations of either the ferroptosis inducer erastin, RSL3 or ML162, always in presence of triacsin C. It was found that the presence of the inhibitor, which caused only a 25% reduction of the cell viability alone, did not rescue the cell viability of these cells to any of the ferroptosis inducers. In fact, the treatment with 1 μM erastin, 1 μM RSL3, or 5 μM ML162 caused a significant decreased of cell viability (with more than 75% of reduction of cell viability), which was not rescued by the presence of triacsin C. These data indicate that both erastin, RSL3 and ML162 were able to induce ferroptotic cell death even if ACSL4 was inhibited. Thus, it was hypothesized that the increased expression of ACSL4 is not the main feature that causes the increased sensitivity of Cav-1-overexpressing RD cells to ferroptosis inducers (Figure 4.13), and that this sensitivity could relate to the higher content of lipid in these cells (Figure 4.11 O), suggesting a more complex metabolic dysregulation in Cav-1-overexpressing cells.

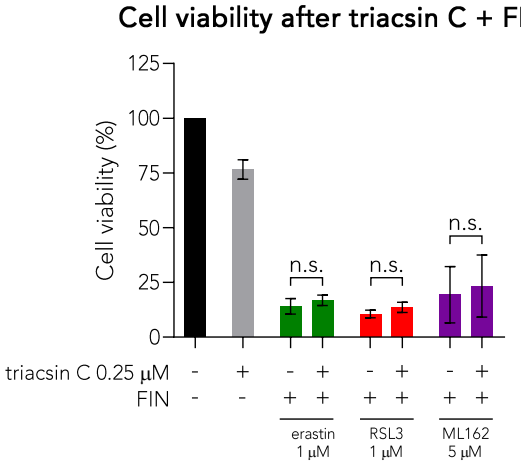


**Figure 4.13 – Triacsin C does not rescue FINs-induced cell death in Cav-1-overexpressing cells.** Cav-1-overexpressing RD cells were pre-treated with 0.25 μM triacsin C for 16h, then cells were treated with 1 μM for erastin and RSL3 and 5 μM for ML162, in presence of 0.25 μM triacsin C for 24 hours, then MTT assay was performed

to verify cell viability. The values are expressed as percentage of viable cells over the not treated cells at the indicated time points. The statistical analysis was performed with two-way ANOVA, using Tukey's method for statistical hypothesis testing.

## *The silencing of ACLS4 fails to revert FINs-induced cytotoxicity in Cav-1-overexpressing RD cells*

Since the chemical inhibition of ACSLs failed to revert the cytotoxic effects of ferroptosis inducers in Cav-1-overexpressing RD cells, and since we wanted to exclude that the results observed were not due to a non-specific effect of triacsin C, a pilot experiment was performed to verify if the specific inhibition of ACSL4 enzyme alone could affect the sensitivity of Cav-1-overexpressing RD cells to ferroptosis inducers. To do so, Cav-1-overexpressing cells were transfected with esiRNAs specific for either ACSL4 or EGFP (used as negative control) mRNA silencing. After 24h of transfection, cells were treated for 24 hours with 0.5 µM RSL3. The efficacy of the silencing was confirmed by western blot assay, which showed a great reduction of ACSL4 protein (Figure 4.14 A). Moreover, the staining of non-polar lipids with Oil Red O showed no differences in the lipid content between control and ACSL4-silenced cells (Figure 4.14 B). Finally, we did not observe any changes in terms of cell viability after RSL3 treatment in Cav-1-overexpressing RD cells silenced for ACSL4 compared to the not silenced ones, as shown in Figure 4.14 C. These data demonstrated that the decreased ACSL4 protein levels do not protect Cav-1-overexpressing cells from the cytotoxic effects of the ferroptosis inducer RSL3, confirming the data from the co-treatment experiments with triacsin C. This suggests that the increased sensitivity of these cells to FINs does not rely solely on the overexpression of ACSL4, but, as mentioned before, on a broader group of alterations possibly caused by Cav-1 overexpression. However, further studies will be required to fully elucidate the role of ACSL4 in Cav-1-overexpressing RD cells.

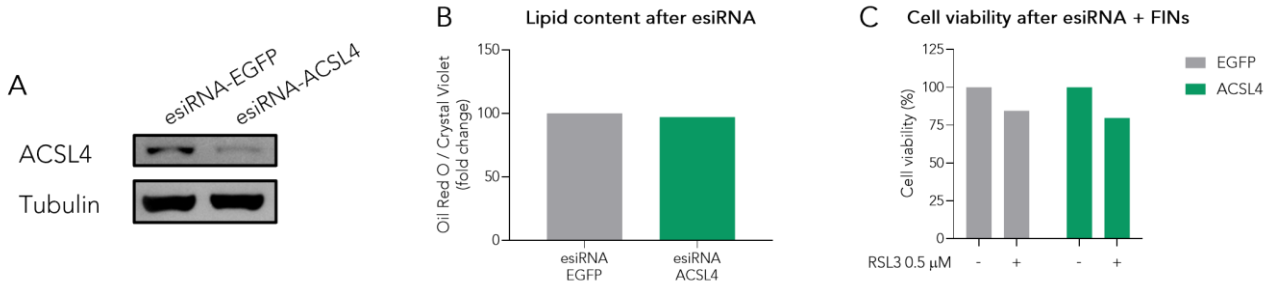


**Figure 4.14 – ACSL4-specific silencing does not reduce FINs-induced cell death in Cav-1-overexpressing cells.** Cav-1-overexpressing cells were transfected with esiRNA targeting EGFP (used as negative control) or ACSL4 mRNA. Then the cells were treated with 0.5 µM RSL3 for 24 hours. The efficiency of the silencing was evaluated by analyzing the protein level of ACLS4 in western blot (A). Cells were analyzed for lipid content (by Oil Red O staining; B). The evaluation of cell viability after RSL3 treatment was performed by MTT assay (C).

### *Treatment of Cav-1-overexpressing cells with different fatty acids increases the lipid content*

Since the modulation of fatty acids content in cells could affect the sensitiveness to ferroptosis, the study aimed to assess if the treatment with either MUFAs or PUFAs could affect the sensitivity of Cav-1-overexpressing cells to ferroptosis. Therefore, the sensitivity of these cells to different fatty acids were first assessed. In detail, a mixture of palmitic (PA) and oleic (OA) acids in a 1:2 ratio was used to simulate the accumulation of MUFAs, while linoleic (LA), α-linolenic (α-LNA), γ-linolenic (γ-LNA) and arachidonic (AA) acids were used to simulate the accumulation of PUFAs. Cells were treated with different concentrations of the considered fatty acids formulations (62.5, 125 and 250 μM) for 24 hours, then were stained with Oil Red O to assess the effective internalization of fatty acids. It was found that all the doses of fatty acids used increased the lipid content of cells (as shown in Figure 4.15 A-C, E), with little to no alterations in terms of cell viability (Figure 4.15 D). From these data, we defined, for each MUFA or PUFA, the lowest doses that was able to increase the lipid content of cells without affecting cell viability. In detail, the doses chosen further experiments were: 62.5 μM of PA:OA mixture, 62.5 μM AA (which increased of 1.1-fold the lipid content), 62.5 μM γ-LNA (which increased of 1.1-fold the lipid content), 250 μM LA (which increased of 1.5-fold the lipid content) and 250 μM α-LNA (which increased of 1.25-fold the lipid content).

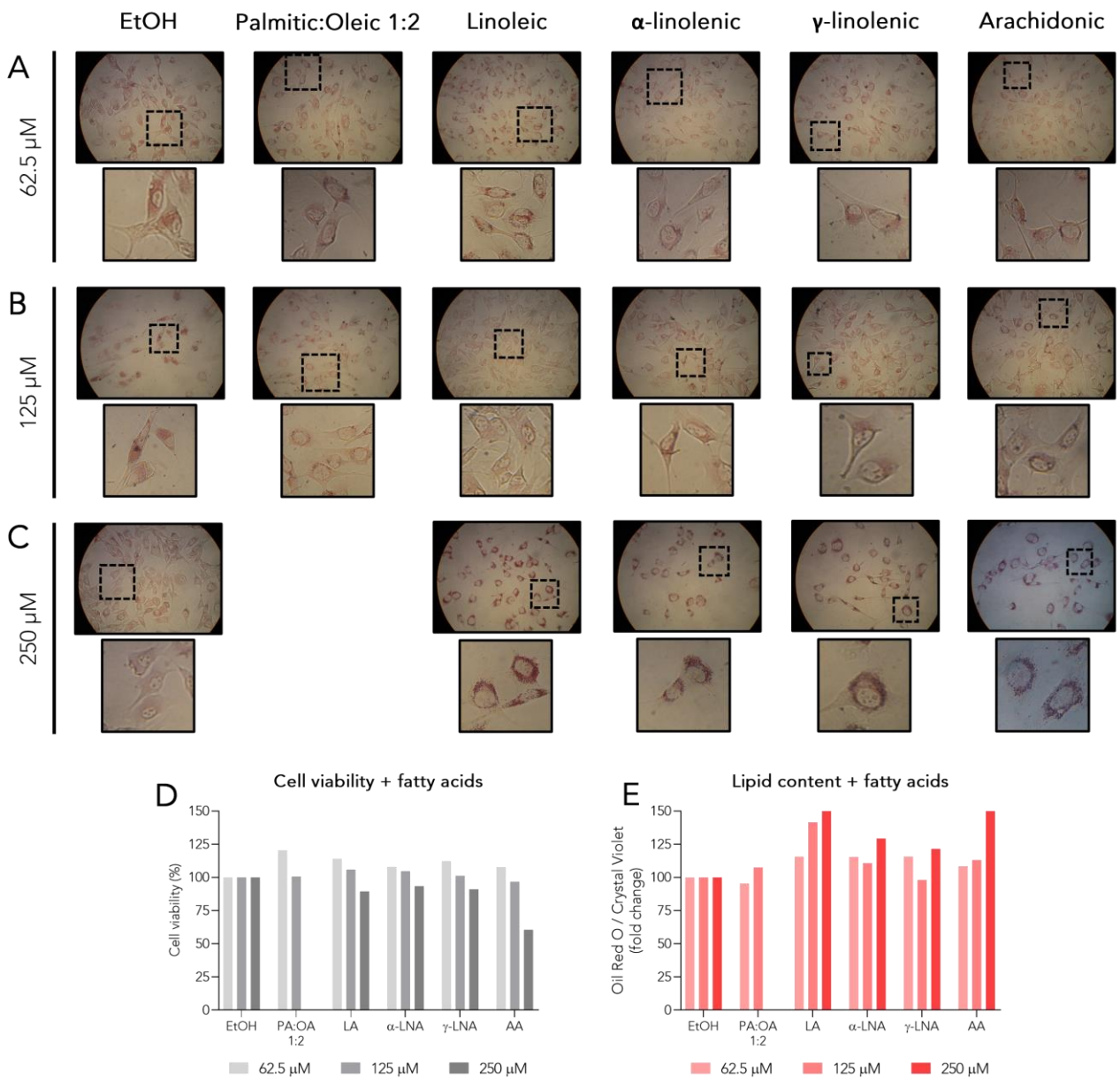


**Figure 4.15 – The exposure to different fatty acids successfully alters the lipid content of Cav-1-overexpressing cells.** Cav-1-overexpressing RD cells were treated for 24 hours with 62.5 (A), 125 (B) and 250 µM (C) of, respectively, a mixture of palmitic (PA) and oleic (OA) acids in a 1:2 ratio, linoleic (LA), α-linolenic (α-LNA), γ-linolenic (γ-LNA) and arachidonic (AA). Cells were stained with Oil Red O to verify lipid uptake, and images at 40X magnification were taken (A-C). The graphs in D and E report, respectively, the cell viability (crystal violet assay) and the lipid content quantification (Oil Red O staining. The data are the result of a single pilot experiment.

## *The modulation of lipid content affects the sensitivity to RSL3 in Cav-1-overexpressing cells*

To test if the modulation of the fatty acid content of Cav-1-overexpressing cells could affect their sensitivity to the ferroptosis inducer RSL3, cells were pre-treated with sublethal concentrations of different fatty acids for 16 hours (in detail, a mixture of PA and OA, in a

1:2 ratio and at a concentration of 62.5 μM, 250 μM LA, 250 μM α-LNA, 62.5 μM γ-LNA or 62.5 μM AA), and then treated with only 0.15 μM RSL3 for 24 hours.

First, to confirm that the pre-treatment with fatty acids could increase the lipid content, Cav-1-overexpressing RD cells treated for 16 hours were stained with Oil Red O. All the treatment conditions increased the intracellular content of lipids (as shown by the images in Figure 4.16 A and by the quantification of Oil Red O staining reported in Figure 4.16 B), with little to no effects on cell viability (Figure 4.16 C). The accumulation of fatty acids in cells was maintained also after 24 more hours, in which fatty acids were removed from the culture medium.

Then, fatty acids-loaded cells were treated with only 0.15 μM RSL3 for 24 hours, and then cell viability was assessed (Figure 4.16 D). It was observed that the single treatment with all the considered fatty acids did not affect the cell viability of Cav-1-overexpressing cells (as indicated by the gray histograms), in line with the results previously reported in Figure 4.16 C. We observed that the PA:OA mixture effectively protected cells from the cytotoxic effect of RSL3, while all the other fatty acids significantly increased RSL3-induced cell mortality. Specifically, the treatment with PA:OA caused about 20% of rescue of the cell death caused by RSL3, confirming that MUFAs protected Cav-1-overexpressing RD cells from ferroptosis. Contrarily, the treatment with LA or α-LNA further enhanced the cytotoxic effect of RSL3, leading to about 50% more reduction of cell viability. Also, the treatment with γ-LNA and AA further promoted RSL3-induced ferroptotic cell death, with a 15-20% more reduction of cell viability compared to RSL3 alone (Figure 4.16 D).

Therefore, these data showed that the treatment with MUFAs protects Cav-1-overexpressing cells from ferroptosis, while, contrarily, the increase in PUFAs content of these cells further sensitizes them to ferroptosis. It could be interesting evaluate the effect of PUFA treatment in presence of ACLS4 inhibition and investigate the mechanisms of the high basal level of lipids in Cav-1-overexpressing RD cells.

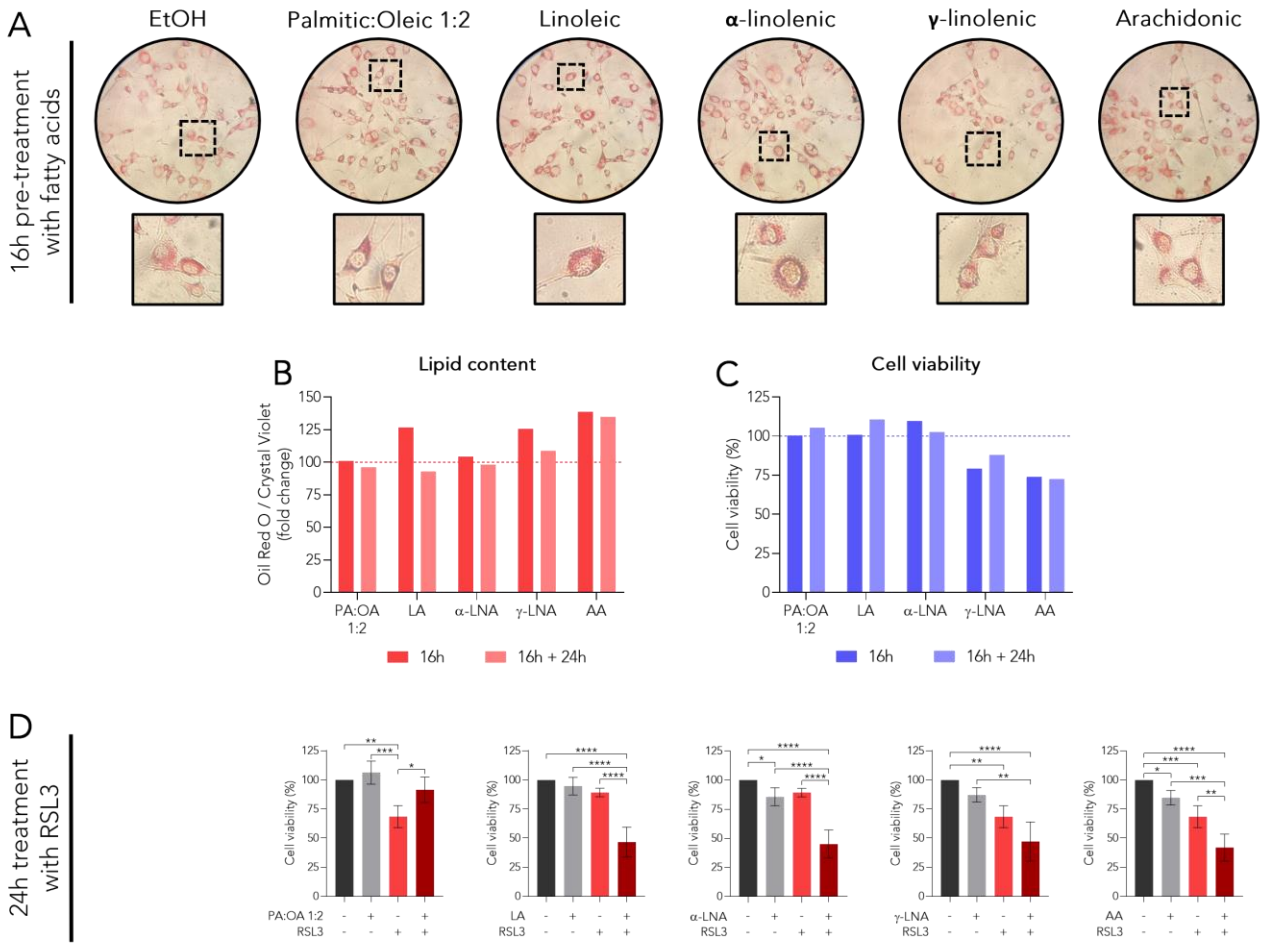


**Figure 4.16 – Pre-treating of Cav-1-overexpressing cells with MUFAs or PUFAs affects their sensitivity to RSL3.** Cav-1-overexpressing RD cells (RD Cav-a F2) were treated with sublethal doses of fatty acids: a mixture of palmitic (PA) and oleic acid (OA), in a 1:2 ratio at a concentration of 62.5 μM (PA:OA), 250 μM linoleic acid (LA), 250 μM α-linolenic acid (α-LNA), 62.5 μM γ-linolenic acid (γ-LNA) or 62.5 μM arachidonic acid (AA). After 16 h, cells were stained with Oil Red O to verify lipid uptake, and images at 40X magnification were taken (A). Lipid content (B) and cell viability, performed by MTT assay (C) were assessed both after 16 hours of treatment with fatty acids and after 16 hours of treatment with fatty acids plus 24 hours in normal medium. For the combined treatments with fatty acids and RSL3, cells were pre-treated with the considered doses of fatty acids for 16 hours; then with only 0.15 μM RSL3, and, after 24 hours of treatment, MTT assay was performed to verify cell viability. The values are expressed as percentage of viable cells over the not treated cells at the indicated time points (D). The statistical analysis was performed with ordinary one-way ANOVA, using Tukey's method for statistical hypothesis testing (* $p < 0.05$; ** $p < 0.01$; *** $p < 0.001$; **** $p < 0.0001$).

# Discussion

Rhabdomyosarcoma (RMS) is an aggressive neoplasia that develops from undifferentiated myocytes, and it mostly occurs in children and adolescents (Skapek *et al.*, 2019). Despite the approved treatment that includes aggressive regimens of both radio- and chemotherapy, RMS often exhibits therapy resistance, leading to tumor recurrence, and is frequently associated with metastatic dissemination (Miwa *et al.*, 2020).

Recently, we demonstrated that iron deprivation significantly reduces the growth of RMS cell lines (Asperti *et al.*, 2023). Since this interesting insight, the current study aimed to investigate if the ribonucleotide reductase inhibitor didox (3,4-dihydroxybenzohydroxamic acid), which also has been demonstrated to have iron chelating properties, could be effective in contrasting RMS progression.

Didox is a synthetic inhibitor of the regulatory subunit of ribonucleotide reductase RRM2, which is responsible for the rapid *de novo* production of deoxyribonucleotides necessary for genome duplication during cell division. RRM2 is also one of the 50 most overexpressed proteins in cancer, where it has been demonstrated to promote tumor proliferation and invasiveness, concomitantly reducing patient prognosis. Therefore, various inhibitors of RRM2 have been developed, the first being hydroxyurea, which exploited good efficacy in the treatment of various malignancies but also caused intense side effects in patients (Saban and Bujak, 2009). To avoid this problem, synthetic derivatives of hydroxyurea have been developed, the most efficient one being didox, which was characterized by greater inhibitory activity on RRM2 and, concomitantly, caused fewer *in vivo* side effects (Elford, Wampler and Riet, 1979; Riet, Wampler and Elford, 1979). Didox has also been tested in clinical trials, where it has been demonstrated inefficient in reducing tumor progression (Carmichael *et al.*, 1990; Rubens *et al.*, 1991). Therefore, more recent studies repurposed the use of didox in combination with approved chemotherapeutic agents, successfully increasing their antitumor effects. (Figul *et al.*, 2003; Al-Abd *et al.*, 2013; Wilson *et al.*, 2021). Moreover, didox has been reported to act as an iron chelator (Fritzer-Szekeres et al., 1997; Asperti et al., 2019). Given this premise, since iron chelation has been demonstrated effective in reducing the growth of rhabdomyosarcoma (Asperti et al., 2023), and since iron is required for the catalytic activity of RRM2, studies aimed to investigate to test if also didox could be effective in counteracting the progression of this aggressive neoplasia. To this aim,

RD and RH30 cell lines were used, representative of the embryonal and alveolar subtypes of RMS, respectively.

The data found that the viability of both cell lines is reduced by a treatment with didox in a dose- and time-dependent manner, with increased potency in RH30 cells, representative of the most aggressive subtype. Also, the treatment with didox reduced far more efficiently the cell viability of RMS cell lines compared to a treatment with its precursor, hydroxyurea. It was also confirmed that didox induced cell death by apoptosis, as widely demonstrated in various studies (Grusch *et al.*, 2001; Raje *et al.*, 2006; Shah *et al.*, 2015), and also caused the increase of mitochondrial ROS production, similarly to what has been reported from previous works (Raje *et al.*, 2006). The study also assessed that didox reduced the motility of RMS cell lines, with increased effects on embryonal RD cells, while it reduced the clonogenicity of both cell lines in a comparable amount between the two subtypes.

Given the iron chelating properties of didox, its effects on the iron status of these cells were analyzed. While no significant variations in the expression of TfR1 were detected, a decrease in the levels of H-ferritin after a treatment with didox 25 μM and 100 μM in, respectively, RH30 and RD cells was observed. Moreover, didox, at low concentrations, increased the content of intracellular iron, a property that is typical of small iron-chelating molecules such as catechol (Torti and Torti, 2013). The fact that we could not see differences in the iron content when cells were treated with higher doses of didox could be due to its inhibitory activity on RRM2, which, at these concentrations, is probably predominant over the iron chelating activity.

Finally, since didox more effectively impaired the cell viability of ARMS cells (which also represents the most aggressive subtype of RMS), RH30 cell line was used to test the *in vivo* antitumor properties of didox. It was found that tumor growth was significantly impaired by the treatment with didox during all the duration of the experiment, as demonstrated by the reduced weight and volume of tumors at the experimental timepoint. Interestingly, didox did not significantly alter the iron content in both liver, spleen, and serum, indicating that the systemic iron handling was not affected by the treatment. Finally, it was found that didox significantly reduced the levels of Ki-67 protein levels in tumors, confirming that the treatment decreased tumor proliferation.

In conclusion, the current study demonstrated that a treatment with didox can efficiently impair the proliferation of RMS tumors, suggesting a new promising therapeutic strategy for the treatment of this aggressive tumor type. Also, given the non-toxicity of didox in clinical trials, the data suggest that the administration of didox in addition to the currently approved chemotherapeutic agents, could increase the success of RMS treatment.

Among the many molecular alterations identified in RMS, increased expression of caveolin-1 has been linked to poorer differentiation and higher proliferation, along with enhanced formation of distant metastases (Codenotti *et al.*, 2019). Moreover, the overexpression of Cav-1 in RD cells (representative of embryonal RMS) resulted in increased sensitivity to ferroptosis inducers (Codenotti *et al.*, 2018). Taking advantage of the link between Cav-1 overexpression in RD cells and the cell susceptibility to ferroptosis, it was aimed to further analyze these cells in terms of antioxidant defense and lipid metabolism.

Initially, Cav-1-overexpressing RD cells were characterized for ferroptosis-related genes and proteins. We observed downregulation of FSP1 (involved in the regeneration of Coenzyme $Q_{10}$, and so, in the neutralization of lipid peroxides), along with increased expression of ACSL4 (involved in the insertion of PUFAs in the cell membrane). Also, higher amounts of lipid peroxides and reduced levels of the mRNAs encoding for GPX4, heme oxygenase 1 and thioredoxin (involved in the antioxidant response of the cell) were detected. These data are in line with the previous findings on these cells, confirming that Cav-1 overexpression in RD cells increased oxidative stress and thus may render them more sensitive to ferroptosis (Codenotti *et al.*, 2018). Moreover, Cav-1 has been previously demonstrated to inhibit the nuclear translocation of Nuclear factor-erythroid 2-related factor 2 (Nrf2), the main regulator of the antioxidant defense system, thereby downregulating the expression of antioxidant proteins and sensitizing cells to oxidative stress (Li *et al.*, 2012; Volonte *et al.*, 2013).

It was observed that ACSL4 was the most expressed member of this enzyme family in Cav-1-overexpressing RD cells, suggesting an increase in the PUFA content of membrane phospholipids, along with the presence of more complex alterations in fatty acids metabolism and handling. It was confirmed by reduced mRNA expression of the main regulators of lipid metabolism, SREBP1 and 2, and of the main players involved in fatty acids synthesis (ACLY, ACC, FASN and SCD1). Increased lipid accumulation was also evident in Cav-1-overexpressing cells. These data suggest that the overexpression of Cav-1 in RD cells also changes lipid metabolism in these cells.

Since ACSL4 is selectively involved in the incorporation of PUFA into cell membrane of PUFAs, which are the final target of the ferroptotic process, studies analyzed the role of this protein in the increased sensitivity of Cav-1-overexpressing cells to ferroptosis. As first approach, we treated cells with the pan-ACSL inhibitor triacsin C. Although triacsin C can inhibit overall ASCLs activity, since it was found that ACSL4 is the mostly expressed ACSL isoform in Cav-1-overexpressing RD cells, it was expected to observe an effect that was mainly due to ASCL4 suppression. We found that control cells were less sensitive to the effects of triacsin C in terms of cell viability, cell motility and clonogenicity, suggesting a higher dependency on the ACSL enzymes in Cav-1-overexpressing cells. To our surprise, a pre-treatment with the inhibitor did not affect FINs-induced mortality in Cav-1-overexpressing cells. Next, we used specific silencing RNAs for the downregulation of the sole ACSL4 in Cav-1-overexpressing RD cells. Preliminary results showed that ASCL4 knockdown did not alter the sensitivity of these cells to ferroptosis inducers. These data suggest that the increased susceptibility to ferroptosis of Cav-1-overexpressing cells is not caused only by the increased expression of ACSL4. Despite the inhibited insertion of PUFAs in the cell membrane, the sensitivity of Cav-1-overexpressing RD cells to ferroptosis inducers may be not affected due to their high lipid content and oxidative status. As a consequence, the impairment of the antioxidant machinery caused by FINs would still be able to promote the formation of PUFA peroxides, thus exacerbating an already precarious balance leading to cell death by ferroptosis. This hypothesis has been partially confirmed by the supplementation with MUFAs, which protected Cav-1-overexpressing cells from the cytotoxic effect of RSL3, while the overloading with exogenous PUFAs increased RSL3-induced cell mortality.

Altogether, these data suggest that the increased sensitivity to ferroptosis inducers in Cav-1-overexpressing cell is caused by a broader range of alterations that involve both lipid metabolism and antioxidant responses, and therefore, further studies will be required to fully understand the role of ACSL4 and lipid metabolism in Cav-1-overexpressing cells.

# 5- Conclusions

Iron plays a fundamental role in the development of cancer. Since a plethora of biological processes, spanning from DNA replication to mitochondrial respiration, require the presence of this essential micronutrient, tumoral cells require higher amounts of iron in order to satisfy their increased metabolic needs, which in turn forces them to handle a greater amount of reactive oxygen species. Due to this, both the deprivation of iron and its overload in cancer cells have detrimental effects on tumor growth. Moreover, it has been reported that different tumor cells are sensitive to ferroptosis, a programmed cell death, caused by the lethal accumulation of lipid peroxides due to an increase of intracellular iron and a decrease of antioxidant capacity. In light of this premise, the work of the present thesis aimed to investigate ferroptosis sensitivity and iron modulation in two different types of tumors, poorly characterized for their iron metabolism: glioblastoma (GBM), the most common tumor of the central nervous system, and rhabdomyosarcoma (RMS), an aggressive and metastatic pediatric cancer that develops from undifferentiated myocytes.

The data obtained from the present work of thesis contributed to the characterization of patients-derived GBM-CSCs, responsible for tumor relapse in glioblastoma, for their expression of ferroptosis- and iron-related genes and proteins. Our results showed that GBM-CSCs expressed iron-related genes and proteins, suggesting a capacity to properly handle iron uptake, export, and storage. Moreover, these cells also express the main genes related to antioxidant defense and ferroptosis. However, these data do not allow to discriminate if GBM-CSCs could be sensitive or resistant to ferroptosis basing on the specific gene and protein expression. Also, the study also reported that ferroptosis inducers can potently reduce the cell viability of GBM-CSC lines *in vitro*, a feature that has been recently discovered in glioma cell lines but had not been verified in GBM-CSCs before. Moreover, our data indicate that ferroptosis inducers can potentiate the effects of the current therapeutical standard-of-care temozolomide. More investigation is required to fully understand the induction of ferroptotic process in GBM-CSC cell lines, and if it could be a potential therapeutic tool to counteract GBM.

In the second part of this PhD thesis, in collaboration with Prof. Fanzani's group (University of Brescia) we investigated if both iron chelation and ferroptosis induction could be effective strategies for the treatment of rhabdomyosarcoma. First, we found that the synthetic RRM2

inhibitor and iron-chelating agent didox effectively counteracted the growth of both embryonal and alveolar RMS cell lines, also reducing the *in vivo* proliferation of alveolar RMS cells, representative of the most aggressive subtype. These data suggest that the use of didox could be an alternative therapeutic approach for the treatment of aggressive RMS. Moreover, it would be of interest to verify if the combination of didox with the currently used therapeutic agents could increase the efficacy of treatments, potentially increasing the prognosis of RMS patients.

Secondly, we investigated the interplay between ferroptosis and lipid metabolism in Cav-1-overexpressing ERMS cell lines, which have been demonstrated more susceptible to ferroptotic cell death. Our data demonstrated that increased levels of Cav-1, which is involved in the aggressiveness and metastatic dissemination of RMS, correlate with the altered expression of the main players of lipid metabolism. Also, since we found that Cav-1-overexpressing cells expressed higher levels of ACSL4, which is involved in the insertion of PUFAs in the cell membrane, we investigated the role of this ligase in the ferroptosis sensitivity of these cells. We demonstrated that, rather than to the increased levels of ACSL4, Cav-1-overexpressing cells are more sensitive to ferroptosis inducers due to their increased lipid content and to the alteration of their antioxidant mechanisms. These data suggest that more profound alterations are responsible for this phenotype, and that more studies will be required to fully clarify the mechanisms involved in the sensitivity to ferroptosis caused by Cav-1 overexpression.

# List of abbreviations

| | |
|---|---|
| AA | Arachidonic acid |
| ACC | Acetyl-CoA carboxylase |
| ACLY | ATP-citrate lyase |
| ACSL | Long-chain-fatty-acid-CoA ligase |
| ARMS | Alveolar Rhabdomyosarcoma |
| CHAC1 | Glutathione-specific gamma-glutamylcyclotransferase 1 |
| CNS | Central Nervous System |
| DFO | Deferoxamine |
| ERMS | Embryonal Rhabdomyosarcoma |
| FASN | Fatty acid synthase |
| Fer-1 | Ferrostatin-1 |
| FIN | Ferroptosis-inducing agent |
| FPN | Ferroportin (also referred to as "SLC40A1") |
| FSP1 | Ferroptosis suppressor protein 1 |
| FtH | Ferritin heavy chain |
| FtL | Ferritin light chain |
| GBM | Glioblastoma |
| GBM-CSC | Glioblastoma Cancer Stem Cell |
| GBM-PNC | Glioblastoma with Primitive Neuronal Component |
| GPX4 | Glutathione peroxidase 4 |
| HMOX1 | Heme oxygenase 1 |
| HU | Hydroxyurea |
| LA | Linoleic acid |
| LIP | Labile iron pool |
| MUFA | Monounsaturated fatty acid |
| NFE2L2 | Nuclear factor erythroid 2-related factor 2 (also referred to as "Nrf2") |
| NQO1 | NAD(P)H dehydrogenase [quinone] 1 |
| OA | Oleic acid |

| | |
|---|---|
| PA | Palmitic acid |
| PNET | Primitive Neuroectodermal Tumor |
| PTGS2 | Prostaglandin-endoperoxide synthase 2 |
| PUFA | Polyunsaturated fatty acid |
| RMS | Rhabdomyosarcoma |
| ROS | Reactive oxygen species |
| SCD1 | Stearoyl-CoA desaturase 1 |
| SLC7A11 | Solute carrier family 7 member 11 (also referred to as "xCT") |
| SREBP | Sterol regulatory element binding protein |
| TfR1 | Transferrin receptor 1 |
| TMZ | Temozolomide |
| α-LNA | α -linolenic acid |
| γ-LNA | γ -linolenic acid |

# References


Abdelaal, G. and Veuger, S. (2021) 'Reversing oncogenic transformation with iron chelation', *Oncotarget*, 12(2), pp. 106–124. doi: 10.18632/oncotarget.27866.

Adamski, V. *et al.* (2017) 'Dormant glioblastoma cells acquire stem cell characteristics and are differentially affected by Temozolomide and AT101 treatment', *Oncotarget*, 8(64), pp. 108064–108078. doi: 10.18632/oncotarget.22514.

Agaram, N. P. (2022) 'Evolving classification of rhabdomyosarcoma', *Histopathology*, 80(1), pp. 98–108. doi: 10.1111/his.14449.

Al-Abd, A. M. *et al.* (2013) 'Didox potentiates the cytotoxic profile of doxorubicin and protects from its cardiotoxicity', *European Journal of Pharmacology*, 718(1–3), pp. 361–369. doi: 10.1016/j.ejphar.2013.08.009.

Arai, M. *et al.* (1999) 'Mitochondrial Phospholipid Hydroperoxide Glutathione Peroxidase Plays a Major Role in Preventing Oxidative Injury to Cells', *Journal of Biological Chemistry*, 274(8), pp. 4924–4933. doi: 10.1074/jbc.274.8.4924.

Arosio, P., Elia, L. and Poli, M. (2017) 'Ferritin, cellular iron storage and regulation', *IUBMB Life*, 69(6), pp. 414–422. doi: 10.1002/iub.1621.

Asperti, M. *et al.* (2019) 'The Antitumor Didox Acts as an Iron Chelator in Hepatocellular Carcinoma Cells.', *Pharmaceuticals (Basel, Switzerland)*, 12(3), p. 129. doi: 10.3390/ph12030129.

Asperti, M. *et al.* (2021) 'H-ferritin suppression and pronounced mitochondrial respiration make Hepatocellular Carcinoma cells sensitive to RSL3-induced ferroptosis.', *Free radical biology & medicine*, 169(April), pp. 294–303. doi: 10.1016/j.freeradbiomed.2021.04.024.

Asperti, M. *et al.* (2023) 'The modulation of iron metabolism affects the Rhabdomyosarcoma tumor growth in vitro and in vivo', *Clinical and Experimental Medicine*, 2(0123456789). doi: 10.1007/s10238-023-01012-5.

Auffinger, B. *et al.* (2014) 'Conversion of differentiated cancer cells into cancer stem-like cells in a glioblastoma model after primary chemotherapy', *Cell Death and Differentiation*, 21(7), pp. 1119–1131. doi: 10.1038/cdd.2014.31.

Bao, S. *et al.* (2006) 'Glioma stem cells promote radioresistance by preferential activation of the DNA damage response', *Nature*, 444(7120), pp. 756–760. doi: 10.1038/nature05236.

Baudrand, R. *et al.* (2016) 'Caveolin 1 modulates aldosterone-mediated pathways of glucose and lipid homeostasis', *Journal of the American Heart Association*, 5(10). doi: 10.1161/JAHA.116.003845.

Beier, D., Schulz, J. B. and Beier, C. P. (2011) 'Chemoresistance of glioblastoma cancer stem cells - much more complex than expected', *Molecular Cancer*, 10(1), p. 128. doi: 10.1186/1476-4598-10-128.

Bersuker, K. *et al.* (2019) 'The CoQ oxidoreductase FSP1 acts parallel to GPX4 to inhibit ferroptosis', *Nature*, 575(7784), pp. 688–692. doi: 10.1038/s41586-019-1705-2.

Bogdan, A. R. *et al.* (2016) 'Regulators of Iron Homeostasis: New Players in Metabolism, Cell Death, and Disease', *Trends in Biochemical Sciences*, 41(3), pp. 274–286. doi: 10.1016/j.tibs.2015.11.012.

Bordini, J. *et al.* (2017) 'Induction of iron excess restricts malignant plasma cells expansion and potentiates bortezomib effect in models of multiple myeloma', *Leukemia*, 31(4), pp. 967–970. doi: 10.1038/leu.2016.346.

Bordini, J. *et al.* (2020) 'Iron Induces Cell Death and Strengthens the Efficacy of Antiandrogen Therapy in Prostate Cancer Models', *Clinical Cancer Research*, 26(23), pp. 6387–6398. doi: 10.1158/1078-0432.CCR-20-3182.

Brat, D. J. *et al.* (2018) 'cIMPACT-NOW update 3: recommended diagnostic criteria for "Diffuse astrocytic glioma, IDH-wildtype, with molecular features of glioblastoma, WHO grade IV"', *Acta Neuropathologica*, 136(5), pp. 805–810. doi: 10.1007/s00401-018-1913-0.

Bridges, R. J., Natale, N. R. and Patel, S. A. (2012) 'System xc- cystine/glutamate antiporter: an update on molecular pharmacology and roles within the CNS', *British Journal of Pharmacology*, 165(1), pp. 20–34. doi: 10.1111/j.1476-5381.2011.01480.x.

Brigelius-Flohé, R. and Maiorino, M. (2013) 'Glutathione peroxidases', *Biochimica et Biophysica Acta - General Subjects*, 1830(5), pp. 3289–3303. doi: 10.1016/j.bbagen.2012.11.020.

Bröer, A. *et al.* (2001) 'Association of 4F2hc with light chains LAT1, LAT2 or y+LAT2 requires different domains.', *The Biochemical journal*, 355(Pt 3), pp. 725–31. doi: 10.1042/bj3550725.

Bronte, G. *et al.* (2017) 'Sorafenib for the treatment of breast cancer', *Expert Opinion on Pharmacotherapy*, 18(6), pp. 621–630. doi: 10.1080/14656566.2017.1309024.

Brown, M. S. and Goldstein, J. L. (1997) 'The SREBP pathway: Regulation of cholesterol metabolism by proteolysis of a membrane-bound transcription factor', *Cell*, 89(3), pp. 331–340. doi: 10.1016/S0092-8674(00)80213-5.

Brown, R. A. M. *et al.* (2020) 'Altered Iron Metabolism and Impact in Cancer Biology, Metastasis, and Immunology', *Frontiers in Oncology*, 10(April). doi: 10.3389/fonc.2020.00476.

Brown, T. J. *et al.* (2016) 'Association of the extent of resection with survival in glioblastoma a systematic review and meta-Analysis', *JAMA Oncology*, 2(11), pp. 1460–1469. doi: 10.1001/jamaoncol.2016.1373.

Brusselmans, K. *et al.* (2005) 'RNA interference-mediated silencing of the acetyl-Coa-carboxylase-α gene induces growth inhibition and apoptosis of prostate cancer cells', *Cancer Research*, 65(15), pp. 6719–6725. doi: 10.1158/0008-5472.CAN-05-0571.

Buccarelli, M. *et al.* (2018) 'Inhibition of autophagy increases susceptibility of glioblastoma stem cells to temozolomide by igniting ferroptosis', *Cell Death and Disease*, 9(8). doi: 10.1038/s41419-018-0864-7.

Buckingham, S. C. *et al.* (2011) 'Glutamate release by primary brain tumors induces epileptic activity', *Nature Medicine*, 17(10), pp. 1269–1274. doi: 10.1038/nm.2453.

Bystrom, L. M. and Rivella, S. (2015) 'Cancer cells with irons in the fire', *Free Radical Biology and Medicine*, 79, pp. 337–342. doi: 10.1016/j.freeradbiomed.2014.04.035.

Cairncross, J. G. *et al.* (2014) 'Benefit from procarbazine, lomustine and vincristine in oligodendroglial tumors is associated with mutation of IDH', *Journal of Clinical Oncology*, 32(8), pp. 783–790. doi: 10.1200/JCO.2013.49.3726.

Calzolari, A. *et al.* (2010) 'Transferrin Receptor 2 Is Frequently and Highly Expressed in Glioblastomas', *Translational Oncology*, 3(2), pp. 123–134. doi: 10.1593/tlo.09274.

Campanella, A. *et al.* (2013) 'Iron increases the susceptibility of multiple myeloma cells to bortezomib', *Haematologica*, 98(6), pp. 971–979. doi: 10.3324/haematol.2012.074872.

Cancer Genome Atlas Research Network *et al.* (2015) 'Comprehensive, Integrative Genomic Analysis of Diffuse Lower-Grade Gliomas', *New England Journal of Medicine*, 372(26), pp. 2481–2498. doi: 10.1056/NEJMoa1402121.

Cao, J. Y. and Dixon, S. J. (2016) 'Mechanisms of ferroptosis', *Cellular and Molecular Life Sciences*, 73(11–12), pp. 2195–2209. doi: 10.1007/s00018-016-2194-1.

Carmichael, J. *et al.* (1990) 'A phase I and pharmacokinetic study of didox administered by 36 hour infusion. The Cancer Research Campaign Phase I/II Clinical Trials Committee.', *British journal of cancer*, 61(3), pp. 447–450.

de Carvalho, C. and Caramujo, M. (2018) 'The Various Roles of Fatty Acids', *Molecules*, 23(10), p. 2583. doi: 10.3390/molecules23102583.

Castro, B. *et al.* (2002) 'Role of γ-glutamyltranspeptidase on the response of poorly and moderately differentiated rhabdomyosarcoma cell lines to buthionine sulfoximine-induced inhibition of glutathione synthesis', *Anti-Cancer Drugs*, 13(3), pp. 281–291. doi: 10.1097/00001813-200203000-00010.

Cavanaugh, P. F. *et al.* (1985) 'Characterization of L1210 Cell Growth Inhibition by the Bacterial Iron Chelators Parabactin and Compound II', *Cancer Research*, 45(10), pp. 4754–4759.

Chabes, A. and Thelander, L. (2000) 'Controlled protein degradation regulates ribonucleotide reductase activity in proliferating mammalian cells during the normal cell cycle and in response to DNA damage and replication blocks', *Journal of Biological Chemistry*, pp. 17747–17753. doi: 10.1074/jbc.M000799200.

Chajès, V. *et al.* (2006) 'Acetyl-CoA carboxylase α is essential to breast cancer cell survival', *Cancer Research*, 66(10), pp. 5287–5294. doi: 10.1158/0008-5472.CAN-05-1489.

Chen, L. *et al.* (2015) 'Erastin sensitizes glioblastoma cells to temozolomide by restraining xCT and cystathionine-γ-lyase function.', *Oncology reports*, 33(3), pp. 1465–74. doi: 10.3892/or.2015.3712.

Chen, X. and Funk, C. D. (2001) 'The N-terminal "β-Barrel" Domain of 5-Lipoxygenase Is Essential for Nuclear Membrane Translocation', *Journal of Biological Chemistry*, 276(1), pp. 811–818. doi: 10.1074/jbc.M008203200.

Chinot, O. L. *et al.* (2014) 'Bevacizumab plus Radiotherapy–Temozolomide for Newly Diagnosed Glioblastoma', *New England Journal of Medicine*, 370(8), pp. 709–722. doi: 10.1056/nejmoa1308345.

Codenotti, S. *et al.* (2018) 'Cell growth potential drives ferroptosis susceptibility in rhabdomyosarcoma and myoblast cell lines', *Journal of Cancer Research and Clinical Oncology*, 144(9), pp. 1717–1730. doi: 10.1007/s00432-018-2699-0.

Codenotti, S. *et al.* (2019) 'Caveolin-1 enhances metastasis formation in a human model of embryonal rhabdomyosarcoma through Erk signaling cooperation', *Cancer Letters*, 449(August 2018), pp. 135–144. doi: 10.1016/j.canlet.2019.02.013.

Codenotti, S. *et al.* (2021) 'Caveolin-1 promotes radioresistance in rhabdomyosarcoma through increased oxidative stress protection and DNA repair', *Cancer Letters*, 505(June 2020), pp. 1–12. doi: 10.1016/j.canlet.2021.02.005.

Cominelli, M. *et al.* (2015) 'EGFR Amplified and Overexpressing Glioblastomas and Association With Better Response to Adjuvant Metronomic Temozolomide', *JNCI: Journal of the National Cancer Institute*, 107(5), pp. 1–13. doi: 10.1093/jnci/djv041.

Conrad, M. and Sato, H. (2012) 'The oxidative stress-inducible cystine/glutamate antiporter, system x c − : cystine supplier and beyond', *Amino Acids*, 42(1), pp. 231–246. doi: 10.1007/s00726-011-0867-5.

Currie, E. *et al.* (2013) 'Cellular fatty acid metabolism and cancer', *Cell Metabolism*, 18(2), pp. 153–161. doi: 10.1016/j.cmet.2013.05.017.

Dächert, J. *et al.* (2020) 'Targeting ferroptosis in rhabdomyosarcoma cells', *International Journal of Cancer*, 146(2), pp. 510–520. doi: 10.1002/ijc.32496.

Das, B., Jain, N. and Mallick, B. (2022) 'Ribonucleotide reductase subunit M2 is a potential prognostic marker and therapeutic target for soft tissue sarcoma', *Gene*, 808(May 2021), p. 145988. doi: 10.1016/j.gene.2021.145988.

Davis, M. E. (2016) 'Glioblastoma: Overview of disease and treatment', *Clinical Journal of Oncology Nursing*, 20(5), pp. 1–8. doi: 10.1188/16.CJON.S1.2-8.

Dirkse, A. *et al.* (2019) 'Stem cell-associated heterogeneity in Glioblastoma results from intrinsic tumor plasticity shaped by the microenvironment', *Nature Communications*, 10(1), pp. 1–16. doi: 10.1038/s41467-019-09853-z.

Dixon, S. J. *et al.* (2012) 'Ferroptosis: An iron-dependent form of nonapoptotic cell death', *Cell*, 149(5), pp. 1060–1072. doi: 10.1016/j.cell.2012.03.042.

Dixon, S. J. *et al.* (2014) 'Pharmacological inhibition of cystine-glutamate exchange induces endoplasmic reticulum stress and ferroptosis', *eLife*, 2014(3), pp. 1–25. doi: 10.7554/eLife.02523.

Dixon, S. J. and Stockwell, B. R. (2019) 'The Hallmarks of Ferroptosis', *Annual Review of Cancer Biology*, 3(1), pp. 35–54. doi: 10.1146/annurev-cancerbio-030518-055844.

Dodson, M., Castro-Portuguez, R. and Zhang, D. D. (2019) 'NRF2 plays a critical role in mitigating lipid peroxidation and ferroptosis', *Redox Biology*, 23(January), p. 101107. doi: 10.1016/j.redox.2019.101107.

Doll, S. *et al.* (2017) 'ACSL4 dictates ferroptosis sensitivity by shaping cellular lipid composition', *Nature Chemical Biology*, 13(1), pp. 91–98. doi: 10.1038/nchembio.2239.

Doll, S. *et al.* (2019) 'FSP1 is a glutathione-independent ferroptosis suppressor', *Nature*, 575(7784), pp. 693–698. doi: 10.1038/s41586-019-1707-0.

Eckel-Passow, J. E. *et al.* (2015) 'Glioma Groups Based on 1p/19q, IDH , and TERT Promoter Mutations in Tumors', *New England Journal of Medicine*, 372(26), pp. 2499–2508. doi: 10.1056/NEJMoa1407279.

Elford, H. L. and Van't Riet, B. (1985) 'Inhibition of nucleoside diphosphate reductase by hydroxybenzohydroxamic acid derivatives', *Pharmacology & Therapeutics*, 29, pp. 239–254.

Elford, H. L., Wampler, G. L. and Riet, B. V. t. (1979) 'New Ribonucleotide Reductase Inhibitors with Antineoplastic Activity', *Cancer Research*, 39(3), pp. 844–851.

Enterline, H. T. and Horn, R. C. (1958) 'Alveolar Rhabdomyosarcoma: A Distinctive Tumor Type', *American Journal of Clinical Pathology*, 29, pp. 356–366. doi: https://doi.org/10.1093/ajcp/29.4.356.

Eyüpoglu, I. Y. *et al.* (2016) 'Supra-complete surgery via dual intraoperative visualization approach (DiVA) prolongs patient survival in glioblastoma', *Oncotarget*, 7(18), pp. 25755–25768. doi: 10.18632/oncotarget.8367.

Faggi, F. *et al.* (2014) 'Phosphocaveolin-1 enforces tumor growth and chemoresistance in rhabdomyosarcoma', *PLoS ONE*, 9(1), pp. 1–13. doi: 10.1371/journal.pone.0084618.

Fan, Q. W. *et al.* (2013) 'EGFR Phosphorylates Tumor-Derived EGFRvIII Driving STAT3/5 and Progression in Glioblastoma', *Cancer Cell*, 24(4), pp. 438–449. doi: 10.1016/j.ccr.2013.09.004.

Fan, Z. *et al.* (2017) 'Nrf2-keap1 pathway promotes cell proliferation and diminishes ferroptosis', *Oncogenesis*, 6(8). doi: 10.1038/oncsis.2017.65.

Fang, S. *et al.* (2018) 'Effects of intracellular iron overload on cell death and identification of potent

cell death inhibitors', *Biochemical and Biophysical Research Communications*, 503(1), pp. 297–303. doi: 10.1016/j.bbrc.2018.06.019.

Fanzani, A. and Poli, M. (2017) 'Iron, oxidative damage and ferroptosis in rhabdomyosarcoma', *International Journal of Molecular Sciences*, 18(8), pp. 1–13. doi: 10.3390/ijms18081718.

Figul, M. *et al.* (2003) 'Combined effects of temozolomide and the ribonucleotide reductase inhibitors didox and trimidox in malignant brain tumor cells', *Cancer Chemotherapy and Pharmacology*, 52(1), pp. 41–46. doi: 10.1007/s00280-003-0611-2.

Foskolou, I. P. *et al.* (2017) 'Ribonucleotide Reductase Requires Subunit Switching in Hypoxia to Maintain DNA Replication', *Molecular Cell*, 66(2), pp. 206-220.e9. doi: 10.1016/j.molcel.2017.03.005.

Frederick, L. *et al.* (2000) 'Diversity and frequency of epidermal growth factor receptor mutations in human glioblastomas', *Cancer Research*, 60(5), pp. 1383–1387.

Fridolfsson, H. N. *et al.* (2012) 'Mitochondria-localized caveolin in adaptation to cellular stress and injury', *The FASEB Journal*, 26(11), pp. 4637–4649. doi: 10.1096/fj.12-215798.

Friedmann Angeli, J. P. *et al.* (2014) 'Inactivation of the ferroptosis regulator Gpx4 triggers acute renal failure in mice', *Nature Cell Biology*, 16(12), pp. 1180–1191. doi: 10.1038/ncb3064.

Fritzer-Szekeres, M. *et al.* (1997) 'Iron binding capacity of didox (3,4-dihydroxybenzohydroxamic acid) and amidox (3,4-dihydroxybenzamidoxime) new inhibitors of the enzyme rebinucleotide reductase', *Life Sciences*, 61(22), pp. 2231–2237. doi: 10.1016/S0024-3205(97)00925-9.

Furukawa, T. *et al.* (1992) 'Iron deprivation decreases ribonucleotide reductase activity and DNA synthesis', *Life Sciences*, 50(26), pp. 2059–2065. doi: 10.1016/0024-3205(92)90572-7.

Van Gaal, J. C. *et al.* (2012) 'Building the bridge between rhabdomyosarcoma in children, adolescents and young adults: The road ahead', *Critical Reviews in Oncology/Hematology*, 82(3), pp. 259–279. doi: 10.1016/j.critrevonc.2011.06.005.

Gai, C. *et al.* (2020) 'Acetaminophen sensitizing erastin-induced ferroptosis via modulation of Nrf2/heme oxygenase-1 signaling pathway in non-small-cell lung cancer', *Journal of Cellular Physiology*, 235(4), pp. 3329–3339. doi: 10.1002/jcp.29221.

Galli, R. *et al.* (2004) 'Isolation and Characterization of Tumorigenic, Stem-like Neural Precursors from Human Glioblastoma', *Cancer Research*, 64(19), pp. 7011–7021. doi: 10.1158/0008-5472.CAN-04-1364.

Galli, R. (2019) 'The Neurosphere Assay (NSA) Applied to Neural Stem Cells (NSCs) and Cancer Stem Cells (CSCs)', in Moll, J. and Carotta, S. (eds) *Target Identification and Validation in Drug Discovery: Methods and Protocols*. 2nd edn. Methods in Molecular Biology, pp. 139–149. doi: 10.1007/978-1-4939-9145-7_9.

Gan, H. K., Cvrljevic, A. N. and Johns, T. G. (2013) 'The epidermal growth factor receptor variant III (EGFRvIII): Where wild things are altered', *FEBS Journal*, 280(21), pp. 5350–5370. doi: 10.1111/febs.12393.

Garnier, D. *et al.* (2019) 'Glioblastoma stem-like cells, Metabolic strategy to kill a challenging target', *Frontiers in Oncology*, 9(MAR), pp. 1–18. doi: 10.3389/fonc.2019.00118.

Gaschler, M. M. and Stockwell, B. R. (2017) 'Lipid peroxidation in cell death', *Biochemical and Biophysical Research Communications*, 482(3), pp. 419–425. doi: 10.1016/j.bbrc.2016.10.086.

Gilbert, M. R. *et al.* (2014) 'A Randomized Trial of Bevacizumab for Newly Diagnosed Glioblastoma', *New England Journal of Medicine*, 370(8), pp. 699–708. doi: 10.1056/nejmoa1308573.

Gimple, R. C. *et al.* (2022) 'Brain cancer stem cells: resilience through adaptive plasticity and

hierarchical heterogeneity', *Nature Reviews Cancer*, 22(9), pp. 497–514. doi: 10.1038/s41568-022-00486-x.

Gokani, S. and Bhatt, L. K. (2022) 'Caveolin-1: A Promising Therapeutic Target for Diverse Diseases', *Current Molecular Pharmacology*, 15(5), pp. 701–715. doi: 10.2174/1874467214666211130155902.

Gomez, D. E. *et al.* (2012) 'Telomere structure and telomerase in health and disease', *International journal of oncology*, 41(5), pp. 1561–9. doi: 10.3892/ijo.2012.1611.

Green, D. R. (2018) 'An Element of Life', *Cell*, 172(3), pp. 389–390. doi: 10.1016/j.cell.2018.01.003.

Griffith, O. W. (1982) 'Mechanism of action, metabolism, and toxicity of buthionine sulfoximine and its higher homologs, potent inhibitors of glutathione synthesis.', *The Journal of biological chemistry*, 257(22), pp. 13704–12. Available at: http://www.ncbi.nlm.nih.gov/pubmed/6128339.

Grusch, M. *et al.* (2001) 'Activation of caspases and induction of apoptosis by novel ribonucleotide reductase inhibitors amidox and didox', *Experimental Hematology*, 29(5), pp. 623–632. doi: 10.1016/S0301-472X(01)00624-5.

Guo, J. *et al.* (2018) 'Ferroptosis: A novel anti-tumor action for cisplatin', *Cancer Research and Treatment*, 50(2), pp. 445–460. doi: 10.4143/crt.2016.572.

Gupta, P. B. *et al.* (2019) 'Phenotypic Plasticity: Driver of Cancer Initiation, Progression, and Therapy Resistance', *Cell Stem Cell*, 24(1), pp. 65–78. doi: 10.1016/j.stem.2018.11.011.

Habermann, K. J. *et al.* (2017) 'Targeting redox homeostasis in rhabdomyosarcoma cells: GSH-depleting agents enhance auranofin-induced cell death', *Cell death & disease*, 8(10), p. e3067. doi: 10.1038/cddis.2017.412.

Hansen-Petrik, M. B. *et al.* (2002) 'Selective inhibition of Δ-6 desaturase impedes intestinal tumorigenesis', *Cancer Letters*, 175(2), pp. 157–163. doi: 10.1016/S0304-3835(01)00715-7.

Hassannia, B. *et al.* (2018) 'Nano-targeted induction of dual ferroptotic mechanisms eradicates high-risk neuroblastoma', *Journal of Clinical Investigation*, 128(8), pp. 3341–3355. doi: 10.1172/JCI99032.

Hassannia, B., Vandenabeele, P. and Vanden Berghe, T. (2019) 'Targeting Ferroptosis to Iron Out Cancer', *Cancer Cell*, 35(6), pp. 830–849. doi: 10.1016/j.ccell.2019.04.002.

Hasselblatt, M. *et al.* (2018) 'Diffuse astrocytoma, IDH-wildtype: A dissolving diagnosis', *Journal of Neuropathology and Experimental Neurology*, 77(6), pp. 422–425. doi: 10.1093/jnen/nly012.

Hatzivassiliou, G. *et al.* (2005) 'ATP citrate lyase inhibition can suppress tumor cell growth', *Cancer Cell*, 8(4), pp. 311–321. doi: 10.1016/j.ccr.2005.09.008.

Hayano, M. *et al.* (2016) 'Loss of cysteinyl-tRNA synthetase (CARS) induces the transsulfuration pathway and inhibits ferroptosis induced by cystine deprivation', *Cell Death and Differentiation*, 23(2), pp. 270–278. doi: 10.1038/cdd.2015.93.

He, C. *et al.* (2012) 'Inhibiting Delta-6 Desaturase Activity Suppresses Tumor Growth in Mice', *PLoS ONE*, 7(10), pp. 1–8. doi: 10.1371/journal.pone.0047567.

Hegi, M. E. *et al.* (2005) 'MGMT Gene Silencing and Benefit from Temozolomide in Glioblastoma', *New England Journal of Medicine*, 352(10), pp. 997–1003. doi: 10.1056/NEJMoa043331.

Hegi, M. E., Rajakannu, P. and Weller, M. (2012) 'Epidermal growth factor receptor: A re-emerging target in glioblastoma', *Current Opinion in Neurology*, 25(6), pp. 774–779. doi: 10.1097/WCO.0b013e328359b0bc.

Hentze, M. W., Muckenthaler, M. U. and Andrews, N. C. (2004) 'Balancing acts: molecular control of mammalian iron metabolism.', *Cell*, 117(3), pp. 285–97. doi: 10.1016/s0092-8674(04)00343-5.

Herrlinger, U. *et al.* (2019) 'Lomustine-temozolomide combination therapy versus standard temozolomide therapy in patients with newly diagnosed glioblastoma with methylated MGMT promoter (CeTeG/NOA–09): a randomised, open-label, phase 3 trial', *The Lancet*, 393(10172), pp. 678–688. doi: 10.1016/S0140-6736(18)31791-4.

Hess, D., Chisholm, J. W. and Igal, R. A. (2010) 'Inhibition of stearoylCoA desaturase activity blocks cell cycle progression and induces programmed cell death in lung cancer cells', *PLoS ONE*, 5(6). doi: 10.1371/journal.pone.0011394.

Hirschhorn, T. and Stockwell, B. R. (2019) 'The development of the concept of ferroptosis', *Free Radical Biology and Medicine*, 133(3), pp. 130–143. doi: 10.1016/j.freeradbiomed.2018.09.043.

Hirschmann-Jax, C. *et al.* (2004) 'A distinct "side population" of cells with high drug efflux capacity in human tumor cells', *Proceedings of the National Academy of Sciences of the United States of America*, 101(39), pp. 14228–14233. doi: 10.1073/pnas.0400067101.

Hochwald, S. N. *et al.* (1997) 'Elevation of glutathione and related enzyme activities in high-grade and metastatic extremity soft tissue sarcoma', *Annals of Surgical Oncology*, 4(4), pp. 303–309. doi: 10.1007/BF02303579.

Horvath, Z. *et al.* (2004) 'Combination chemotherapy of BCNU and didox acts synergystically in 9L glioma cells', *Nucleosides, Nucleotides and Nucleic Acids*, 23(8–9), pp. 1531–1535. doi: 10.1081/NCN-200027746.

Hsu, N. Y. *et al.* (2011) 'Expression status of ribonucleotide reductase small subunits hRRM2/p53R2 as prognostic biomarkers in stage I and II non-small cell lung cancer', *Anticancer Research*, 31(10), pp. 3475–3481.

Huang, Y. *et al.* (2005) 'Cystine-glutamate transporter SLC7A11 in cancer chemosensitivity and chemoresistance', *Cancer Research*, 65(16), pp. 7446–7454. doi: 10.1158/0008-5472.CAN-04-4267.

Ibrahim, O. and O'Sullivan, J. (2020) 'Iron chelators in cancer therapy', *BioMetals*, 33(4–5), pp. 201–215. doi: 10.1007/s10534-020-00243-3.

Ichimura, K. *et al.* (2009) 'IDH1 mutations are present in the majority of common adult gliomas but rare in primary glioblastomas', *Neuro-Oncology*, 11(4), pp. 341–347. doi: 10.1215/15228517-2009-025.

Imai, H. and Nakagawa, Y. (2003) 'Biological significance of phospholipid hydroperoxide glutathione peroxidase (PHGPx, GPx4) in mammalian cells', *Free Radical Biology and Medicine*, 34(2), pp. 145–169. doi: 10.1016/S0891-5849(02)01197-8.

Imoto, S. *et al.* (2018) 'Haemin-induced cell death in human monocytic cells is consistent with ferroptosis', *Transfusion and Apheresis Science*, 57(4), pp. 524–531. doi: 10.1016/j.transci.2018.05.028.

Ivanov, S. D. *et al.* (2015) 'Effects of iron ions and iron chelation on the efficiency of experimental radiotherapy of animals with gliomas', *Bulletin of Experimental Biology and Medicine*, 158(6), pp. 800–803. doi: 10.1007/s10517-015-2865-1.

Jaksch-Bogensperger, H. *et al.* (2020) 'Ferritin in glioblastoma', *British Journal of Cancer*, 122(10), pp. 1441–1444. doi: 10.1038/s41416-020-0808-8.

Kagan, V. E. *et al.* (2017) 'Oxidized arachidonic and adrenic PEs navigate cells to ferroptosis', *Nature Chemical Biology*, 13(1), pp. 81–90. doi: 10.1038/nchembio.2238.

Karsy, M. *et al.* (2012) 'Established and emerging variants of glioblastoma multiforme: Review of morphological and molecular features', *Folia Neuropathologica*, 50(4), pp. 301–321. doi: 10.5114/fn.2012.32361.

Kaseb, H., Kuhn, J. and Babiker, H. M. (2021) *Rhabdomyosarcoma*, *StatPearls*. Available at: http://www.ncbi.nlm.nih.gov/pubmed/29939543.

Keating, G. M. (2017) 'Sorafenib: A Review in Hepatocellular Carcinoma', *Targeted Oncology*, 12(2), pp. 243–253. doi: 10.1007/s11523-017-0484-7.

Ketteler, J. and Klein, D. (2018) 'Caveolin-1, cancer and therapy resistance', *International Journal of Cancer*, 143(9), pp. 2092–2104. doi: 10.1002/ijc.31369.

Khasraw, M. *et al.* (2022) 'New Approaches to Glioblastoma', *Annual Review of Medicine*, 73(1), pp. 279–292. doi: 10.1146/annurev-med-042420-102102.

Killela, P. J. *et al.* (2013) 'TERT promoter mutations occur frequently in gliomas and a subset of tumors derived from cells with low rates of self-renewal', *Proceedings of the National Academy of Sciences of the United States of America*, 110(15), pp. 6021–6026. doi: 10.1073/pnas.1303607110.

Kim, J. *et al.* (2015) 'Spatiotemporal Evolution of the Primary Glioblastoma Genome', *Cancer Cell*, 28(3), pp. 318–328. doi: 10.1016/j.ccell.2015.07.013.

Kim, J. Y. *et al.* (2001) 'Human cystine/glutamate transporter: cDNA cloning and upregulation by oxidative stress in glioma cells', *Biochimica et Biophysica Acta - Biomembranes*, 1512(2), pp. 335–344. doi: 10.1016/S0005-2736(01)00338-8.

Koundouros, N. and Poulogiannis, G. (2020) 'Reprogramming of fatty acid metabolism in cancer', *British Journal of Cancer*, 122(1), pp. 4–22. doi: 10.1038/s41416-019-0650-z.

Kraft, V. A. N. *et al.* (2020) 'GTP Cyclohydrolase 1/Tetrahydrobiopterin Counteract Ferroptosis through Lipid Remodeling', *ACS Central Science*, 6(1), pp. 41–53. doi: 10.1021/acscentsci.9b01063.

Kram, H. *et al.* (2022) 'Glioblastoma Relapses Show Increased Markers of Vulnerability to Ferroptosis', *Frontiers in Oncology*, 12(April), pp. 1–14. doi: 10.3389/fonc.2022.841418.

von Krusenstiern, A. N. *et al.* (2023) 'Identification of essential sites of lipid peroxidation in ferroptosis', *Nature Chemical Biology*. doi: 10.1038/s41589-022-01249-3.

Kulkarni, S. *et al.* (2002) 'Molecular Basis of the Specific Subcellular Localization of the C2-like Domain of 5-Lipoxygenase', *Journal of Biological Chemistry*, 277(15), pp. 13167–13174. doi: 10.1074/jbc.M112393200.

Labussière, M. *et al.* (2014) 'TERT promoter mutations in gliomas, genetic associations and clinico-pathological correlations', *British Journal of Cancer*, 111(10), pp. 2024–2032. doi: 10.1038/bjc.2014.538.

Lachaier, E. *et al.* (2014) 'Sorafenib induces ferroptosis in human cancer cell lines originating from different solid tumors.', *Anticancer research*, 34(11), pp. 6417–22. Available at: http://www.ncbi.nlm.nih.gov/pubmed/25368241.

Lacroix, M. *et al.* (2001) 'A multivariate analysis of 416 patients with glioblastoma multiforme: prognosis, extent of resection, and survival', *Journal of Neurosurgery*, 95(2), pp. 190–198. doi: 10.3171/jns.2001.95.2.0190.

Lan, X. *et al.* (2017) 'Fate mapping of human glioblastoma reveals an invariant stem cell hierarchy', *Nature*, 549(7671), pp. 227–232. doi: 10.1038/nature23666.

Lane, D. J. R. *et al.* (2015) 'Cellular iron uptake, trafficking and metabolism: Key molecules and mechanisms and their roles in disease', *Biochimica et Biophysica Acta - Molecular Cell Research*, 1853(5), pp. 1130–1144. doi: 10.1016/j.bbamcr.2015.01.021.

Laneuville, O. *et al.* (1995) 'Fatty Acid Substrate Specificities of Human Prostaglandin-endoperoxide H Synthase-1 and −2', *Journal of Biological Chemistry*, 270(33), pp. 19330–19336. doi:

10.1074/jbc.270.33.19330.

Latunde-Dada, G. O. (2017) 'Ferroptosis: Role of lipid peroxidation, iron and ferritinophagy', *Biochimica et Biophysica Acta (BBA) - General Subjects*, 1861(8), pp. 1893–1900. doi: 10.1016/j.bbagen.2017.05.019.

Lee, J. Y. *et al.* (2020) 'Polyunsaturated fatty acid biosynthesis pathway determines ferroptosis sensitivity in gastric cancer', *Proceedings of the National Academy of Sciences of the United States of America*, 117(51), pp. 32433–32442. doi: 10.1073/pnas.2006828117.

Lei, G. *et al.* (2020) 'The role of ferroptosis in ionizing radiation-induced cell death and tumor suppression', *Cell Research*, 30(2), pp. 146–162. doi: 10.1038/s41422-019-0263-3.

Li, J. *et al.* (1994) 'Partial characterization of a cDNA for human stearoyl-CoA desaturase and changes in its mRNA expression in some normal and malignant tissues', *International Journal of Cancer*, 57(3), pp. 348–352. doi: 10.1002/ijc.2910570310.

Li, Q. *et al.* (2017) 'Inhibition of neuronal ferroptosis protects hemorrhagic brain', *JCI Insight*, 2(7). doi: 10.1172/jci.insight.90777.

Li, S. *et al.* (2021) 'RSL3 Drives Ferroptosis through NF- κ B Pathway Activation and GPX4 Depletion in Glioblastoma', *Oxidative Medicine and Cellular Longevity*, 2021. doi: 10.1155/2021/2915019.

Li, W. *et al.* (2012) 'Caveolin-1 inhibits expression of antioxidant enzymes through direct interaction with nuclear erythroid 2 p45-related factor-2 (Nrf2)', *Journal of Biological Chemistry*, 287(25), pp. 20922–20930. doi: 10.1074/jbc.M112.352336.

Li, W. *et al.* (2022) 'Identification of novel biomarkers in prostate cancer diagnosis and prognosis', *Journal of Biochemical and Molecular Toxicology*, (October 2021). doi: 10.1002/jbt.23137.

Liu, G. *et al.* (2006) 'Analysis of gene expression and chemoresistance of CD133+ cancer stem cells in glioblastoma', *Molecular Cancer*, 5, pp. 1–12. doi: 10.1186/1476-4598-5-67.

Loras, A. *et al.* (2023) 'Neural Stem Cells as Potential Glioblastoma Cells of Origin', *Life*, 13(4), pp. 1–13. doi: 10.3390/life13040905.

Louandre, C. *et al.* (2013) 'Iron-dependent cell death of hepatocellular carcinoma cells exposed to sorafenib', *International Journal of Cancer*, 133(7), pp. 1732–1742. doi: 10.1002/ijc.28159.

Louis, D. N. *et al.* (2016) 'The 2016 World Health Organization Classification of Tumors of the Central Nervous System: a summary', *Acta Neuropathologica*, 131(6), pp. 803–820. doi: 10.1007/s00401-016-1545-1.

Louis, D. N. *et al.* (2021) 'The 2021 WHO Classification of Tumors of the Central Nervous System: a summary', *Neuro-Oncology*, 23(8), pp. 1231–1251. doi: 10.1093/neuonc/noab106.

Lu, S. C. (2013) 'Glutathione synthesis', *Biochimica et Biophysica Acta (BBA) - General Subjects*, 1830(5), pp. 3143–3153. doi: 10.1016/j.bbagen.2012.09.008.

Luo, S. *et al.* (2021) 'Caveolin-1 Regulates Cellular Metabolism: A Potential Therapeutic Target in Kidney Disease', *Frontiers in Pharmacology*, 12(December), pp. 1–21. doi: 10.3389/fphar.2021.768100.

Lv, Y. *et al.* (2022) 'Ferroptosis: From regulation of lipid peroxidation to the treatment of diseases', *Cell Biology and Toxicology*, (0123456789). doi: 10.1007/s10565-022-09778-2.

Lyons, S. A. *et al.* (2007) 'Autocrine glutamate signaling promotes glioma cell invasion', *Cancer Research*, 67(19), pp. 9463–9471. doi: 10.1158/0008-5472.CAN-07-2034.

Mackenzie, E. L., Iwasaki, K. and Tsuji, Y. (2008) 'Intracellular iron transport and storage: From

molecular mechanisms to health implications', *Antioxidants and Redox Signaling*, 10(6), pp. 997–1030. doi: 10.1089/ars.2007.1893.

Magtanong, L. *et al.* (2019) 'Exogenous Monounsaturated Fatty Acids Promote a Ferroptosis-Resistant Cell State', *Cell Chemical Biology*, 26(3), pp. 420-432.e9. doi: 10.1016/j.chembiol.2018.11.016.

Magtanong, L. *et al.* (2022) 'Context-dependent regulation of ferroptosis sensitivity', *Cell Chemical Biology*, 29(9), pp. 1409-1418.e6. doi: 10.1016/j.chembiol.2022.06.004.

Mai, T. T. *et al.* (2017) 'Salinomycin kills cancer stem cells by sequestering iron in lysosomes', *Nature Chemistry*, 9(10), pp. 1025–1033. doi: 10.1038/nchem.2778.

Mastroberardino, L. *et al.* (1998) 'Amino-acid transport by heterodimers of 4F2hc/CD98 and members of a permease family', *Nature*, 395(6699), pp. 288–291. doi: 10.1038/26246.

Melhem, J. M. *et al.* (2022) 'Updates in IDH-Wildtype Glioblastoma', *Neurotherapeutics*, 19(6), pp. 1705–1723. doi: 10.1007/s13311-022-01251-6.

Menendez, J. A. and Lupu, R. (2007) 'Fatty acid synthase and the lipogenic phenotype in cancer pathogenesis', *Nature Reviews Cancer*, 7(10), pp. 763–777. doi: 10.1038/nrc2222.

Meyer, M. *et al.* (2015) 'Single cell-derived clonal analysis of human glioblastoma links functional and genomic heterogeneity', *Proceedings of the National Academy of Sciences of the United States of America*, 112(3), pp. 851–856. doi: 10.1073/pnas.1320611111.

Migita, T. *et al.* (2008) 'ATP citrate lyase: Activation and therapeutic implications in non-small cell lung cancer', *Cancer Research*, 68(20), pp. 8547–8554. doi: 10.1158/0008-5472.CAN-08-1235.

Million, L. *et al.* (2011) 'Influence of Noncompliance With Radiation Therapy Protocol Guidelines and Operative Bed Recurrences for Children With Rhabdomyosarcoma and Microscopic Residual Disease: A Report From the Children's Oncology Group', *International Journal of Radiation Oncology*Biology*Physics*, 80(2), pp. 333–338. doi: 10.1016/j.ijrobp.2010.01.058.

Mishima, E. *et al.* (2022) 'A non-canonical vitamin K cycle is a potent ferroptosis suppressor', *Nature*, 608(7924), pp. 778–783. doi: 10.1038/s41586-022-05022-3.

Missiaglia, E. *et al.* (2012) 'PAX3/FOXO1 fusion gene status is the key prognostic molecular marker in rhabdomyosarcoma and significantly improves current risk stratification', *Journal of Clinical Oncology*, 30(14), pp. 1670–1677. doi: 10.1200/JCO.2011.38.5591.

Mitchell, K. *et al.* (2021) 'The evolution of the cancer stem cell state in glioblastoma: emerging insights into the next generation of functional interactions', *Neuro-Oncology*, 23(2), pp. 199–213. doi: 10.1093/neuonc/noaa259.

Miwa, S. *et al.* (2020) 'Recent advances and challenges in the treatment of rhabdomyosarcoma', *Cancers*, 12(7), pp. 1–18. doi: 10.3390/cancers12071758.

Molinaro, A. M. *et al.* (2019) 'Genetic and molecular epidemiology of adult diffuse glioma', *Nature Reviews Neurology*, 15(7), pp. 405–417. doi: 10.1038/s41582-019-0220-2.

Monti, E. and Fanzani, A. (2016) 'Uncovering metabolism in rhabdomyosarcoma', *Cell Cycle*, 15(2), pp. 184–195. doi: 10.1080/15384101.2015.1071746.

Mousa, R., Notis Dardashti, R. and Metanis, N. (2017) 'Selenium and Selenocysteine in Protein Chemistry', *Angewandte Chemie - International Edition*, 56(50), pp. 15818–15827. doi: 10.1002/anie.201706876.

Murata, M. *et al.* (1995) 'VIP21/caveolin is a cholesterol-binding protein', *Proceedings of the National Academy of Sciences of the United States of America*, 92(22), pp. 10339–10343. doi:

10.1073/pnas.92.22.10339.

Musiałek, M. W. and Rybaczek, D. (2021) 'Hydroxyurea—the good, the bad and the ugly', *Genes*, 12(7). doi: 10.3390/genes12071096.

Nemeth, E. and Ganz, T. (2021) 'Hepcidin-ferroportin interaction controls systemic iron homeostasis', *International Journal of Molecular Sciences*, 22(12). doi: 10.3390/ijms22126493.

Nohturfft, A. and Shao, C. Z. (2009) 'Coordination of lipid metabolism in membrane biogenesis', *Annual Review of Cell and Developmental Biology*, 25, pp. 539–566. doi: 10.1146/annurev.cellbio.24.110707.175344.

Noushmehr, H. *et al.* (2010) 'Identification of a CpG Island Methylator Phenotype that Defines a Distinct Subgroup of Glioma', *Cancer Cell*, 17(5), pp. 510–522. doi: 10.1016/j.ccr.2010.03.017.

Ntambi, J. M. and Miyazaki, M. (2004) 'Regulation of stearoyl-CoA desaturases and role in metabolism', *Progress in Lipid Research*, 43(2), pp. 91–104. doi: 10.1016/S0163-7827(03)00039-0.

Nwosu, Z. C. *et al.* (2016) 'Caveolin-1 in the regulation of cell metabolism: A cancer perspective', *Molecular Cancer*, 15(1), pp. 1–12. doi: 10.1186/s12943-016-0558-7.

O'Leary, B. *et al.* (2016) 'Craniospinal irradiation with concomitant and adjuvant temozolomide—a feasibility assessment of toxicity in patients with glioblastoma with a PNET component', *Journal of Neuro-Oncology*, 127(2), pp. 295–302. doi: 10.1007/s11060-015-2033-5.

Olzmann, J. A. and Carvalho, P. (2019) 'Dynamics and functions of lipid droplets', *Nature Reviews Molecular Cell Biology*, 20(3), pp. 137–155. doi: 10.1038/s41580-018-0085-z.

Orzan, F. *et al.* (2020) 'A simplified integrated molecular and immunohistochemistry-based algorithm allows high accuracy prediction of glioblastoma transcriptional subtypes', *Laboratory Investigation*, 100(10), pp. 1330–1344. doi: 10.1038/s41374-020-0437-0.

Ostrom, Q. T. *et al.* (2022) 'CBTRUS Statistical Report: Primary Brain and Other Central Nervous System Tumors Diagnosed in the United States in 2015–2019', *Neuro-Oncology*, 24(Supplement_5), pp. v1–v95. doi: 10.1093/neuonc/noac202.

Papanikolaou, G. and Pantopoulos, K. (2005) 'Iron metabolism and toxicity', *Toxicology and Applied Pharmacology*, 202(2), pp. 199–211. doi: 10.1016/j.taap.2004.06.021.

Parisi, S. *et al.* (2015) 'Temozolomide and Radiotherapy versus Radiotherapy Alone in High Grade Gliomas: A Very Long Term Comparative Study and Literature Review', *BioMed Research International*, 2015, pp. 1–7. doi: 10.1155/2015/620643.

Patton, R. B. and Horn, R. G. (1962) 'Rhabdomyosarcoma: Clinical and pathological features and comparison with human fetal and embryonal skeletal muscle', *Surgery*. doi: 10.5555/uri:pii:0039606062900582.

Perry, A. *et al.* (2009) 'Malignant gliomas with primitive neuroectodermal tumor-like components: A clinicopathologic and genetic study of 53 cases', *Brain Pathology*, 19(1), pp. 81–90. doi: 10.1111/j.1750-3639.2008.00167.x.

Pezeshkian, W., Chevrot, G. and Khandelia, H. (2018) 'The role of caveolin-1 in lipid droplets and their biogenesis', *Chemistry and Physics of Lipids*, 211(November 2017), pp. 93–99. doi: 10.1016/j.chemphyslip.2017.11.010.

Pineda, M. *et al.* (1999) 'Identification of a membrane protein, LAT-2, that co-expresses with 4F2 heavy chain, an L-type amino acid transport activity with broad specificity for small and large zwitterionic amino acids', *Journal of Biological Chemistry*, 274(28), pp. 19738–19744. doi: 10.1074/jbc.274.28.19738.

Pizer, E. S. *et al.* (2000) 'Malonyl-coenzyme-A is a potential mediator of cytotoxicity induced by fatty-acid synthase inhibition in human breast cancer cells and xenografts', *Cancer Research*, 60(2), pp. 213–218.

Polewski, M. D. *et al.* (2016) 'Increased Expression of System xc− in Glioblastoma Confers an Altered Metabolic State and Temozolomide Resistance', *Molecular Cancer Research*, 14(12), pp. 1229–1242. doi: 10.1158/1541-7786.MCR-16-0028.

Pratibha, R. *et al.* (2006) 'Enzymatic studies of cisplatin induced oxidative stress in hepatic tissue of rats', *European Journal of Pharmacology*, 532(3), pp. 290–293. doi: 10.1016/j.ejphar.2006.01.007.

Prelaj, A. *et al.* (2018) 'Therapeutic approach in glioblastoma multiforme with primitive neuroectodermal tumor components: Case report and review of the literature', *Oncology Letters*, 15(5), pp. 6641–6647. doi: 10.3892/ol.2018.8102.

Puig, S. *et al.* (2017) 'The elemental role of iron in DNA synthesis and repair', *Metallomics*, 9(11), pp. 1483–1500. doi: 10.1039/c7mt00116a.

Quan, J., Bode, A. M. and Luo, X. (2021) 'ACSL family: The regulatory mechanisms and therapeutic implications in cancer', *European Journal of Pharmacology*, 909(April), p. 174397. doi: 10.1016/j.ejphar.2021.174397.

Raje, N. *et al.* (2006) 'Didox, a ribonucleotide reductase inhibitor, induces apoptosis and inhibits DNA repair in multiple myeloma cells', *British Journal of Haematology*, 135(1), pp. 52–61. doi: 10.1111/j.1365-2141.2006.06261.x.

Ramadan, F. *et al.* (2020) 'Signaling pathways in Rhabdomyosarcoma invasion and metastasis', *Cancer and Metastasis Reviews*, 39(1), pp. 287–301. doi: 10.1007/s10555-020-09860-3.

Raudenska, M. *et al.* (2020) 'Caveolin-1 in oncogenic metabolic symbiosis', *International Journal of Cancer*, 147(7), pp. 1793–1807. doi: 10.1002/ijc.32987.

Recht, L. *et al.* (1990) 'Transferrin receptor in normal and neoplastic brain tissue: Implications for brain-tumor immunotherapy', *Journal of Neurosurgery*, 72(6), pp. 941–945. doi: 10.3171/jns.1990.72.6.0941.

Reinartz, R. *et al.* (2017) 'Functional Subclone profiling for prediction of treatment-induced intratumor population shifts and discovery of rational drug combinations in human glioblastoma', *Clinical Cancer Research*, 23(2), pp. 562–574. doi: 10.1158/1078-0432.CCR-15-2089.

Reuss, D. E. *et al.* (2015) 'Adult IDH wild type astrocytomas biologically and clinically resolve into other tumor entities', *Acta Neuropathologica*, 130(3), pp. 407–417. doi: 10.1007/s00401-015-1454-8.

Riet, B. V. t., Wampler, G. L. and Elford, H. L. (1979) 'Synthesis of Hydroxy-and Amino-Substituted Benzohydroxamic Acids: Inhibition of Ribonucleotide Reductase and Antitumor Activity', *Journal of Medicinal Chemistry*, 22(5), pp. 589–592. doi: 10.1021/jm00191a027.

Ring, A. *et al.* (2006) 'Caveolin-1 is required for fatty acid translocase (FAT/CD36) localization and function at the plasma membrane of mouse embryonic fibroblasts', *Biochimica et Biophysica Acta - Molecular and Cell Biology of Lipids*, 1761(4), pp. 416–423. doi: 10.1016/j.bbalip.2006.03.016.

Robe, P. A. *et al.* (2009) 'Early termination of ISRCTN45828668, a phase 1/2 prospective, randomized study of sulfasalazine for the treatment of progressing malignant gliomas in adults', *BMC Cancer*, 9, p. 372. doi: 10.1186/1471-2407-9-372.

Robenek, M. J. *et al.* (2004) 'Lipids partition caveolin-1 from ER membranes into lipid droplets: updating the model of lipid droplet biogenesis.', *The FASEB journal : official publication of the Federation of American Societies for Experimental Biology*, 18(7), pp. 866–868. doi: 10.1096/fj.03-0782fje.

Robert, S. M. *et al.* (2015) 'SLC7A11 expression is associated with seizures and predicts poor survival in patients with malignant glioma', *Science Translational Medicine*, 7(289). doi: 10.1126/scitranslmed.aaa8103.

Robert, S. M. and Sontheimer, H. (2014) 'Glutamate transporters in the biology of malignant gliomas', *Cellular and Molecular Life Sciences*, 71(10), pp. 1839–1854. doi: 10.1007/s00018-013-1521-z.

Rodriguez, R., Schreiber, S. L. and Conrad, M. (2021) 'Persister cancer cells: Iron addiction and vulnerability to ferroptosis', *Molecular Cell*, (2021), pp. 1–13. doi: 10.1016/j.molcel.2021.12.001.

Roetto, A. *et al.* (2010) 'Comparison of 3 Tfr2-deficient murine models suggests distinct functions for Tfr2-α and Tfr2-β isoforms in different tissues', *Blood*, 115(16), pp. 3382–3389. doi: 10.1182/blood-2009-09-240960.

Röhrig, F. and Schulze, A. (2016) 'The multifaceted roles of fatty acid synthesis in cancer', *Nature Reviews Cancer*, 16(11), pp. 732–749. doi: 10.1038/nrc.2016.89.

Rossi, S., Poliani, P. L., Cominelli, M., *et al.* (2011) 'Caveolin 1 is a marker of poor differentiation in Rhabdomyosarcoma', *European Journal of Cancer*, 47(5), pp. 761–772. doi: 10.1016/j.ejca.2010.10.018.

Rossi, S., Poliani, P. L., Missale, C., *et al.* (2011) 'Caveolins in rhabdomyosarcoma', *Journal of Cellular and Molecular Medicine*, 15(12), pp. 2553–2568. doi: 10.1111/j.1582-4934.2011.01364.x.

Rossier, G. *et al.* (1999) 'LAT2, a New Basolateral 4F2hc/CD98-associated Amino Acid Transporter of Kidney and Intestine', *Journal of Biological Chemistry*, 274(49), pp. 34948–34954. doi: 10.1074/jbc.274.49.34948.

Rubens, R. D. *et al.* (1991) 'Phase II trial of didox in advanced breast cancer', *British Journal of Cancer*, 64(6), pp. 1187–1188. doi: 10.1038/bjc.1991.488.

Ruskoski, T. B. and Boal, A. K. (2021) 'The periodic table of ribonucleotide reductases', *Journal of Biological Chemistry*, 297(4), p. 101137. doi: 10.1016/j.jbc.2021.101137.

Saban, N. and Bujak, M. (2009) 'Hydroxyurea and hydroxamic acid derivatives as antitumor drugs', *Cancer Chemotherapy and Pharmacology*, 64(2), pp. 213–221. doi: 10.1007/s00280-009-0991-z.

Safa, A. R. *et al.* (2015) 'Glioblastoma stem cells (GSCs) epigenetic plasticity and interconversion between differentiated non-GSCs and GSCs', *Genes and Diseases*, 2(2), pp. 152–163. doi: 10.1016/j.gendis.2015.02.001.

Sanai, N., Alvarez-Buylla, A. and Berger, M. S. (2005) 'Mechanisms of disease: Neural stem cells and the origin of gliomas', *The New England Journal of Medicine*, 353(8), pp. 811–822.

Santos, C. R. and Schulze, A. (2012) 'Lipid metabolism in cancer', *FEBS Journal*, 279(15), pp. 2610–2623. doi: 10.1111/j.1742-4658.2012.08644.x.

Sato, H. *et al.* (2005) 'Redox imbalance in cystine/glutamate transporter-deficient mice', *Journal of Biological Chemistry*, 280(45), pp. 37423–37429. doi: 10.1074/jbc.M506439200.

Savaskan, N. E. and Eyüpoglu, I. Y. (2010) 'xCT modulation in gliomas: Relevance to energy metabolism and tumor microenvironment normalization', *Annals of Anatomy - Anatomischer Anzeiger*, 192(5), pp. 309–313. doi: 10.1016/j.aanat.2010.07.003.

Sbodio, J. I., Snyder, S. H. and Paul, B. D. (2019) 'Regulators of the transsulfuration pathway', *British Journal of Pharmacology*, 176(4), pp. 583–593. doi: 10.1111/bph.14446.

Scaglia, N., Matías Caviglia, J. and Ariel Igal, R. (2005) 'High stearoyl-CoA desaturase protein and activity levels in simian virus 40 transformed-human lung fibroblasts', *Biochimica et Biophysica Acta*

*(BBA) - Molecular and Cell Biology of Lipids*, 1687(1–3), pp. 141–151. doi: 10.1016/j.bbalip.2004.11.015.

Schonberg, D. L. *et al.* (2015) 'Preferential Iron Trafficking Characterizes Glioblastoma Stem-like Cells', *Cancer Cell*, 28(4), pp. 441–455. doi: 10.1016/j.ccell.2015.09.002.

Schott, C. *et al.* (2015) 'Oncogenic RAS mutants confer resistance of RMS13 rhabdomyosarcoma cells to oxidative stress-induced ferroptotic cell death', *Frontiers in Oncology*, 5(JUN), pp. 1–7. doi: 10.3389/fonc.2015.00131.

Sehm, T., Fan, Z., *et al.* (2016) 'Sulfasalazine impacts on ferroptotic cell death and alleviates the tumor microenvironment and glioma-induced brain edema', *Oncotarget*, 7(24), pp. 36021–36033. doi: 10.18632/oncotarget.8651.

Sehm, T., Rauh, M., *et al.* (2016) 'Temozolomide toxicity operates in a xCT/SLC7a11 dependent manner and is fostered by ferroptosis', *Oncotarget*, 7(46), pp. 74630–74647. doi: 10.18632/oncotarget.11858.

Seitz, G. *et al.* (2010) 'Inhibition of glutathione-S-transferase as a treatment strategy for multidrug resistance in childhood rhabdomyosarcoma', *International journal of oncology*, 36(2), pp. 491–500. Available at: http://www.spandidos-publications.com/ijo/36/2/491.

Sen, U., Coleman, C. and Sen, T. (2023) 'Stearoyl coenzyme A desaturase-1: multitasker in cancer, metabolism, and ferroptosis', *Trends in Cancer*, xx(xx), pp. 1–10. doi: 10.1016/j.trecan.2023.03.003.

Shah, K. N. *et al.* (2015) 'Targeting ribonucleotide reductase M2 and NF-κB activation with didox to circumvent tamoxifen resistance in breast cancer', *Molecular Cancer Therapeutics*, 14(11), pp. 2411–2421. doi: 10.1158/1535-7163.MCT-14-0689.

Shah, R., Margison, K. and Pratt, D. A. (2017) 'The Potency of Diarylamine Radical-Trapping Antioxidants as Inhibitors of Ferroptosis Underscores the Role of Autoxidation in the Mechanism of Cell Death', *ACS Chemical Biology*, 12(10), pp. 2538–2545. doi: 10.1021/acschembio.7b00730.

Shern, J. F. *et al.* (2014) 'Comprehensive genomic analysis of rhabdomyosarcoma reveals a landscape of alterations affecting a common genetic axis in fusion-positive and fusion-negative tumors', *Cancer Discovery*, 4(2), pp. 216–231. doi: 10.1158/2159-8290.CD-13-0639.

Shimada, K. *et al.* (2016) 'Global survey of cell death mechanisms reveals metabolic regulation of ferroptosis', *Nature Chemical Biology*, 12(7), pp. 497–503. doi: 10.1038/nchembio.2079.

Shintoku, R. *et al.* (2017) 'Lipoxygenase-mediated generation of lipid peroxides enhances ferroptosis induced by erastin and RSL3', *Cancer Science*, 108(11), pp. 2187–2194. doi: 10.1111/cas.13380.

Singh, N. *et al.* (2021) 'Mechanisms of temozolomide resistance in glioblastoma - a comprehensive review', *Cancer Drug Resistance*, 4(1), pp. 17–43. doi: 10.20517/cdr.2020.79.

Skapek, S. X. *et al.* (2019) 'Rhabdomyosarcoma', *Nature Reviews Disease Primers*, 5(1), p. 1. doi: 10.1038/s41572-018-0051-2.

Śledzińska, P. *et al.* (2021) 'Prognostic and Predictive Biomarkers in Gliomas', *International Journal of Molecular Sciences*, 22(19), p. 10373. doi: 10.3390/ijms221910373.

Smart, E. J. *et al.* (1996) 'A role for caveolin in transport of cholesterol from endoplasmic reticulum to plasma membrane', *Journal of Biological Chemistry*, 271(46), pp. 29427–29435. doi: 10.1074/jbc.271.46.29427.

SongTao, Q. *et al.* (2012) 'IDH mutations predict longer survival and response to temozolomide in secondary glioblastoma', *Cancer Science*, 103(2), pp. 269–273. doi: 10.1111/j.1349-7006.2011.02134.x.

Sottoriva, A. *et al.* (2013) 'Intratumor heterogeneity in human glioblastoma reflects cancer evolutionary dynamics', *Proceedings of the National Academy of Sciences of the United States of America*, 110(10), pp. 4009–4014. doi: 10.1073/pnas.1219747110.

Soupene, E. and Kuypers, F. A. (2008) 'Mammalian long-chain acyl-CoA synthetases', *Experimental Biology and Medicine*, 233(5), pp. 507–521. doi: 10.3181/0710-MR-287.

Stichel, D. *et al.* (2018) 'Distribution of EGFR amplification, combined chromosome 7 gain and chromosome 10 loss, and TERT promoter mutation in brain tumors and their potential for the reclassification of IDHwt astrocytoma to glioblastoma', *Acta Neuropathologica*, 136(5), pp. 793–803. doi: 10.1007/s00401-018-1905-0.

Stockwell, B. R. (2022) 'Ferroptosis turns 10: Emerging mechanisms, physiological functions, and therapeutic applications', *Cell*, 185(14), pp. 2401–2421. doi: 10.1016/j.cell.2022.06.003.

Stockwell, B. R. and Jiang, X. (2020) 'The Chemistry and Biology of Ferroptosis', *Cell chemical biology*, 27(4), pp. 365–375. doi: 10.1016/j.chembiol.2020.03.013.

Stockwell, B. R., Jiang, X. and Gu, W. (2020) 'Emerging Mechanisms and Disease Relevance of Ferroptosis', *Trends in Cell Biology*, 30(6), pp. 478–490. doi: 10.1016/j.tcb.2020.02.009.

Stupp, R. *et al.* (2005) 'Radiotherapy plus Concomitant and Adjuvant Temozolomide for Glioblastoma', *New England Journal of Medicine*, 352(10), pp. 987–996. doi: 10.1056/NEJMoa043330.

Stupp, R. *et al.* (2009) 'Effects of radiotherapy with concomitant and adjuvant temozolomide versus radiotherapy alone on survival in glioblastoma in a randomised phase III study: 5-year analysis of the EORTC-NCIC trial', *The Lancet Oncology*, 10(5), pp. 459–466. doi: 10.1016/S1470-2045(09)70025-7.

Sturm, D. *et al.* (2016) 'New Brain Tumor Entities Emerge from Molecular Classification of CNS-PNETs', *Cell*, 164(5), pp. 1060–1072. doi: 10.1016/j.cell.2016.01.015.

Su, Y. *et al.* (2020) 'Ferroptosis, a novel pharmacological mechanism of anti-cancer drugs', *Cancer Letters*, 483, pp. 127–136. doi: 10.1016/j.canlet.2020.02.015.

Sui, X. *et al.* (2018) 'RSL3 drives ferroptosis through GPX4 inactivation and ros production in colorectal cancer', *Frontiers in Pharmacology*, 9(NOV), pp. 1–8. doi: 10.3389/fphar.2018.01371.

Sun, H. *et al.* (2013) 'Prognostic significance of IDH mutation in adult low-grade gliomas: a meta-analysis', *Journal of Neuro-Oncology*, 113(2), pp. 277–284. doi: 10.1007/s11060-013-1107-5.

Sun, Y. *et al.* (2018) 'Glutathione depletion induces ferroptosis, autophagy, and premature cell senescence in retinal pigment epithelial cells', *Cell Death & Disease*, 9(7), p. 753. doi: 10.1038/s41419-018-0794-4.

Sun, Y. *et al.* (2021) 'Fin56-induced ferroptosis is supported by autophagy-mediated GPX4 degradation and functions synergistically with mTOR inhibition to kill bladder cancer cells', *Cell Death & Disease*, 12(11), p. 1028. doi: 10.1038/s41419-021-04306-2.

Suvà, M. L. and Tirosh, I. (2020) 'The Glioma Stem Cell Model in the Era of Single-Cell Genomics', *Cancer Cell*, 37(5), pp. 630–636. doi: 10.1016/j.ccell.2020.04.001.

Suwala, A. K. *et al.* (2021) 'Glioblastomas with primitive neuronal component harbor a distinct methylation and copy-number profile with inactivation of TP53, PTEN, and RB1', *Acta Neuropathologica*, 142(1), pp. 179–189. doi: 10.1007/s00401-021-02302-6.

Szekeres, T., Fritzer-Szekeres, M. and Elford, H. L. (1997) 'The enzyme ribonucleotide reductase: Target for antitumor and anti-HIV therapy', *Critical Reviews in Clinical Laboratory Sciences*, 34(6), pp. 503–528. doi: 10.3109/10408369709006424.

Takano, T. *et al.* (2001) 'Glutamate release promotes growth of malignant gliomas', *Nature Medicine*, 7(9), pp. 1010–1015. doi: 10.1038/nm0901-1010.

Takeuchi, S. *et al.* (2013) 'Increased xCT expression correlates with tumor invasion and outcome in patients with glioblastomas', *Neurosurgery*, 72(1), pp. 33–41. doi: 10.1227/NEU.0b013e318276b2de.

Tesfay, L. *et al.* (2019) 'Stearoyl-CoA Desaturase 1 Protects Ovarian Cancer Cells from Ferroptotic Cell Death', *Cancer Research*, 79(20), pp. 5355–5366. doi: 10.1158/0008-5472.CAN-19-0369.

Tesileanu, C. M. S. *et al.* (2020) 'Survival of diffuse astrocytic glioma, IDH1/2 wildtype, with molecular features of glioblastoma, WHO grade IV: a confirmation of the cIMPACT-NOW criteria', *Neuro-Oncology*, 22(4), pp. 515–523. doi: 10.1093/neuonc/noz200.

Thakur, A. *et al.* (2022) 'Glioblastoma: Current Status, Emerging Targets, and Recent Advances', *Journal of Medicinal Chemistry*, 65(13), pp. 8596–8685. doi: 10.1021/acs.jmedchem.1c01946.

Torrents, D. *et al.* (1998) 'Identification and Characterization of a Membrane Protein (y + L Amino Acid Transporter-1) That Associates with 4F2hc to Encode the Amino Acid Transport Activity y + L', *Journal of Biological Chemistry*, 273(49), pp. 32437–32445. doi: 10.1074/jbc.273.49.32437.

Torti, S. V. *et al.* (2018) 'Iron and Cancer', *Annual Review of Nutrition*, 38(1), pp. 97–125. doi: 10.1146/annurev-nutr-082117-051732.

Torti, S. V. and Torti, F. M. (2013) 'Iron and cancer: more ore to be mined', *Nature Reviews Cancer*, 13(5), pp. 342–355. doi: 10.1038/nrc3495.

Torti, S. V. and Torti, F. M. (2020) 'Iron and cancer: 2020 vision', *Cancer Research*, 80(24), pp. 5435–5448. doi: 10.1158/0008-5472.CAN-20-2017.

Tosi, F. *et al.* (2014) 'Delta-5 and delta-6 desaturases: Crucial enzymes in polyunsaturated fatty acid-related pathways with pleiotropic influences in health and disease', *Advances in Experimental Medicine and Biology*, 824, pp. 61–81. doi: 10.1007/978-3-319-7320-0_7.

Trigatti, B. L., Anderson, R. G. W. and Gerber, G. E. (1999) 'Identification of caveolin-1 as a fatty acid binding protein', *Biochemical and Biophysical Research Communications*, 255(1), pp. 34–39. doi: 10.1006/bbrc.1998.0123.

Ursini, F. and Maiorino, M. (2020) 'Lipid peroxidation and ferroptosis: The role of GSH and GPx4', *Free Radical Biology and Medicine*, 152, pp. 175–185. doi: 10.1016/j.freeradbiomed.2020.02.027.

Veale, D. *et al.* (1988) 'A phase 1 and pharmacokinetic study of didox: A ribonucleotide reductase inhibitor', *British Journal of Cancer*, 58(1), pp. 70–72. doi: 10.1038/bjc.1988.164.

Verhaak, R. G. W. *et al.* (2010) 'Integrated Genomic Analysis Identifies Clinically Relevant Subtypes of Glioblastoma Characterized by Abnormalities in PDGFRA, IDH1, EGFR, and NF1', *Cancer Cell*, 17(1), pp. 98–110. doi: 10.1016/j.ccr.2009.12.020.

Volonte, D. *et al.* (2013) 'Inhibition of nuclear factor-erythroid 2-related factor (Nrf2) by caveolin-1 promotes stress-induced premature senescence', *Molecular Biology of the Cell*, 24(12), pp. 1852–1862. doi: 10.1091/mbc.E12-09-0666.

Volonte, D. *et al.* (2016) 'Caveolin-1 controls mitochondrial function through regulation of m-AAA mitochondrial protease', *Aging*, 8(10), pp. 2355–2369. doi: 10.18632/aging.101051.

Volonte, D., Liu, Y. and Galbiati, F. (2005) 'The modulation of caveolin-1 expression controls satellite cell activation during muscle repair', *The FASEB Journal*, 19(2), pp. 1–36. doi: 10.1096/fj.04-2215fje.

Wang, C. *et al.* (2020) 'Stearoyl-CoA desaturase 1 (SCD1) facilitates the growth and anti-ferroptosis of gastric cancer cells and predicts poor prognosis of gastric cancer', *Aging*, 12(15), pp. 15374–15391. doi: 10.18632/AGING.103598.

Wang, J. *et al.* (2016) 'Clonal evolution of glioblastoma under therapy', *Nature Genetics*, 48(7), pp. 768–776. doi: 10.1038/ng.3590.

Wang, Q. *et al.* (2017) 'Tumor Evolution of Glioma-Intrinsic Gene Expression Subtypes Associates with Immunological Changes in the Microenvironment', *Cancer Cell*, 32(1), pp. 42-56.e6. doi: 10.1016/j.ccell.2017.06.003.

Wang, S. *et al.* (2017) 'Caveolin-1: An Oxidative Stress-Related Target for Cancer Prevention', *Oxidative Medicine and Cellular Longevity*, 2017. doi: 10.1155/2017/7454031.

Wang, S. *et al.* (2021) 'Overexpression of RRM2 is related to poor prognosis in oral squamous cell carcinoma', *Oral Diseases*, 27(2), pp. 204–214. doi: 10.1111/odi.13540.

Wang, X. *et al.* (2019) 'RSL3 induced autophagic death in glioma cells via causing glycolysis dysfunction', *Biochemical and Biophysical Research Communications*, 518(3), pp. 590–597. doi: 10.1016/j.bbrc.2019.08.096.

Wang, Yu *et al.* (2022) 'Acetyl-CoA Carboxylases and Diseases', *Frontiers in Oncology*, 12(March), pp. 1–10. doi: 10.3389/fonc.2022.836058.

Wei, X. *et al.* (2020) 'Molecular basis for acetyl-CoA production by ATP-citrate lyase', *Nature Structural and Molecular Biology*, 27(1), pp. 33–41. doi: 10.1038/s41594-019-0351-6.

Wenzel, S. E. *et al.* (2017) 'PEBP1 Wardens Ferroptosis by Enabling Lipoxygenase Generation of Lipid Death Signals', *Cell*, 171(3), pp. 628-641.e26. doi: 10.1016/j.cell.2017.09.044.

White, B. (2009) 'Dietary fatty acids', *American family physician*, 80(4), pp. 345–50. Available at: http://www.ncbi.nlm.nih.gov/pubmed/19678602.

Wijnenga, M. M. J. *et al.* (2017) 'Molecular and clinical heterogeneity of adult diffuse low-grade IDH wild-type gliomas: assessment of TERT promoter mutation and chromosome 7 and 10 copy number status allows superior prognostic stratification', *Acta Neuropathologica*, 134(6), pp. 957–959. doi: 10.1007/s00401-017-1781-z.

Williamson, D. *et al.* (2010) 'Fusion gene-negative alveolar rhabdomyosarcoma is clinically and molecularly indistinguishable from embryonal rhabdomyosarcoma', *Journal of Clinical Oncology*, 28(13), pp. 2151–2158. doi: 10.1200/JCO.2009.26.3814.

Wilson, E. A. *et al.* (2021) 'Molecular Targeting of RRM2, NF-κB, and Mutant TP53 for the Treatment of Triple-Negative Breast Cancer', *Molecular cancer therapeutics*, 20(4), pp. 655–664. doi: 10.1158/1535-7163.MCT-20-0373.

Wong, A. J. *et al.* (1987) 'Increased expression of the epidermal growth factor receptor gene in malignant gliomas is invariably associated with gene amplification.', *Proceedings of the National Academy of Sciences of the United States of America*, 84(19), pp. 6899–6903. doi: 10.1073/pnas.84.19.6899.

Woo, J. H. *et al.* (2015) 'Elucidating Compound Mechanism of Action by Network Perturbation Analysis', *Cell*, 162(2), pp. 441–451. doi: 10.1016/j.cell.2015.05.056.

Wood, M. D. *et al.* (2016) 'Protein analysis of glioblastoma primary and posttreatment pairs suggests a mesenchymal shift at recurrence', *Journal of Neuropathology and Experimental Neurology*, 75(10), pp. 925–935. doi: 10.1093/jnen/nlw068.

Wu, G. *et al.* (2004) 'Glutathione Metabolism and Its Implications for Health', *The Journal of Nutrition*, 134(3), pp. 489–492. doi: 10.1093/jn/134.3.489.

Xie, X. P. *et al.* (2022) 'Quiescent human glioblastoma cancer stem cells drive tumor initiation, expansion, and recurrence following chemotherapy', *Developmental Cell*, 57(1), pp. 32-46.e8. doi:

10.1016/j.devcel.2021.12.007.

Xie, Y. *et al.* (2016) 'Ferroptosis: Process and function', *Cell Death and Differentiation*, 23(3), pp. 369–379. doi: 10.1038/cdd.2015.158.

Xu, G., Zheng, H. and Li, J. Y. (2019) 'Next-generation whole exome sequencing of glioblastoma with a primitive neuronal component', *Brain Tumor Pathology*, 36(3), pp. 129–134. doi: 10.1007/s10014-019-00334-1.

Xu, T. *et al.* (2019) 'Molecular mechanisms of ferroptosis and its role in cancer therapy', *Journal of Cellular and Molecular Medicine*, 23(8), pp. 4900–4912. doi: 10.1111/jcmm.14511.

Yagoda, N. *et al.* (2007) 'RAS-RAF-MEK-dependent oxidative cell death involving voltage-dependent anion channels', *Nature*, 447(7146), pp. 864–868. doi: 10.1038/nature05859.

Yan, H. *et al.* (2009) 'IDH1 and IDH2 Mutations in Gliomas', *New England Journal of Medicine*, 360(8), pp. 765–773. doi: 10.1056/NEJMoa0808710.

Yan, K. *et al.* (2014) 'Glioma cancer stem cells secrete Gremlin1 to promote their maintenance within the tumor hierarchy', *Genes and Development*, 28(10), pp. 1085–1100. doi: 10.1101/gad.235515.113.

Yan, R. *et al.* (2019) 'Structure of the human LAT1–4F2hc heteromeric amino acid transporter complex', *Nature*, 568(7750), pp. 127–130. doi: 10.1038/s41586-019-1011-z.

Yanagida, O. *et al.* (2001) 'Human L-type amino acid transporter 1 (LAT1): Characterization of function and expression in tumor cell lines', *Biochimica et Biophysica Acta - Biomembranes*, 1514(2), pp. 291–302. doi: 10.1016/S0005-2736(01)00384-4.

Yang, L. J., Zhou, C. F. and Lin, Z. X. (2014) 'Temozolomide and radiotherapy for newly diagnosed glioblastoma multiforme: A systematic review', *Cancer Investigation*, 32(2), pp. 31–36. doi: 10.3109/07357907.2013.861474.

Yang, P. *et al.* (2015) 'IDH mutation and MGMT promoter methylation in glioblastoma: results of a prospective registry', *Oncotarget*, 6(38), pp. 40896–40906. doi: 10.18632/oncotarget.5683.

Yang, W.-H. and Chi, J.-T. (2020) 'Hippo pathway effectors YAP/TAZ as novel determinants of ferroptosis', *Molecular & Cellular Oncology*, 7(1), p. 1699375. doi: 10.1080/23723556.2019.1699375.

Yang, W. S. *et al.* (2014) 'Regulation of Ferroptotic Cancer Cell Death by GPX4', *Cell*, 156(1–2), pp. 317–331. doi: 10.1016/j.cell.2013.12.010.

Yang, W. S. and Stockwell, B. R. (2008) 'Synthetic Lethal Screening Identifies Compounds Activating Iron-Dependent, Nonapoptotic Cell Death in Oncogenic-RAS-Harboring Cancer Cells', *Chemistry & Biology*, 15(3), pp. 234–245. doi: 10.1016/j.chembiol.2008.02.010.

Yang, W. S. and Stockwell, B. R. (2016) 'Ferroptosis: Death by Lipid Peroxidation', *Trends in Cell Biology*, 26(3), pp. 165–176. doi: 10.1016/j.tcb.2015.10.014.

Yant, L. J. *et al.* (2003) 'The selenoprotein GPX4 is essential for mouse development and protects from radiation and oxidative damage insults', *Free Radical Biology and Medicine*, 34(4), pp. 496–502. doi: 10.1016/S0891-5849(02)01360-6.

Ye, L. F. *et al.* (2020) 'Radiation-Induced Lipid Peroxidation Triggers Ferroptosis and Synergizes with Ferroptosis Inducers', *ACS Chemical Biology*, 15(2), pp. 469–484. doi: 10.1021/acschembio.9b00939.

Ye, L. F. and Stockwell, B. R. (2017) 'Transforming Lipoxygenases: PE-Specific Enzymes in Disguise', *Cell*, 171(3), pp. 501–502. doi: 10.1016/j.cell.2017.10.006.

Ye, Z. *et al.* (2020) 'Ferroptosis: Final destination for cancer?', *Cell Proliferation*, 53(3). doi: 10.1111/cpr.12761.

Ye, Z. C. and Sontheimer, H. (1999) 'Glioma cells release excitotoxic concentrations of glutamate', *Cancer Research*, 59(17), pp. 4383–4391.

Yechieli, R. L. *et al.* (2021) 'Rhabdomyosarcoma', *Pediatric Blood & Cancer*, 68(S2), pp. 1–8. doi: 10.1002/pbc.28254.

Yoon, H. and Lee, S. (2022) 'Fatty Acid Metabolism in Ovarian Cancer: Therapeutic Implications', *International Journal of Molecular Sciences*, 23(4). doi: 10.3390/ijms23042170.

Yuan, H. *et al.* (2016) 'Identification of ACSL4 as a biomarker and contributor of ferroptosis', *Biochemical and Biophysical Research Communications*, 478(3), pp. 1338–1343. doi: 10.1016/j.bbrc.2016.08.124.

Yuan, T. *et al.* (2007) 'Glut-4 is translocated to both caveolae and non-caveolar lipid rafts, but is partially internalized through caveolae in insulin-stimulated adipocytes', *Cell Research*, 17(9), pp. 772–782. doi: 10.1038/cr.2007.73.

Zanganeh, S. *et al.* (2016) 'Iron oxide nanoparticles inhibit tumour growth by inducing pro-inflammatory macrophage polarization in tumour tissues', *Nature Nanotechnology*, 11(11), pp. 986–994. doi: 10.1038/nnano.2016.168.

Zhang, Y. *et al.* (2019) 'Imidazole Ketone Erastin Induces Ferroptosis and Slows Tumor Growth in a Mouse Lymphoma Model', *Cell Chemical Biology*, 26(5), pp. 623-633.e9. doi: 10.1016/j.chembiol.2019.01.008.

Zhao, R. *et al.* (2020) 'FADS1 promotes the progression of laryngeal squamous cell carcinoma through activating AKT/mTOR signaling', *Cell Death and Disease*, 11(4). doi: 10.1038/s41419-020-2457-5.

Zhao, Y. *et al.* (2020) 'The role of Erastin in ferroptosis and its prospects in cancer therapy', *OncoTargets and Therapy*, 13, pp. 5429–5441. doi: 10.2147/OTT.S254995.

Zheng, J. and Conrad, M. (2020) 'The Metabolic Underpinnings of Ferroptosis', *Cell Metabolism*, 32(6), pp. 920–937. doi: 10.1016/j.cmet.2020.10.011.

Zhu, Z. *et al.* (2018) 'Glutathione reductase mediates drug resistance in glioblastoma cells by regulating redox homeostasis', *Journal of Neurochemistry*, 144(1), pp. 93–104. doi: 10.1111/jnc.14250.

Zitka, O. *et al.* (2012) 'Redox status expressed as GSH:GSSG ratio as a marker for oxidative stress in paediatric tumour patients', *Oncology Letters*, 4(6), pp. 1247–1253. doi: 10.3892/ol.2012.931.

# Ringraziamenti

Niente di quello che è stato scritto fino a questo punto sarebbe mai stato realizzato senza l'aiuto di tanti colleghi, collaboratori e amici.

I primi ringraziamenti vanno alla Prof.ssa Poli per aver diretto e coordinato la pianificazione degli esperimenti e la stesura di questa tesi. Grazie, inoltre, alla dott.ssa Asperti e alla dott.ssa Gryzik per il supporto pratico nella realizzazione degli esperimenti e per i consigli pratici. Grazie mille a tutti i membri, presenti e passati, del Laboratorio di Biologia Molecolare per aver fatto volare questi tre anni e per aver reso il mio percorso di dottorato un'esperienza, oltre che impegnativa, anche significativa a livello personale.

Grazie mille al Prof. Fanzani e alla dott.ssa Codenotti per la pianificazione e la realizzazione dei progetti sul rabdomiosarcoma, e al Prof. Poliani, alla dott.ssa Pagani e alla dott.ssa Somenza per la collaborazione del progetto glioblastoma. Grazie a chiunque abbia supportato questo percorso, sia in modo pratico che con suggerimenti preziosi.

Grazie, infine, a chi ha reso possibile questo percorso di dottorato al di fuori del laboratorio. Grazie agli amici per i momenti di svago, e soprattutto alla mia famiglia per il continuo appoggio nei momenti più difficili. Un grazie a Chiara, per la sua spensieratezza contagiosa, e un grazie enorme a Sara, per essermi sempre accanto e per essere capace di darmi forza in ogni situazione.